Design And Analysis Of Wireless Power Transfer Using High Frequency Resonant Inductive Coupling By Changing The Coil Geometry

A Study On Improving Wireless Power Coil Magnetics

Master of Science Thesis

Adarsh Bandi
Nagendra Gouthamas
Chalmers University Of Technology
Gothenburg, Sweden 2024

Master Of Science Thesis 2024

Design And Analysis Of Wireless Power Transfer Using High Frequency Resonant Inductive Coupling By Changing The Coil Geometry

A Study On Improving Wireless Power Coil Magnetics

Adarsh Bandi
Nagendra Gouthamas

Department of Electrical Engineering
Division of Electric Power Engineering
Chalmers University of Technology
Gothenburg, Sweden 2024

Design And Analysis Of Wireless Power Transfer Using High Frequency Resonant Inductive Coupling By Changing The Coil Geometry

A Study On Improving Wireless Power Coil Magnetics

Adarsh Bandi
Nagendra Gouthamas

Supervisor: Prof.Torbjörn Thiringer and Res.Fredrik Larsson
Examiner: Prof.Torbjörn Thiringer, Chalmers University of Technology

Master Of Science Thesis 2024
Department of Electrical Engineering
Division of Electric Power Engineering
Chalmers University of Technology
SE-412 96 Gothenburg
Sweden

Assisted by
Power Board Design Department
Division of Power Solutions
Ericsson AB
SE-417 56 Gothenburg
Sweden

Typeset in LaTeX

Design And Analysis Of Wireless Power Transfer Using High Frequency Resonant Inductive Coupling By Changing The Coil Geometry

A Study On Improving Wireless Power Coil Magnetics

Adarsh Bandi
Nagendra Gouthamas
Division of Electric Power Engineering
Chalmers University of Technology
SE-412 96 Gothenburg
Sweden

Abstract

In this thesis, we have developed a wireless power transfer system for a space of dimensions (15cm x 15cm x 15cm), utilizing a series-connected transmitter (Tx) coil to generate an equally distributed electromagnetic field inside the space. This field can be picked up by a solenoid receiver (Rx) coil placed anywhere within the space to power a DC load. To develop the proposed system, we have studied a conventional wireless power transfer system from Wurth Electronics and investigated various coil geometries for both Tx and Rx.

The conventional wireless power system has been examined regarding the influence of coil geometry, alignment between the transmitter (Tx) and receiver (Rx), as well as the coil parameters on efficiency. The wireless power system from Wurth Electronics is tested with different Rx coil geometries to evaluate interoperability between various Tx and Rx coil geometries, as well as to compare the coupling coefficient and magnetic field density of different Rx coil geometries with misalignment in order to evaluate most suitable Rx coil geometry for the proposed wireless power system. The different Rx coil geometries investigated are: concentric, solenoid, and center-tapped circular coil. The comparison is based on different alignment conditions between the transmitter and receiver coils. We find, from the results obtained by investigating different Rx coil geometries with the conventional system, that the solenoid coil geometry with a core provides a stable coupling coefficient under various misalignment conditions. Thus, the solenoid Rx geometry can be optimized to enhance coupling between the transmitter and receiver coils. Additionally, test results show that the use of center-tapped circular coils in wireless power power system helps in improving range from 30mm to 180mm compared to conventional wireless power system with concentric coils. However, the improved range is only achievable with significantly higher number of coil turns compared to concentric coils which reduces efficiency. Also, a unique BJT based automatically switching transmitter circuit is required for the center-tapped circular coils which makes it a non-viable solution due to inefficiency of the BJTs.

Further a suitable transmitter coil geometry is investigated for use in combination

with the solenoid receiver to demonstrate the proposed wireless power system within a space of dimensions (15 cm x 15 cm x 15 cm). Three different transmitter coils are investigated: the concentric coil, 2-series connected concentric coil, and 8-series connected concentric coil. A half-bridge transmitter circuit is designed to drive the various transmitter coils. The experimental and simulation results indicate that the concentric transmitter coil with a large diameter enhances high power transfer and better range due to a more effective distribution of the magnetic field.

However, when using a solenoid receiver coil, the power transfer efficiency drops by 28% compared to the efficiency of 75% under aligned operation. Consequently, the concentric transmitter coil is designed with the coil turns distributed into smaller areas, forming a 2-series connected coil. Test results reveal that it was possible to transfer 10W of power at an efficiency of 75% when the coils were perfectly aligned. In contrast, when the coils were misaligned, power transfer efficiency of up to 48% was achieved. This is in contrast to the power transfer efficiency of 6% under misaligned conditions in the conventional wireless power system.

The 2-series connected concentric Tx coil is then extended to an 8-series connected concentric Tx coil to form a space of dimensions (15 cm x 15 cm x 15 cm) in combination with a solenoid Rx coil. Simulation results indicate that the coupling coefficient between Tx & Rx improved by approximately 11% and measurement results show that power transfer efficiency improved by 4% compared to the 2-series connected concentric Tx coil. Similarly, when the solenoid Rx coil was rotated or misaligned with the Tx coil, the efficiency improved by approximately 33% compared to the 2-series connected concentric Tx coil. The increase in efficiency and coupling with Tx and Rx is mainly due to distribution of coil turns into smaller areas and then connecting them in series which improved the magnetic field distribution compared to other coil geometries. Hence, the 8-series connected concentric coil as Tx and solenoid as Rx are selected as the suitable Tx and Rx coils, respectively, for the proposed wireless power system. In comparison to the conventional wireless power system, the efficiency remains approximately the same at 80% when the coils were perfectly aligned and efficiency improved by more than 60% when the coils were misaligned.

Keywords: Wireless power transfer, coil geometry, coil parameter, alignment, coupling coefficient, series connected concentric coil.

Acknowledgements

We extend our heartfelt gratitude to our supervisor and examiner, Prof. Torbjörn Thiringer, for your support, guidance, and expertise. This project was conducted at Chalmers and in Ericsson facilities under the supervision of researcher Fredrik Larsson. We sincerely thank Fredrik for the tremendous support and trust extended throughout the project, as well as for the invaluable opportunity to work at Ericsson Labs. We are equally grateful to our colleagues at Ericsson for their continuous help and support.

Our appreciation extends to Wurth Electronics and Infineon for their support in providing coil samples and a half-bridge evaluation board. The simulations undertaken would not have been possible without the support of Ansys.

We also take this moment to express our gratitude to all who contributed to this project and enriched our learning experience during this time. Finally, we extend our heartfelt thanks to our family and friends for their unwavering interest in our work and their continuous, unconditional love and support.

Adarsh Bandi
Nagendra Gouthamas
Gothenburg, Sweden 2024.

List of Acronyms

Below is the list of acronyms that have been used throughout this thesis:

WPT	Wireless power transfer
WE	Wurth electronik
Tx	Transmitter
Rx	Receiver
EMF	Electromotive force
MOSFET	Metal oxide semiconductor field effect transistor
BJT	Bi-polar juntion transistor
SS	Series-series
SP	Series-parallel
PS	Parallel-series
PP	Parallel-parallel
NFT	Near field technology
FFT	Far field technology
VMA	Vertical misalignment
LMA	Lateral misalignment
AMA	Angular misalignment
DC	Direct current
AC	Alternating current
FEM	Finite element method
LED	Light emitting diode
$\mathbf{f}_r$	Resonant frequency
BW	Bandwidth
PWM	Pulse width modulation
GaN	Gallium Nitride
IC	Integrated circuit
mm	millimetre
cm	Centimetre
3D	Three dimension
NA	Not applicable
SWG	Standard wire gauge
PCB	Printed circuit board
VR	Vertical Rotation
HR	Horizontal Rotation

Contents

1
Introduction

1.1 Background

The Wireless power transfer(WPT) is the transfer of electrical energy from a power source to a distant electrical load without using discrete conductors. The wireless power system was first demonstrated in the 1890's by Nikola Tesla who laid down the basic principles for the wireless power technology[1]. Tesla's idea of wireless power transfer using high frequency magnetic coupling at resonance was groundbreaking and was ahead of his time. However, due to fewer applications of the wireless power technology and an underdeveloped power electronics sector became a restriction and set limitations in implementing the wireless power technology[3].

The wireless power system is the transfer of electrical energy based on the fundamentals of time-varying electric, magnetic, or electromagnetic fields. Today the wireless power technology can be classified into two major categories; near field wireless power technology and far field wireless power technology. The wireless power technology based on the resonant inductive coupling is the most popular and has been used for mid and high power applications across different industries. The resonant inductive coupling outperforms the other WPT techniques in terms of power transfer efficiency and capability, ease of control, and safety. Therefore, the WPT finds its application in electric vehicle charging solutions and changing of portable electronics.

The conventional wireless power technologies based on the resonant inductive coupling for charging the portable electronic devices and the electric vehicles use identical coil geometries on the transmitter and the receiver side. In such wireless power systems, it is required to align the receiver coil with the transmitter coil perfectly in order to achieve better power transfer efficiency and capability. The low degree of freedom on the receiver side is inconvenient and does not make the system true wireless since the receiver is bound to be placed at a certain location in the vicinity of the transmitter. The other major challenges in the wireless power are the efficiency and range. The efficiency drop in wireless power is due to a number of reasons, like range, flux leakage, losses in the power converter, and coupling. The main challenge in achieving a greater range between the transmitter and the receiver is due to the limited ability of the transmitter to distribute its magnetic fields over a long distance.

A method to improve the coupling between the transmitter and the receiver coil is to utilize multiple coils on the transmitter to generate equally distributed electromagnetic field which will enable power delivery to the receiver contained anywhere in the vicinity of the transmitter. The equally distributed magnetic field will improve the coupling between the transmitter and the receiver in all alignment conditions and thereby improving the overall efficiency of the wireless power system.

In this thesis, the main objective of the thesis is to implement the wireless power transfer in a room of dimension (3m X 3m X 2.5m), however the idea is demonstrated in a test space of (15cm X 15cm X 15cm) which can be extended to a bigger test space. We study a conventional wireless power system from Wurth Electronics to understand the working and challenges in the wireless power system. The conventional wireless power system is then utilized to investigate suitable Rx coil geometry. Further, a half-bridge Tx converter is designed to investigate suitable Tx coil geometry. All the different coil geometries investigated are tested under aligned and misaligned condition. From the investigation of different coil geometries for Tx and Rx, a suitable Tx coil and a receiver coil are selected to demonstrate the equal distribution of electromagnetic field in an enclosed space which will enable better coupling with the receiver and improve the efficiency of power transfer.

1.2 Objective

The objective of the thesis is to determine the feasibility of using a wireless power system to supply power to a DC electrical load in a space with dimensions of (15cm x 15cm x 15cm) by generating an electromagnetic field in the space. In order to achieve this objective, different coil geometries will be tested to investigate suitable transmitter and receiver coil geometries. Power transfer of up to 10W will be demonstrated in the given space. A half-bridge transmitter circuit will be developed to reduce losses in the power electronics that will drive the transmitter coils to generate an electromagnetic field in the given space. Additionally, the thesis will focus on improving the coupling factor between the transmitter and the receiver coil and the efficiency of power transfer.

In summary, the thesis will address the following research questions:

- What is the best coil geometry for the transmitter and receiver to construct the proposed wireless power transfer setup?
- Is the center-tapped circular coil geometry suitable for wireless power transfer?
- Is it beneficial to distribute Tx coil turns into smaller areas to improve coupling with Rx?

2

Theory

2.1 Wireless power transfer

Wireless power transfer (WPT) is the transfer of electrical power from a power source to a load without wires and is based on technologies using time-varying electric, magnetic, or electromagnetic fields. The wireless power transfer works based on the principle of electromagnetic induction. Faraday's laws of electromagnetic induction explains the relationship between the electric field and the magnetic field. This law is the basic working principle of most of the electrical motors, generators, transformers, inductors, etc. Faraday's law of electromagnetic induction states that, "Whenever a conductor is placed in a varying magnetic field, an electromotive force is induced". The induced voltage(EMF) is proportional to the rate of change of magnetic flux with the time and can be expressed as

$$\varepsilon = -N\frac{\Delta\phi}{\Delta t} \tag{2.1}$$

where ε is the induced voltage, N is the number of turns, $\Delta\phi$ is the change in magnetic flux, and Δt is the change in time.

Faraday's first law: Whenever a conductor is placed in a varying magnetic field an EMF gets induced across the conductor (called as induced emf), and if the conductor is a closed circuit then induced current flows through it.

Faraday's second law: Faraday's second law of electromagnetic induction states that, "the magnitude of induced emf is equal to the rate of change of flux linkages with the coil". The flux linkages is the product of number of turns and the flux associated with the coil.

The minus sign in Faraday's law of induction is very important. The minus means that the emf creates a current (I) and magnetic field (B) that oppose the change in flux ($\Delta\phi$) which is known as Lenz's law. Lenz's law states that, "an induced electric current flows in a direction such that the current opposes the change that induced it". Thus, Faraday's law of electromagnetic induction and Ampere's circuit law is used to mathematically describe power transfer using resonant inductive coupling.

2.1.1 Maxwell's equations

The time varying magnetic field in the inductive power transfer plays an important role. In time varying fields, the electric field(E) and the magnetic field(H) are closely related and mutually coupled. The electric field and magnetic field together form an electromagnetic wave. Maxwell's equations provide a unified mathematical relationship between the electrical and the magnetic fields. Maxwell's equations in integral form can be expressed as[1],

$$\oiint_{\partial v} D.da = Q_v \tag{2.2}$$

$$\oiint_{\partial v} B.da = 0 \tag{2.3}$$

$$\oint_{\partial A} E.ds = -\iint_{A} \frac{\partial B}{\partial t}.da \tag{2.4}$$

$$\oint_{\partial A} H.ds = \iint_{A} (J + \frac{\partial D}{\partial t}).da \tag{2.5}$$

where, E is electrical field intensity vector in (V/m), D is electrical flux density vector in (As/m^2), H is magnetic field intensity vector in (A/m), B is magnetic flux density vector in (Wb/m^2), and J is current density in (A/m^2).

Maxwell's equation expressed in (2.2) is also called as Gauss's law which describes that the electrical flux density(D) in an enclosed area(da) will have the same total charge(Q_v) which is withing the enclosed area. Gauss's law for magnetism is expressed in (2.3) and it describes that the enclosed area(da) has the same amount of magnetic flux lines(B) coming in and going out forming a closed loop and hence no magnetic charge is built up at any point in space. In general, the net magnetic flux out of any closed surface is zero.

Faraday's law of magnetic induction is expressed in (2.4) and describes that the time changing magnetic field(B) generates an electrical field(E) or it can be described as the line integral of the electric field around a closed loop is equal to the negative of the rate of change of the magnetic flux through the area enclosed by the loop. Eq(2.5) is also called Ampere's law which describes that the magnetic field intensity(H) integrated along a closed area is equal to the current flowing through the surface enclosed by the area.

2.1.2 Magnetic flux density and induced voltage

The electric field is produced by the static charges while the magnetic field is produced by the moving electric charges. The generation of the magnetic field around a current carrying conductor can be explained by Ampere's law. The direction of the magnetic field around a conductor can be identified using the

right hand rule. If the thumb is pointed towards the direction of the current then the fingers curl in the direction of the magnetic field. The magnetic field produced by a current carrying circular coil is shown in figure 2.1.

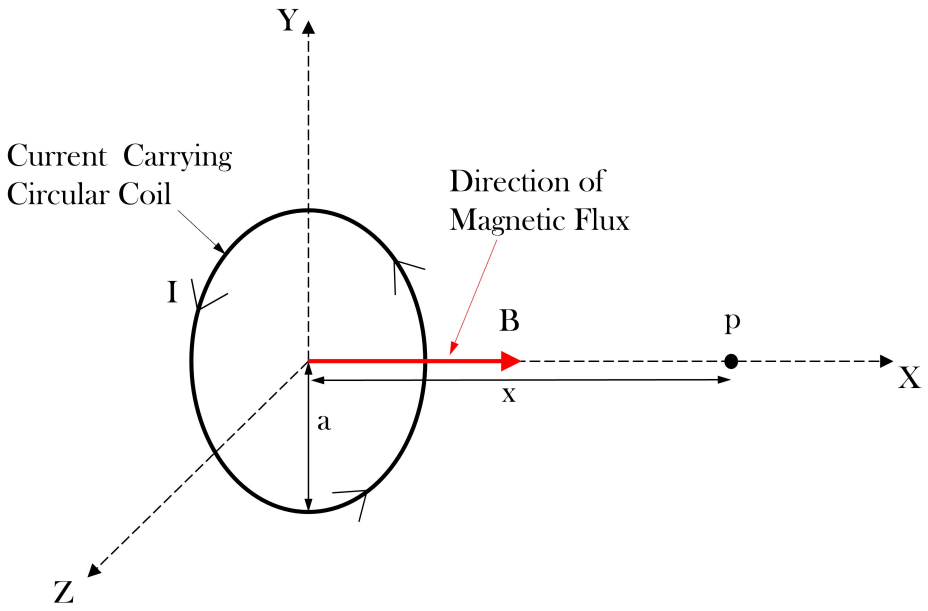

Figure 2.1: Magnetic flux generated by a current carrying circular coil

The magnetic field produced by the current carrying conductor can be described using Biot-Savart law. The magnetic field at any point in space produced by a current carrying conductor can be calculated using Biot-Savart equation,

$$B = -\frac{\mu}{4\Pi}\oint_{l}\frac{Idl\hat{r}}{r^2} \tag{2.6}$$

where I is the current flowing in the circuilar coil, dl is current element, r is referred to the displacement vector from the current element to a point where the magnetic field is calculated, $\hat{r}$ is the unit vector of r, μ is the permeability, and a is the radius of the circular coil.

Biot-Savart law states that a segement of the current carrying conductor produces a magnetic field and this segment is called the current element which is a vector quantity. From (2.6) it is also evident that the magnetic field(db) is proportional to the current flowing in the coil segment(dl). Biot-Savart equation can also be used to calculate the magnetic field at any point p on the axis of the circular coil of radius a and current I at a distance of x as shown in figure 2.1 which can be expressed as

$$B = \frac{2\Pi\mu NIa^2}{4\Pi(x^2+a^2)^{\frac{3}{2}}} \tag{2.7}$$

where N is the number of turns, I is the current in each turn, and x is the distance

from the center of the coil to the point p where the magnetic field B is calculated.

The magnetic flux density at the center of the coil can be expressed using (2.7) by substituting x=0 and we get,

$$B = \frac{\mu_0 NI}{2a} \tag{2.8}$$

In conclusion, the relationship between the magnetic field db generated by the current element dl with current I can be expressed as

$$dB \propto \frac{Idl \sin\theta}{r^2} \tag{2.9}$$

where θ is the angle between the displacement vector r and direction of current in the current element dl.

Faraday's law of electromagnetic induction states that the changing magnetic field produces an electric field E. Consider another circular coil is introduced in figure 2.1 as shown in figure 2.2.

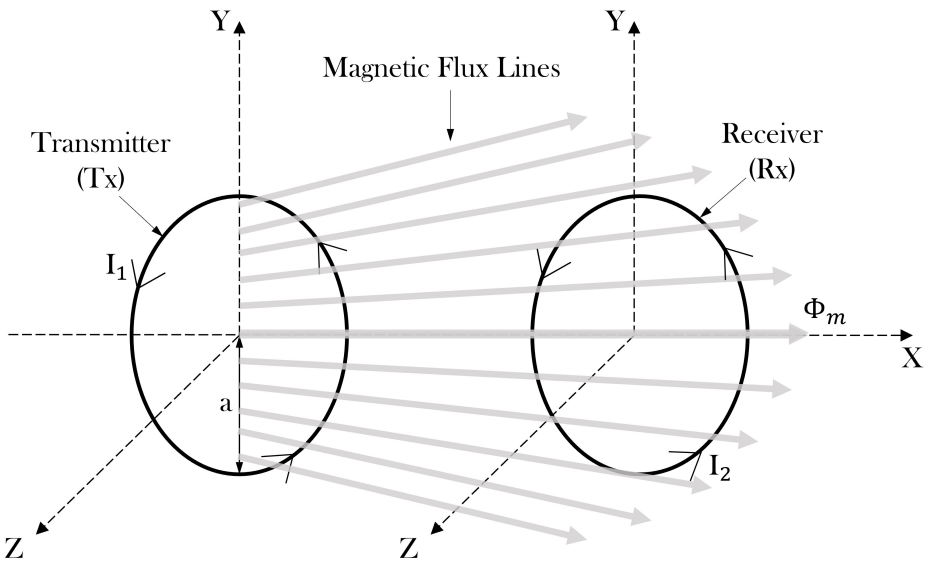

Figure 2.2: Magnetic flux between two circular coils

In figure 2.2, current I_1 flows in the Tx coil and generates a magnetic flux. According to the law of electromagnetic induction, the generated flux linking with the Rx coil induces voltage in it. The Tx and the Rx coil are separated by an air gap and hence only a part of the magnetic flux generated by the Tx links with the Rx coil which is referred to as Φ_m. The total magnetic flux linked with the Rx coil can be expressed as

$$\Phi_m = \int_a Bda \tag{2.10}$$

where B is the total magnetic flux density generated by the Tx coil and a is the total surface area of the Rx coil. The induced voltage in the Rx coil can be expressed as

$$E(t) = -\frac{d\Phi_m}{dt} \tag{2.11}$$

If the Rx coil consists of N turns and Φ_m is the flux through one turn, an emf is produced in all the turns and can be expressed as

$$E(t) = -N\frac{d\Phi_m}{dt} \tag{2.12}$$

In conclusion, the induced voltage depends on the following factors:

- Increasing the number of turns on the receiver coil induces higher voltage as the area of the conductor linking with the flux lines increases[6].
- Increasing the strength of the magnetic field generated by the Tx coil induces more voltage in the Rx coil.
- Increasing the radius of the coil induces higher voltage because area is directly proportional to the induced voltage[6].
- The induced voltage can be improved by using stranded wires for operation at high frequency to reduce AC resistance thereby reducing the voltage drop in the coil.

2.1.3 Types of wireless power transfer systems

There are different technologies for transmitting the electrical energy by means of electro-magnetic waves. The wireless power system can be divided based on the electromagnetic principle used as shown in figure 2.3.

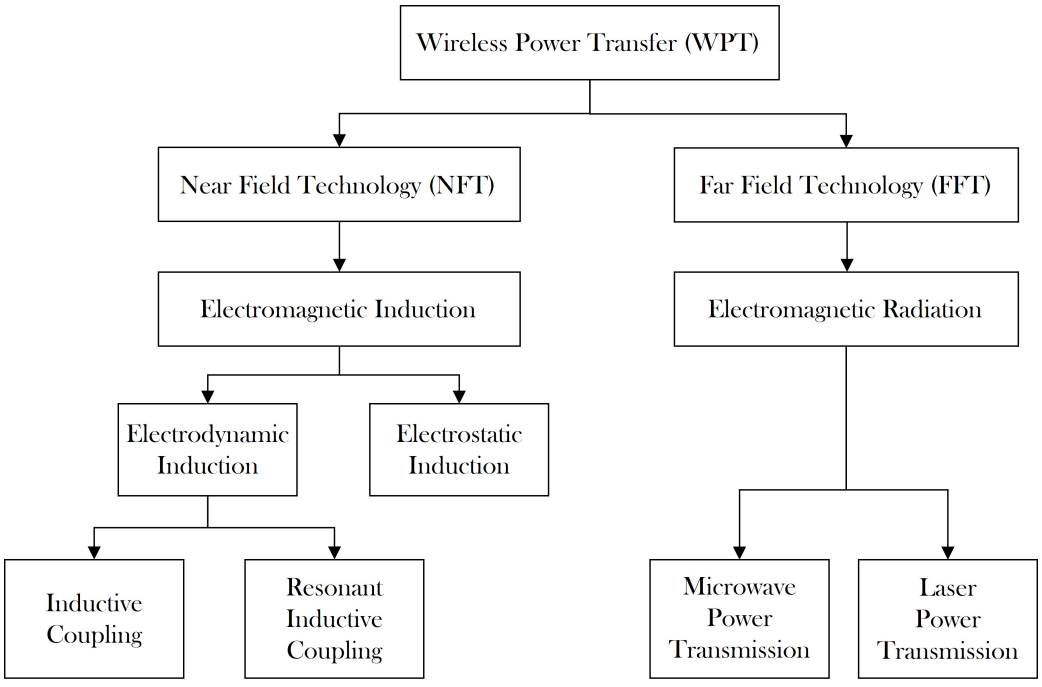

Figure 2.3: Different types of wireless power systems

The wireless power technology is mainly classified based on the distance of power transmission, maximum power, and method used to achieve the wireless power transfer. The first classification is based on how far the electrical power can be transferred from the source to the load without any physical contact. There are methods capable of transferring power to loads at large distance away from the source while the other methods could only transfer power to the load at a distance of few centimeters from the source. Hence, the first division is based on whether the power transfer is of near field or far field.

2.1.3.1 Near field technology(NFT)

The near field power transfer is a non-radiative power transfer technology where the phenomenon used is the electromagnetic induction. The near field technology is subdivided as

- Electromagnetic induction
- Electromagnetic resonance
- Electrostatic induction

In electromagnetic induction, the power transfer takes place through mutual coupling with the coils tightly coupled. The WPT with the electromagnetic induction works up to a distance of 1/6 of the wavelength of the transmission frequency[1]. The WPT using electromagnetic resonance has largely extended the potential of NFT. In this method, a capacitor is either connected in series or in parallel combination to the coils to form a resonant LC tank. The transmitter and the receiver are made to resonate at the same frequency, maximizing the power transfer to the load. The electrostatic induction is a method where the electric field acts as the energy carrier medium. The electrostatic induction is also called as capacitive coupling since the power is transferred between two electrodes that forms a capacitance[1].

2.1.3.2 Far field technology(FFT)

The far field power transfer is a radiative power transfer technology where the phenomenon used is the electromagnetic radiation and the power can be delivered to a load far away from the source. The electromagnetic radiation can be concentrated to a focal point enabling wireless power transfer over longer distance. The two most popular methods of far field technology are

- Micro wave power transmission
- Laser power transmission

The microwave power transfer involves conversion of electrical power into microwaves and transfer of the microwaves using an antenna. The transferred microwaves are then converted into electrical power at the receiver. The wireless power technology using laser radiation is the transfer of photonic energy using a laser in a form either as heat or electricity. The method used in the WPT using laser radiation is same as the method used in the production of solar energy.

2.1.4 Resonant inductive coupling

The basic building block of the wireless power system using the resonant inductive coupling is the resonant circuit. A simple resonant circuit with an AC source, transmitter coil, receiver coil, capacitor C1 and C2 connected in parallel to the Tx and the Rx coil respectively, and a load R is shown in figure 2.4.

The resonant inductive coupling is the transfer of electrical energy between two coils that are tuned to resonant at the same frequency while the coils are coupled together by a magnetic field. In the resonant inductive coupling, the energy in the resonant circuit oscillates between electric energy stored in the capacitor and magnetic energy stored in the inductor. The transmitter and the receiver coil are connected with a capacitor either in series or in parallel combination to compensate for the inductive reactance of the transmitter coil and the receiver coil. The compensation of the inductive reactance in both the transmitter and the receiver circuit forms the basic operating principle for the WPT using the resonant inductive coupling and enables resonance in both the Tx and the Rx circuit.

The coils in the resonant inductive coupling can be loosely coupled and can transfer power over a range of few times the coil diameters with high Q-factor of the coils to maintain good efficiency. The WPT using the resonant inductive coupling improves the efficiency of the power transfer drastically and improves the power transfer range when compared to the WPT using non-resonant inductive coupling.

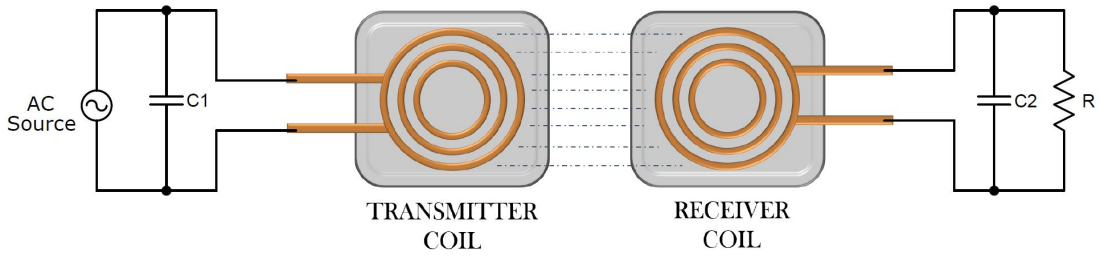

Figure 2.4: Wireless power system using resonant inductive coupling

2.2 Resonant circuits

A simple resonating circuit consists of a resistor R, an inductor L and a capacitor C, connected either in series or in parallel to an AC source with variable frequency. The circuit is said to be at resonance when the frequecy of the power supply exactly matches the natural frequency of the circuit's LC combination. The resonant circuits are used in the power supply circuits to obtain high frequency output voltage or current, low switching loss, and low switching noise. The resonant circuits can be mainly classified based on circuit topology as shown in figure 2.5.

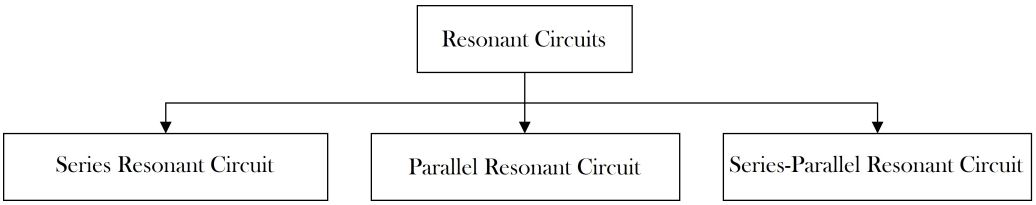

Figure 2.5: Types of resonant circuits

In the series resonant circuit, the inductor and the capacitor are connected in series with the AC source where the inductive and capacitive reactances are equal in magnitude ($X_L = X_C$) and cancel each other as they are 180° apart in phase. When the circuit is at resonance, it acts as a purely resistive circuit due to low or zero impedance of the circuit and the value of the impedance therefore becomes $Z = R$. The series resonant circuit is also called as an acceptor circuit because the current flowing in the circuit is at its highest possible point and is in phase with the applied voltage. Unlike series resonant circuit, the parallel resonant circuit offers maximum impedance at resonance and limits the circuit current. The parallel resonant circuit is also called as the rejecter circuit because it suppresses the circuit current whose frequency is equal to the resonant value.

The series and parallel resonant circuits with very low resistance will have significant affect on the impedance at resonance and the resonant condition can be easily calculated using the expression,

$$f_r = \frac{1}{2\Pi\sqrt{LC}} \tag{2.13}$$

However, when a significant value of resistance is added to an LC circuit, (2.13) becomes invalid. The resistor can be added in a number of combination to the series or parallel resonant circuit. The series-parallel resonant circuit can be mainly classified as,

- Series LC circuit with R in parallel
- Parallel LC circuit with R in series

The added resistance in the LC circuit lead to an anti-resonance condition. At anti-resonance, the affects of peak or low impedance occurs at frequencies other than the frequency that gives equal inductive and capacitive reactances.

2.2.1 Parallel resonant circuit

In the parallel resonant circuit, the RLC components are connected in parallel to the AC source and parallel resonance occurs when the supply frequency produces zero phase difference between the supply voltage and the current. Figure 2.6 shows the parallel resonant RLC circuit with a current source and figure 2.7 shows the phasor diagram for the parallel resonance.

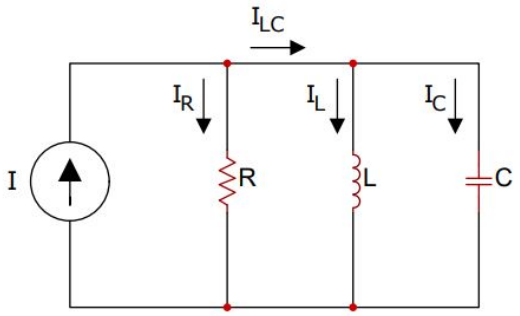

Figure 2.6: Parallel resonant circuit

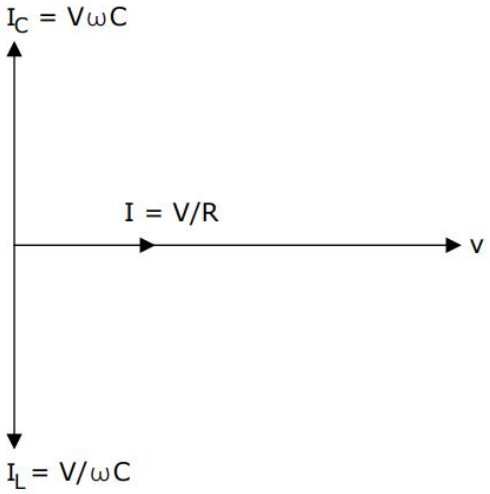

Figure 2.7: Phasor diagram

The parallel resonant circuit is similar to the series resonant circuit as the reactive components in both the circuits are influenced by the supply frequency. However, the parallel resonant circuit is influenced by the current flowing in each branch of the parallel LC tank. At resonant frequency, the impedance of the parallel resonant circuit is maximised as the circuit acts like an open circuit with the total current being determined only by resistor R. Thus at resonance, the impedance of the parallel circuit is maximum and is equal to the resistance of the circuit. Keeping L and C constant, the amount of current flowing in the circuit can be controlled by varying the value of resistance R. The total impedance in the parallel resonant circuit can be expressed as

$$Z_{total} = R \,\|\, Z_L \,\|\, Z_C = \frac{R}{1 - jR(\frac{1}{X_C} + \frac{1}{X_L})} = \frac{R}{1 + jR(\omega C - \frac{1}{\omega L})} \tag{2.14}$$

If the resonance occurs at ω_r and $X_L = X_C$ then the imaginary part of Z_{total} becomes zero and hence the resonant frequency can be expressed as

$$\begin{aligned} \omega_r C &= \frac{1}{\omega_r L} \\ \omega_r &= \frac{1}{\sqrt{LC}} \\ f_r &= \frac{1}{2\Pi\sqrt{LC}} \end{aligned} \tag{2.15}$$

The parallel resonant circuit and series resonant circuit produces the same equation for the resonant frequency as expressed in (2.15). Hence, it makes no difference to the resonance if the inductor or the capacitor is connected in series or in parallel.

2.2.1.1 Frequency response of parallel resonant circuit

The frequency response of the parallel resonant circuit with change in the impedance of the circuit is shown in figure 2.8. As the frequency of the applied voltage is increased beyond the resonant value f_r of the circuit, the inductive reactance increases and the capacitive reactance decreases. As a result of this, the current in the inductive branch decreases and the current in the capacitive branch increases. Since the inductive and the capacitive reactance are not equal beyond the resonant value, the total current in the circuit increases and leads the voltage applied. Similarly, when the frequency of the applied voltage is less than the resonant value, the total impedance of the circuit decreases and the total current increases which is lagging the applied voltage. The parallel resonant circuit offers maximum impedance at the resonant frequency, and offers less impedance to other frequencies. Hence, the impedance of the circuit at resonance is called dynamic impedance (Z_d). The maximum dynamic impedance of the parallel resonant circuit is given by

$$Z_d = \frac{L}{RC} \tag{2.16}$$

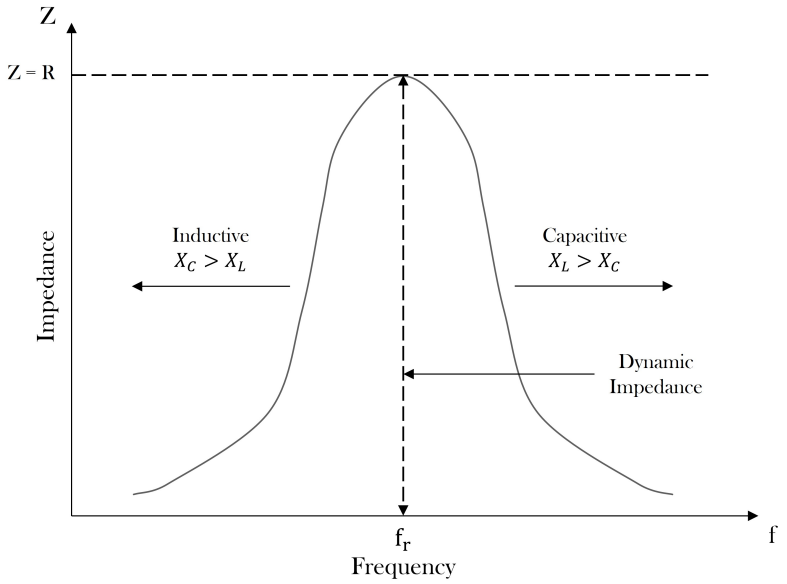

Figure 2.8: Plot of impedance vs frequency in parallel resonant circuit

Figure 2.9 shows the circuit current as a function of frequency. The plot shows that if the frequency of the applied voltage is varied from the low value to the maximum value through the resonant frequency, the current magnitude decreases from its maximum value at low frequency to a minimum value at the resonant frequency. The total current is minimum when the circuit is at resonance as the total impedance of the circuit is at its maximum value *(Z=R)*. The impedance reduces as the frequency is varied on either side of the resonant value. The parallel resonant circuit is also called as a rejecter circuit because it rejects or suppresses the current whose frequency is equal to the resonant value.

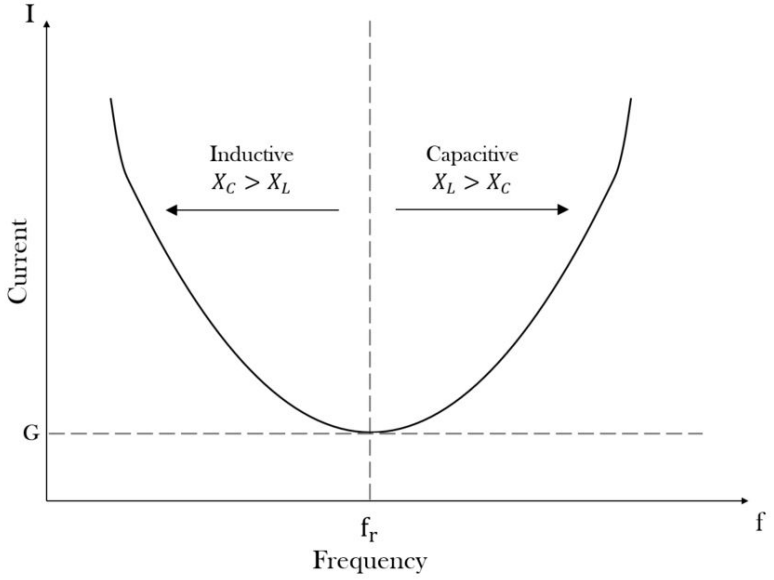

Figure 2.9: Plot of current vs frequency in parallel resonant circuit

2.2.1.2 Q-factor and bandwidth

The quality factor or Q-factor is a dimensionless quantity and is used to define how well the system can oscillate or gives a measure for the quality of a resonant circuit. A high Q-factor corresponds to the oscillations going further and a low Q-factor corresponds to the oscillations that attenuate faster. The Q-factor of the parallel resonant circuit with the resonant frequency f_r can be expressed as

$$\begin{aligned} Q &= 2\pi \frac{Maximum\,energy\,stored}{Energy\,dissipated\,for\,a\,period} \\ Q &= 2\Pi \frac{\frac{1}{2}CV^2}{\frac{1}{2}\frac{V^2}{R}T} \\ Q &= 2\Pi f_r CR \end{aligned} \tag{2.17}$$

At resonant condition,

$$\begin{aligned} 2\Pi f_r C &= \frac{1}{2\Pi f_r L} \\ Q &= \frac{R}{2\Pi f_r L} \end{aligned} \tag{2.18}$$

From (2.18) it can be implied that the circuit with a high Q-factor can store more energy compared to the energy dissipated. The reponse of the parallel resonant circuit is shown in figure 2.10. A high Q-factor is due to low resistance in series with the inductor which produces a high peak with a narrow response curve. While a low Q-factor is due to high resistance in series with inductor that produces a lower peak with a wide response curve.

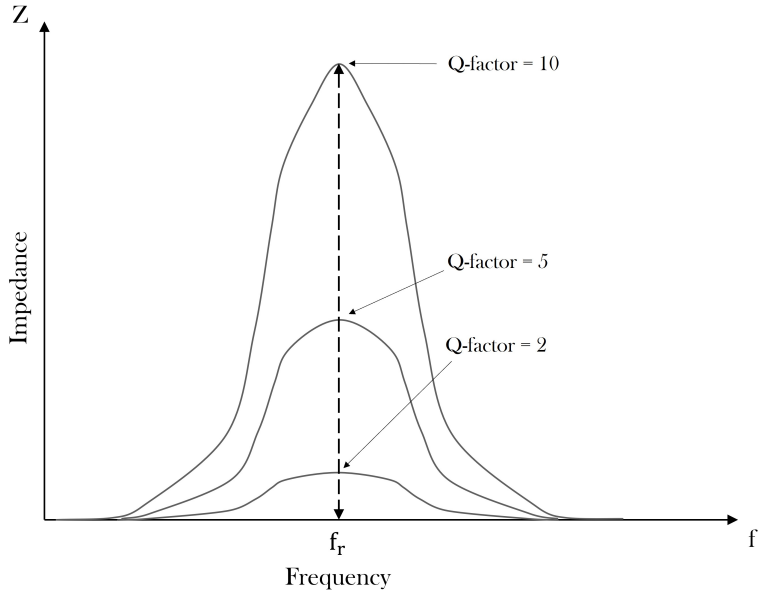

Figure 2.10: Response of parallel resonant circuit with change in Q-factor

The impedance curve is used to define the bandwidth of the parallel resonant circuit. The bandwidth of the parallel resonant circuit is shown in figure 2.11. The bandwidth of the resonant circuit is measured between the half-power frequencies where the power dissipated in the circuit is half of the power dissipated at the resonant frequency. The upper and lower cutoff frequencies are denoted as f_H and f_L respectively. The 100% impedance point is when Z=R where the power dissipated is I^2R and at 0.707*Z the power dissipated is 0.5*I^2R. The bandwidth of the circuit can be expressed as

$$BW = f_H - f_L = \Delta f \tag{2.19}$$

The Q-factor of the parallel resonant circuit can also be defined as ratio between the resonant frequency and the bandwidth which implies that a high Q-factor has a narrow bandwidth. Also, the bandwidth and the frequency response for a system with fixed resonant frequency can be altered by changing the ratio between the inductor and the capacitor or by changing the value of resistance R.

$$Q = \frac{f_r}{BW} \tag{2.20}$$

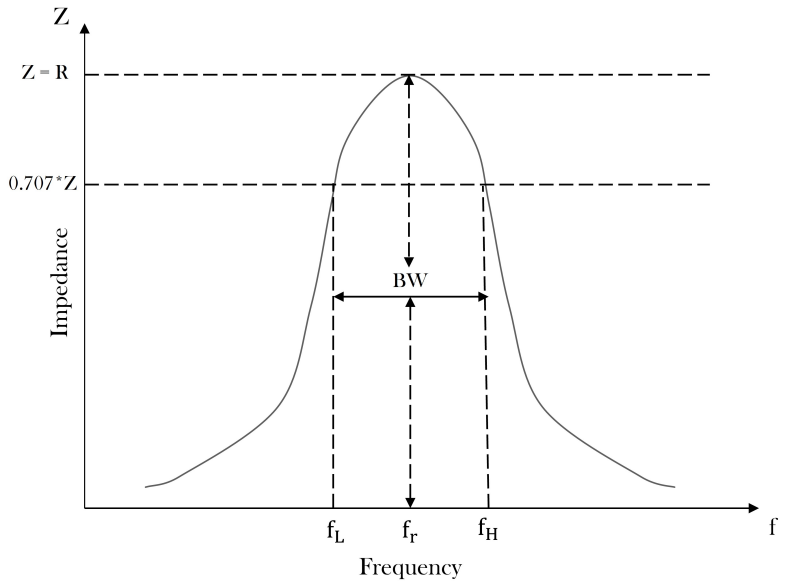

Figure 2.11: Bandwidth of parallel resonant circuit

2.3 Analytical model of WPT

The transmitter and receiver coils together form a transformer. Therefore, the equivalent circuit of transformer can be used to analyse the wireless power transfer circuit. The circuit diagram of inductive power transfer is shown in figure 2.12.

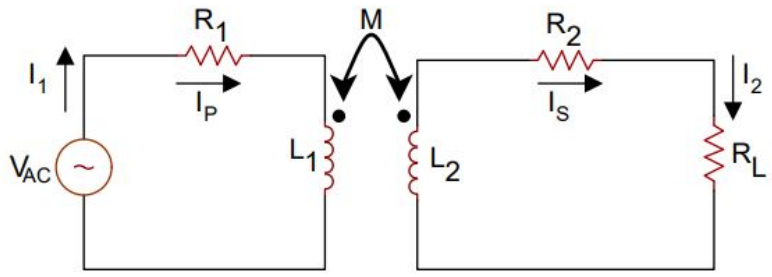

Figure 2.12: Circuit diagram of inductive power transfer

In this model, there is no core and the air gap between the Tx and Rx coil is large which results in increased leakage inductance. The equivalent model of inductive power transfer considering leakage inductance is shown in figure 2.13.

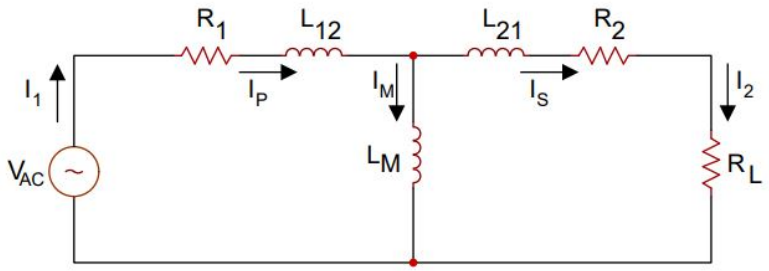

Figure 2.13: Equivalent circuit diagram of inductive power transfer

From figure 2.13

$$V_{AC} = V_1 = (R_1 + j\omega L_{12} + j\omega L_M) I_P + j\omega L_M I_S \tag{2.21}$$

$$0 = (R_L + R_2 + j\omega L_{21} + j\omega L_M) I_S + j\omega L_M I_P \tag{2.22}$$

Input impedance of the network as seen by the source is expressed as

$$Z_{in} = \frac{V_1}{I_P} = \frac{(R_1 + j\omega L_{12} + j\omega L_M) I_P + j\omega L_M I_S}{I_P} \tag{2.23}$$

From 2.22

$$I_S = \frac{-j\omega L_M I_P}{R_L + R_2 + j\omega L_{21} + j\omega L_M} \tag{2.24}$$

Substituting 2.24 in 2.23, we get

$$Z_{in} = \frac{(R_1 + j\omega L_{12} + j\omega L_M)(R_L + R_2 + j\omega L_{21} + j\omega L_M) + \omega^2 M^2}{R_L + R_2 + j\omega L_b + j\omega L_M} \tag{2.25}$$

The efficiency of power transfer from source V_1 to load R_L can be expressed as

$$\eta = \frac{R_L |I_2|^2}{R_L |I_2|^2 + R_2 |I_S|^2 + R_1 |I_P|^2} \tag{2.26}$$

$$\eta = \frac{R_L}{R_L + R_2 + R_1 \left[\frac{|I_P|}{|I_2|}\right]^2} \tag{2.27}$$

From 2.22

$$\frac{I_P}{I_2} = \frac{R_L + R_2 + j\omega L_{21} + j\omega L_M}{-j\omega L_M}$$

$$\left[\frac{|I_P|}{|I_2|}\right]^2 = \left[\frac{R_L + R_2}{\omega L_M}\right]^2 + \left[\frac{L_{21} + L_M}{L_M}\right]^2 \tag{2.28}$$

substituting 2.28 in 2.27, we get

$$\eta = \frac{R_L}{(R_L + R_2)\left[1 + \frac{R_1(R_2+R_L)}{\omega^2 L_M^2}\right] + R_1 \left[\frac{L_{21}+L_M}{L_M}\right]^2} \tag{2.29}$$

From 2.29, the condition for maximum efficiency can be derived. Therefore, maximum efficiency is achieved when 2.30 is fulfilled. The condition for 2.30 is satisfied when $\frac{R_1(R_2+R_L)}{\omega^2 L_M^2}$ tends to zero.

$$\omega \gg \frac{\sqrt{R_1 (R_2 + R_L)}}{L_M} \tag{2.30}$$

Hence, the maximum theoretical efficiency for power transfer is given by

$$\eta_{max} = \frac{R_L}{R_L + R_2 + R_1 \left[\frac{L_{21}+L_M}{L_M}\right]^2} \tag{2.31}$$

2.4 Compensation of leakage inductance

In a transformer model, the flux generated by the primary circuit links with the secondary circuit, but not all the flux generated is mutual flux. There are magnetic field lines which do not follow the magnetic circuit resulting in leakage flux. The distance between the Tx and the Rx coils in the wireless power system affects the coupling of the system and generates leakage inductance. The leakage inductance increases the reactive power and reduces the efficiency of the system. Hence, there is a requirement for compensation of the reactive power using capacitors on both the transmitter and the receiver side to ensure that the system operates at a power factor close to unity.

2.4.1 Compensation topologies

The capacitive compensation is formed by two capacitances, C_1 at the transmitter side and C_2 at the reciever side. Depending on the capacitor connection, there are four basic compensation topologies available,

- Series - Series(SS) compensation
- Series - Parallel(SP) compensation
- Parallel - Series(PS) compensation
- Parallel - Parallel(PP) compensation

The four different compensation topologies are represented as shown in figure 2.14. The selection of the topologies is made according to the application since each topology behaves differently for variation in the parameters.

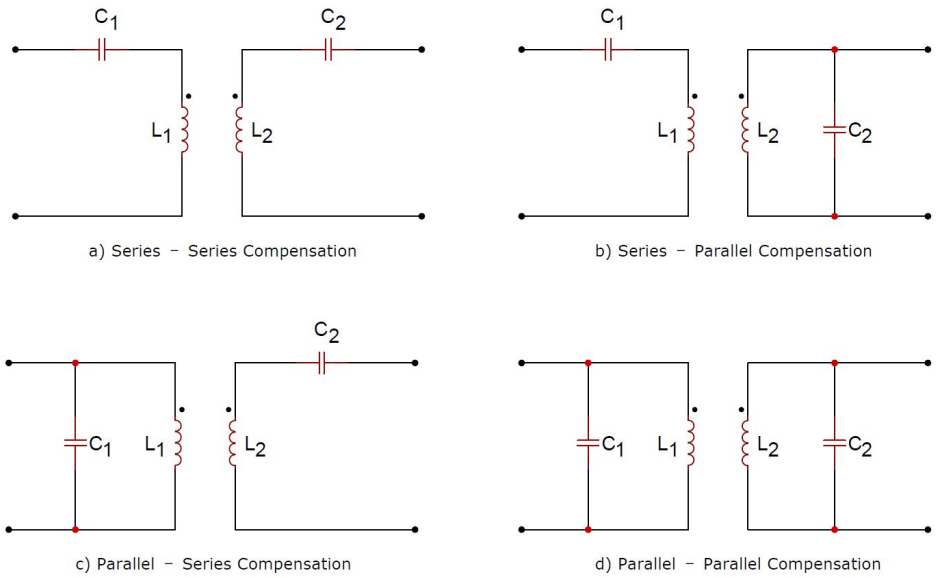

Figure 2.14: Capacitive compensation topologies

The secondary compensation capacitance C_2 is chosen such that it compensates the secondary leakage inductance and the mutual inductance. The secondary compensation capacitor C_2 is independent of type of topology and it is expressed as sum of the secondary leakage inductance and the mutual inductance as

$$\begin{aligned} X_{C2} &= X_{L21} + X_M \\ C_2 &= \frac{1}{(2\Pi f_r)^2(L_{21} + L_M)} \\ C_2 &= \frac{1}{\omega_r^2(L_{21} + L_M)} \end{aligned} \tag{2.32}$$

The expression for the primary compensation capacitor C_1 is dependent on the type of topology and it differs for each topology. The capacitor C_1 is chosen such that the total impedance seen by the supply is purely resistive. This will ensure that the high frequency inverter will have minimum VA rating. Similar to the secondary compensation capacitance, the capacitive reactance X_{C1} should also be equal to the inductive reactance of the transmitter coil.

2.4.1.1 Series-series compensation topology

The equivalent circuit of series-series topology is shown in figure 2.15. The SS topology helps in constant current operation with zero phase shift and hence it is suitable for battery charging and low power applications. The main advantage of the SS topology is that the compensation capacitances are independent of the coupling coefficient k and load. However, the power transfer efficiency for large distance between the coils in relatively low[5]. The expression for the capacitor C_1 in SS topology is given as[1]

$$C_1 = \frac{1}{\omega_r^2.(L_{12} + L_M)} \tag{2.33}$$

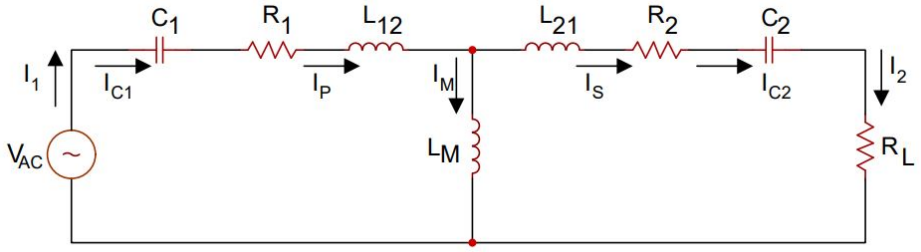

Figure 2.15: Equivalent circuit diagram of SS compensation topology

2.4.1.2 Analytical model of PP compensation topology

The PP topology requires a relatively large primary capacitance for loosely coupled coils and it is most commonly used for industrial applications. The power transfer efficiency in the PP topology for a large distance between the transmitter and receiver coil is better compared to the rest of the topologies. The main advantage of the PP topology is the high power factor and high efficiency at low mutual inductance and a large distance between the Tx and Rx coils[5].

The network diagram for the Parallel-Parallel compensation topology is shown in figure 2.16. In figure 2.16, R_1 and R_2 refers to the Tx and Rx coil resistance, L_{12} and L_{21} refers to the Tx and Rx coil leakage inductance, L_M refers to the mutual inductance between the Tx and Rx coil, and I_P and I_S refers to the current flowing through the Tx and Rx coils respectively.

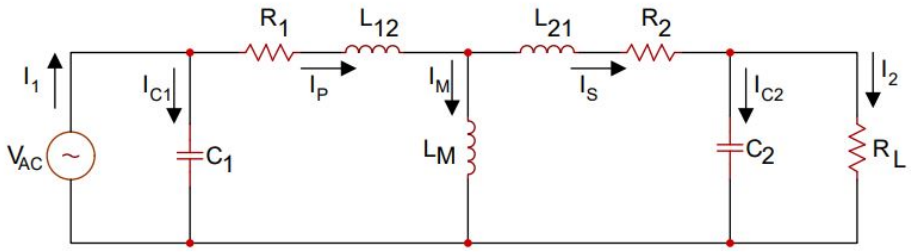

Figure 2.16: Equivalent circuit diagram of PP compensation topology

The input impedance as seen by the voltage source is expressed as

$$Z_{in} = \frac{1}{j\omega C_1 + \frac{1}{R_1 + j\omega(L_a + M) + \frac{\omega^2 M^2 (1 + R_L C_2 \omega)}{(R_L + R_2 + j\omega(L_b + M))(1 + R_L C_2 \omega)}}} \tag{2.34}$$

The input impedance can also be expressed in terms of admittance as

$$Y_{in} = j\omega C_1 + \frac{1}{R_1 + j\omega\left(L_a + M\right) + \frac{\omega^2 M^2 (1+R_L C_2 \omega)}{\left(R_L + R_2 + j\omega(L_b+M)\right)(1+R_L C_2 \omega)}} \tag{2.35}$$

The primary capacitance is chosen such that the imaginary part of the impedance as seen by the source is zero,

$$Im(Y_{in}) = 0 \tag{2.36}$$

WKT

$$C_2 = \frac{1}{\omega_r^2 (L_{21} + L_M)} \tag{2.37}$$

substituting 2.37 in 2.36 we get

$$C_1 = \frac{(L_{21} + L_M)^2 \left[(L_{12} + L_M)(L_{21} + L_M) - L_M^2\right] C_2}{\left[(L_{12} + L_M)(L_{21} + L_M) - L_M^2\right]^2 + L_M^4 R_L^2 (L_{21} + L_M) C_2} \tag{2.38}$$

The effect of primary and secondary resistance are neglected in calculating the compensation capacitor C_1.

The efficiency of power transfer from source V_{AC} to load R_L is given by 2.26.

From figure 2.16

$$\begin{aligned} I_S &= I_{C2} + I_2 \\ I_S &= j\omega C_2 V_L + \frac{V_L}{R_L} \\ I_S &= V_L \left[\frac{1 + j\omega C_2 R_L}{R_L}\right] \\ \frac{|I_S|}{|I_2|} &= \sqrt{1 + R_L^2 C_2^2 \omega_r^2} \end{aligned} \tag{2.39}$$

similarly

$$\frac{|I_P|}{|I_2|} = \frac{\sqrt{R_2^2 + \left[(L_{21} + L_M)\omega_0 + R_2 R_L C_2 \omega_r\right]^2}}{\omega_r L_M} \tag{2.40}$$

substituting 2.39 and 2.40 in 2.26, we get

$$\eta = \frac{R_L}{R_L + R_2 + \frac{R_2 R_L^2}{\omega^2 (L_{21}+L_M)} + \frac{R_1 R_2^2}{\omega^2 L_M^2} + \frac{R_1 \left[(L_{21}+L_M)\omega^2 + \frac{R_2 R_L}{\omega^2 (L_{21}+L_M)}\right]^2}{\omega^2 L_M^2}} \tag{2.41}$$

rearranging 2.41

$$\eta = \frac{R_L}{R_L + R_2 + \frac{R_1(L_{21}+L_M)^2}{L_M^2}\left[1 + \frac{R_2R_L^2L_M^2 + R_1R_2^2(L_{21}+L_M)^2}{\omega_r^2(L_{21}+L_M)^2L_M^2}\right]} \tag{2.42}$$

From 2.42, the condition for maximum efficiency can be derived. If $\left[\frac{R_2R_L^2L_M^2 + R_1R_2^2(L_{21}+L_M)^2}{\omega_r^2(L_{21}+L_M)^2L_M^2}\right]$ tends to zero, maximum efficiency can be achieved.

Therefore,

$$\omega_r \gg \left[\frac{\sqrt{R_2R_L^2L_M^2 + R_1R_2^2\left(L_{21}+L_M\right)^2}}{\left(L_{21}+L_M\right)L_M}\right] \tag{2.43}$$

Hence, the maximum theoretical efficiency can be achieved when condition given by 2.43 is fulfilled. The maximum theoretical efficiency can be expressed as

$$\eta_{max,PP} = \frac{R_L}{R_L + R_2 + \frac{R_1(L_{21}+L_M)^2}{L_M^2}} \tag{2.44}$$

2.5 Coil geometries for wireless power technology

The efficiency of the wireless power technology using time-varying resonant magnetic coupling largely depends on the Tx and Rx coil geometries, Q-factor of the coils, coupling coefficient, and air-gap between the coils. An alternating current applied to the Tx coil generates electromagnetic waves which is dependent on the coil geometry besides applied current and frequency. An electromagnetic coil is designed by winding isolated conductors in the shape of a coil, spiral, or helix. The electromagnetic coil parameters such as inductance, resistance, and magnitude of the desired magnetic field influence the design of the coil. The coils used in the wireless power technology can be divided based on the geometry and core type as shown in figure 2.17.

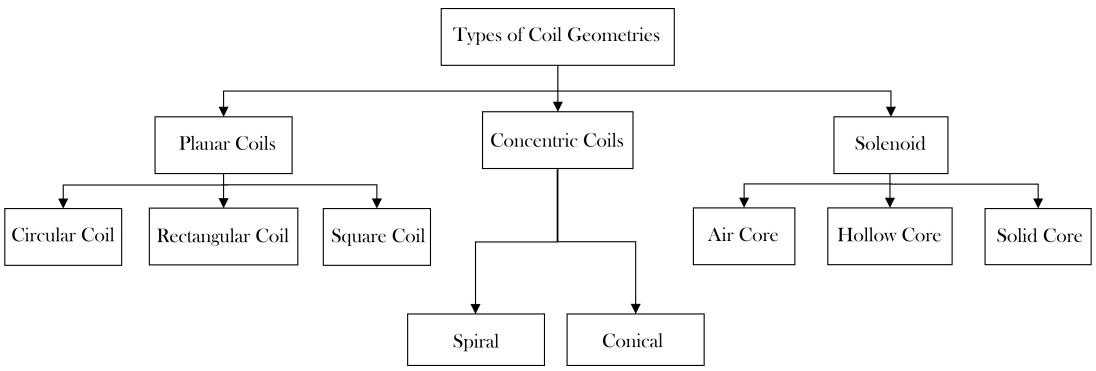

Figure 2.17: Types of coil geometries

In this thesis, planar circular coils, concentric coils, and solenoids are used both as Tx and Rx coils. The different types of coil geometries used in this thesis are discussed below.

2.5.1 Circular coils

If the current carrying conductor is wound to be a loop, the resulting geometry will be a circular coil. The electric current applied to the circular loop generates a magnetic field that is concentrated at the center of the loop. The strength of the magnetic field at the center of the circular coil can be improved by increasing the number of loops on the coil. A single layer circular coil with N turns is shown in figure 2.18.

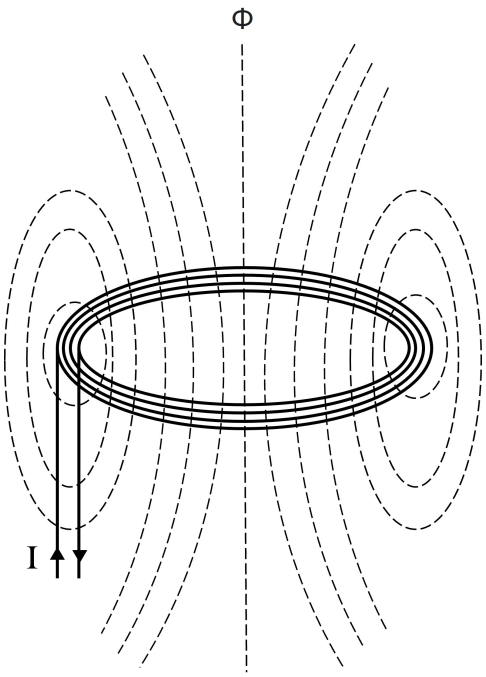

Figure 2.18: Magnetic field lines of single layer circular coil

The magnetic field produced by a current carrying circular loop can be described using Biot-Savart law. The magnetic field produced by the circular loop at any point in space as explained in section (2.1.2) can be calculated as

$$B = -\frac{\mu}{4\Pi}\oint_{l}\frac{Idl\hat{r}}{r^2}$$

Biot-Savart law can also be used to calculate the magnetic field at any point on the axis of the circular loop as explained in section (2.1.2) using the equation

$$B = \frac{2\Pi\mu NIa^2}{4\Pi(x^2+a^2)^{\frac{3}{2}}}$$

The magnetic flux density is maximum at the center of the circular loop as all the field lines are concentrated at the center which can be determined by

$$B = \frac{\mu_0 NI}{2a}$$

The following factors affect the magnetic field in the circular coil:

- The magnitude of the magnetic field in a circular coil is directly proportional to the magnitude of current through the loop i.e., $B \propto I$.
- The magnitude of the magnetic field is inversely proportional to the radius of the circular coil i.e., $B \propto \frac{1}{r}$.
- The magnitude of the magnetic field in the circular coil also depends on the number of loops in the coil. The more the number of loops, higher the magnitude of the magnetic field.
- The self-inductance of the circular coil is influenced by the coil geometric parameters such as the inner and outer radius of the wire, inner and outer radius of the coil, and number of turns.

2.5.1.1 Inductance of a circular coil

The self-inductance of a single turn circular coil as shown in figure 2.19(i) can be analytically expressed as[7]

$$L = \mu_0 x \left(ln\left(\frac{8x}{a}\right) - 2 \right) \tag{2.45}$$

where μ_0 ($= 4\pi * 10^{-7}$) is the permeability of free space, x is radius of coil, and a is radius of wire. Using Maxwell's expression in elliptic integrals, the mutual inductance between two single turn circular coils as shown in figure 2.19(ii) can be analytically expressed as[7]

$$M = \mu_0 \sqrt{xy} k^{\frac{3}{2}} C(k) = \mu_0 \sqrt{xy} \left[\left(\frac{2}{\sqrt{k}} - \sqrt{k} \right) F(k) - \frac{2}{\sqrt{k}} E(k) \right] \tag{2.46}$$

where x and y are the radii of two circular coils, functions C(k), F(k) and E(k) are the complete elliptic integrals of the first and second order, and

$$k = \frac{4xy}{(x+y)^2 + h^2} \tag{2.47}$$

where h is the distance between the circular coil centers.

Similarly, the analytical expression for the self-inductances and the mutual inductance for the circular coils with N turns can be expressed as

$$\begin{aligned} L_1 &= \mu_0 N_1^2 x \left(ln\left(\frac{8x}{a_1}\right) - 2 \right) \\ L_2 &= \mu_0 N_2^2 y \left(ln\left(\frac{8y}{a_2}\right) - 2 \right) \\ M &= \mu_0 N_1 N_2 \sqrt{xy} k^{\frac{3}{2}} C(k) \end{aligned} \tag{2.48}$$

where x and y are the coil radius of coil 1 and coil 2 respectively, a_1 and a_2 are the wire radius of coil 1 and coil 2 respectively, and N_1 and N_2 are the number of turns in coil 1 and coil 2 respectively.

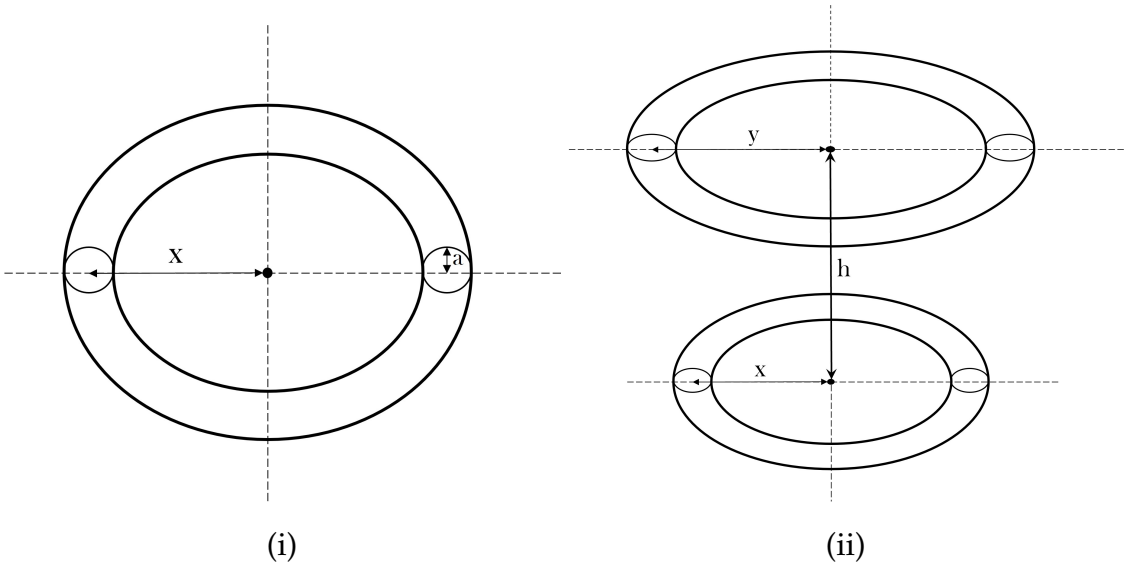

Figure 2.19: (i) Single turn circular coil with coil radius x and wire radius a. (ii) Two single turn circular coil with coil radius x and y respectively with a distance of h between them

2.5.2 Concentric coils

The concentric coils are generally flat spirals of isolated conductors mounted on a substrate or a magnetic shielding as shown in figure 2.20. Each turn in the concentric coil has a different radius which is a function of the pitch factor. The pitch factor determines the distance between each turn of the coil. The electromagnetic behaviour of the concentric coil is similar to the circular coil with the maximum flux density at the center of the coil and the strength of the magnetic field depends on number of turns N, magnitude of current, and inner and outer radius of the coil. The magnetic flux density B at any point in space and on the axis of the concentric coil can be calculated similar to the circular coil as explained in section (2.1.2) using Biot-Savart equations.

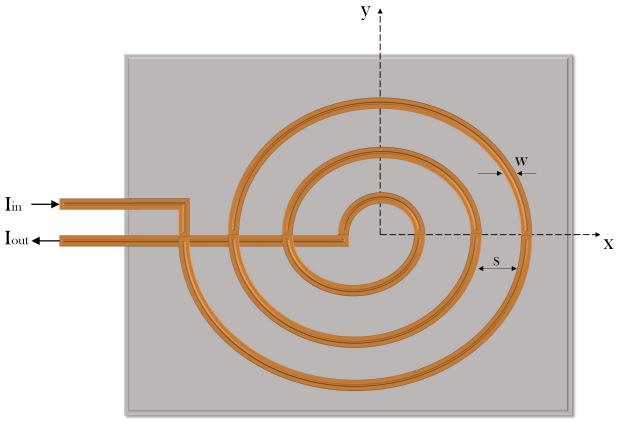

Figure 2.20: Single layer concentric coil

The following factors affect the magnetic field in the concentric coil:

- The magnitude of the magnetic field in a circular coil is directly proportional to the magnitude of current through the loop i.e., $B \propto I$.
- The magnitude of the magnetic field in the circular coil also depends on the number of loops in the coil. The more the number of loops, higher the magnitude of the magnetic field.
- The insertion of a material with high permeability as a substrate or magnetic shielding increases the magnitude of the magnetic field in the concentric coil.
- The self-inductance of the concentric coil is influenced by the geometric parameters such as the inner and outer radius of the coil, pitch factor, and number of turns.

2.5.2.1 Inductance of a concentric coil

The self-inductance of the concentric coil with N turn as shown in figure 2.21(i) can be approximated by using the concept of average of diameter of the concentric coil[8]. The geometrical parameters of the concentric coil is shown in figure 2.21(ii). In figure 2.21(ii), w is the wire diameter, s is the distance between the turn, d_{inner} and d_{outer} are the inner and outer diameter of the coil, respectively. The analytical expression for the self-inductance of the concentric coil can be expressed as[8]

$$L = \frac{\mu_0 N^2 d_{avg}}{2}\left[ln\left(\frac{2.46}{\gamma}\right) + 0.20\gamma^2\right] \tag{2.49}$$

$$\gamma = \frac{d_{outer} - d_{inner}}{d_{outer} + d_{inner}} \tag{2.50}$$

$$d_{avg} = \frac{d_{outer} + d_{inner}}{2} \tag{2.51}$$

The mutual inductance between two concentric coils C_1 and C_2 as shown in figure 2.22 can be expressed using Neumann's equation as[8]

$$M = \frac{\mu_0}{4\Pi} \oint_{C_1} \oint_{C_2} \frac{dl_1 dl_2}{R} \tag{2.52}$$

where μ_0 is the permeability of free space, dl_1 and dl_2 are line elements, R is the separation distance between the two line elements, and θ is the angle of revolution relative to x-axis.

The outer radius R of the coil is determined using the equation

$$R = R_i + a\theta \tag{2.53}$$

where R_i is the initial radius of the coil and a is the pitch factor given by,

$$a = \frac{s}{2\pi} \tag{2.54}$$

$$\theta = 2\pi N \tag{2.55}$$

Using (2.53), the equation for coil 1 and coil 2 can be expressed as

$$R_A = R_{i1} + a_1\theta_1 \tag{2.56}$$

$$R_B = R_{i2} + a_2\theta_2 \tag{2.57}$$

The tangential line elements dl_1 and dl_2 can be expressed as

$$dl_1 = (R_{i1} + a_1\theta_1)d\theta_1 \tag{2.58}$$

$$dl_2 = (R_{i2} + a_2\theta_2)d\theta_2 \tag{2.59}$$

The dot product of dl_1 and dl_2 is given by

$$dl_1.dl_2 = (R_{i1} + a_1\theta_1)(R_{i2} + a_2\theta_2)cos(\theta_2 - \theta_1)d\theta_1 d\theta_2 \tag{2.60}$$

The distance R between the line elements dl_1 and dl_2 can be expressed using the cosine law as

$$R^2 = (R_{i1}+a_1\theta_1)^2+(R_{i2}+a_2\theta_2)^2-2(R_{i1}+a_1\theta_1)(R_{i2}+a_2\theta_2)cos(\theta_2-\theta_1)d\theta_1 d\theta_2+h^2 \tag{2.61}$$

Substituting (2.60) and (2.61) in (2.52), the mutual inductance between perfectly aligned concentric coils can be expressed as

$$M = \frac{\mu_0}{4\Pi} \int_{2\Pi} \int_{N} \frac{j d\theta_1 d\theta_2}{\sqrt{(R_{i1} + a_1\theta_1)^2 + (R_{i2} + a_2\theta_2)^2 - 2j + h^2}} \tag{2.62}$$

where

$$j = (R_{i1} + a_1\theta_1)(R_{i2} + a_2\theta_2)\, cos\,(\theta_2 - \theta_1)$$

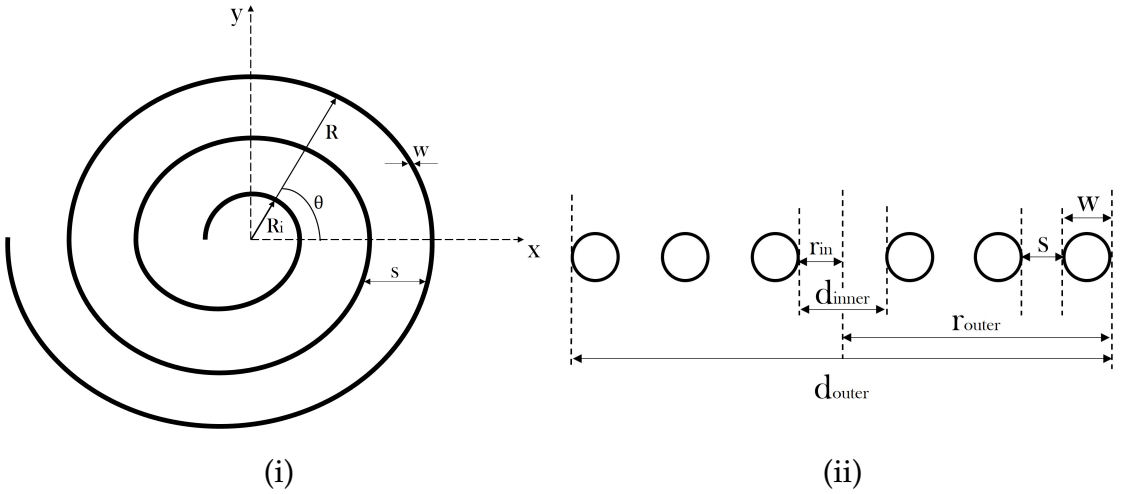

Figure 2.21: (i) Concentric coil with N turns. (ii) Cross-section of concentric coil

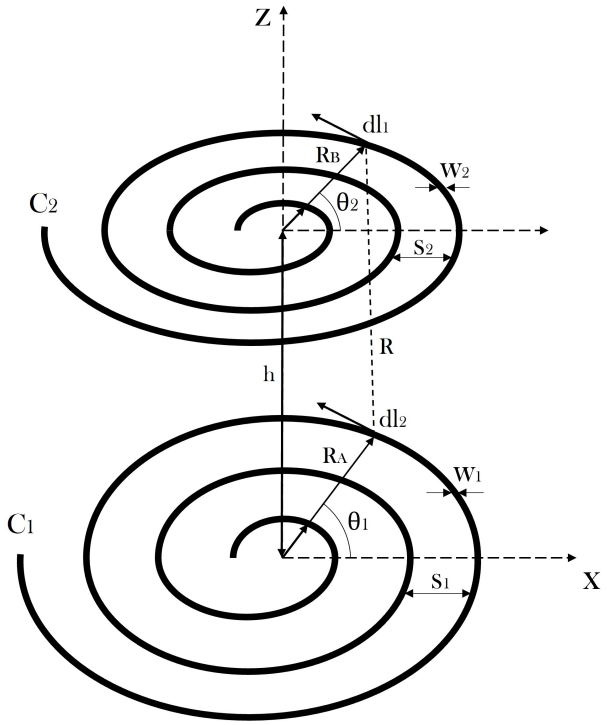

Figure 2.22: Two perfectly aligned concentric coils

2.5.3 Solenoid

A solenoid is a coil of wire wound in the axial direction with electric current flowing through it. The current flowing in the solenoid generates a magnetic field that starts from the north pole and ends at the south pole similar to a bar magnet. The magnetic field produced by the solenoid is stronger along the axis of the solenoid since the magnetic flux generated by each turn of the coil is concentrated at the center. Whereas the magnetic flux outside the solenoid is considerably low.

The magnetic field due to current flowing in the solenoid can be expressed using Ampere's law as

$$\oint B.dl = \mu_0 I_{enc} \tag{2.63}$$

The line integral of B around the coil of length l with current enclosed in the coil to be product of number of turns N and current I in each turn will give us

$$B = \frac{\mu_0 NI}{l} \tag{2.64}$$

where μ_0 is the permeability of free space, N is the number of turns, I is the current. The equation described in (2.64) gives an expression for the magnetic field generated by the solenoid with air core. However, with the introduction of a ferromagnetic core increases the magnitude of the magnetic field in the solenoid due to high permeability of the core. The expression for the magnetic field within a core can be expressed as

$$B = \frac{\mu_0 \mu_r NI}{l} \tag{2.65}$$

where μ_r is relative permeability of the core. From (2.64) and (2.65), it is clear that the magnitude of the magnetic field in a solenoid with core will be higher than the solenoid with air core. Also, the magnetic field in the solenoid with hollow core will be less than the magnetic field of the solenoid with solid core.

The following factors affect the magnetic field in the solenoid:

- The magnitude of the magnetic field in the solenoid is directly proportional to the magnitude of current through it i.e., $B \propto I$.
- The magnitude of the magnetic field in the solenoid also depends on the number of loops in the coil. The more the number of loops, higher the magnitude of the magnetic field.
- The insertion of a core material with high permeability increases the magnitude of the magnetic field in a solenoid.
- The self-inductance of the concentric coil is influenced by the geometric parameters such as the cross-sectional area of the wire,length of the coil, and number of turns.

2.5.3.1 Inductance of a solenoid

The self-inductance of a coil with N turns is expressed as

$$L_1 = L_{11} = N_1 \frac{\phi_{11}}{I_1} \tag{2.66}$$

The self-inductance for a solenoid as shown in figure 2.23 can be determined using (2.66). The magnetic flux density due to current in the solenoid can be expressed as

$$B = \frac{\mu NI}{l} \tag{2.67}$$

where N is the number of turns, and l is the length of the solenoid.

The magnetic flux flowing through the solenoid is the product of magnetic field and cross-sectional area of the solenoid. Therefore, the magnetic flux per turn is given by

$$\phi = B.A \tag{2.68}$$

where A is the cross-sectional area of the solenoid.

Substituting (2.67) and (2.68) in (2.66), we get self-inductance of the solenoid as

$$L = \frac{\mu N^2 A}{l} \tag{2.69}$$

From (2.69), the self-inductance of the solenoid depends on the coil parameters such number of turns on the coil, cross-sectional area of the coil, and length of the coil. The self-inductance of a solenoid can also be increased by selecting a core with high permeability.

The mutual inductance between two coaxial solenoids with N_1 and N_2 turns with currents I_1 and I_2 respectively is derived below. The mutual inductance of coil 2 with respect to coil 1 (M_{21}) is given by

$$M_{21} = \frac{N_2 \Phi_{21}}{I_1} \tag{2.70}$$

Similarly, the mutual inductance of coil 1 with respect to coil 2 (M_{12}) is given by

$$M_{12} = \frac{N_1 \Phi_{12}}{I_2} \tag{2.71}$$

From (2.70) and (2.71), we can write

$$M = \frac{N_1 \Phi_{12}}{I_2} = \frac{N_2 \Phi_{21}}{I_1} \tag{2.72}$$

The magnetic flux Φ_{21} can be expressed as,

$$\Phi_{21} = B_1.A = \left(\frac{\mu N_1 I_1}{l_1}\right) A \tag{2.73}$$

Substituting (2.73) in (2.72), we get the mutual inductance between two coaxial solenoids as

$$M = \frac{\mu N_1 N_2 A}{l_1} \tag{2.74}$$

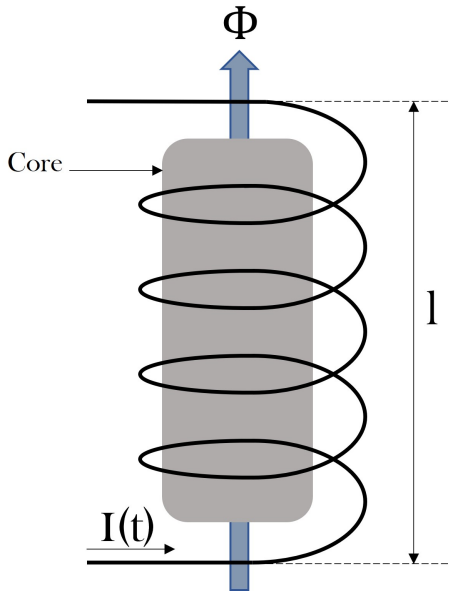

Figure 2.23: Solenoid with N turns

2.6 Material selection for coils

The selection of material for designing electromagnetic coils for wireless power transfer is critical in order to obtain maximum efficiency. The type of material selected for designing the coils contribute in the resistive losses, and losses due to skin and proximity effect when operating at higher frequency. Also, the Q-factor of the coil material plays a vital role in the material selection. The Q-factor is a measure of the performance of the coil. When operating at higher frequencies, the effective resistance of the coil increases due to the skin and the proximity effect which reduces the quality or the Q-factor of the coil.

A simple circuit model for an ideal inductor can be represented by connecting a resistance in series as shown in figure 2.24.

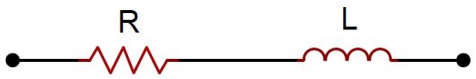

Figure 2.24: A simple circuit model of ideal inductor with series resistance

In case of direct current, the current density is distributed or homogenous over the entire cross-section of the conductor. The DC resistance of the conductor depends on the cross-sectional area of the wire, length of the wire and electrical conductivity of the material used which is expressed as

$$R_{DC} = \frac{l}{\sigma A} \tag{2.75}$$

where σ is the electrical conductivity [S/m] of the material used for the wire, l is the length of the wire [m], and A is the cross-sectional area of the wire [m^2]. In order to get low resistance in the wire, the electrical conductivity of the material should be high. The electrical conductivity of copper is $5.8 * 10^7$[S/m] which is higher compared to the electrical conductivity of aluminium and iron.

In case of alternating current, the current density is not homogenous over the cross-section of the conductor and with increasing frequency, the current density is accumulated at the surface of the conductor and it is reduced at the center of the conductor. This effect is known as the skin-effect which reduces the effective conducting area in the wire as shown in figure 2.25.

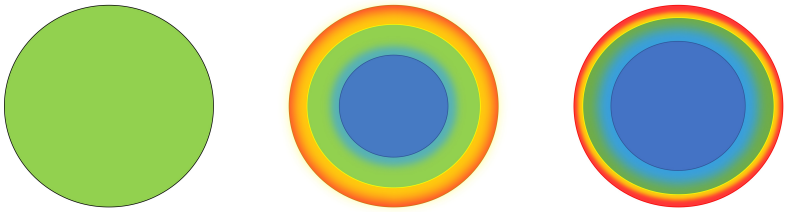

Figure 2.25: Illustration of skin effect at different frequencies

The skin-effect is caused by the magnetic field generated by the current flowing in the circumference of the conductor which opposes the current to flow at the center of the conductor. At higher frequencies using AC, the main resistance comes from the skin-effect. The skin depth is used to describe how a high frequency alternating current penetrates the conductor. The skin depth is defined as the distance from the circumference where the current density is reduced by 63% of the surface current density. The skin depth is expressed as

$$\delta = \sqrt{\frac{2}{\mu \sigma_{cu} \omega}} \tag{2.76}$$

where σ_{cu} is the conductivity of copper, $\mu = \mu_0 \mu_r$ is the permeability, and $\omega = 2\pi f$ is the frequency of the current. When the frequency increases, the skin depth decreases. The effective current carrying area of a conductor is determined by the skin depth. Thus, a conductor thicker than the skin depth will not be an effective use of the conductor. The skin depth in a conductor is illustrated in figure 2.26.

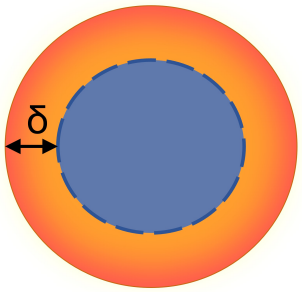

Figure 2.26: Illustration of skin depth in a conductor

Another effect that adds to the loss when operating at high frequency is the proximity effect. The external field generated by the high frequency current in the conductor influences the current distribution in the nearby conductors or the conductors located in the proximity. The proximity effect is more in the solid conductors compared to the stranded conductors since the surface area of the stranded conductor is smaller than the solid conductor. The AC resistance for a conductor with circular cross-section can be expressed as

$$R = \frac{L}{\sigma \pi r^2}, r \ll \delta \tag{2.77}$$

$$R = \frac{L}{2\sigma \pi r \delta}, r \gg \delta \tag{2.78}$$

where r is the radius of the conductor and L is the length of the conductor. Hence, conductors with $r \gg \delta$ have higher higher resistance compared to conductors with $r \ll \delta$. In order to reduce the AC resistance at high frequency, different conductors are used to design the coil which are discussed below.

2.6.1 Litz wire

The litz wires are used typically in applications operating within the frequency range of 10kHz - 5MHz [11]. The cross-section of a litz wire with n strands is shown in figure 2.27. The litz wire consists of individual insulated magnetic wires that are bunched or braided together. Each strand in the litz wire is smaller that the skin depth to ensure effective use of the conducting area. The multiple strands in the wire allows current to divide uniformly between the strands. Also, the strands are bunched together such that the location of each strand alternate between the center of the wire and the circumference of the wire. The multiple strand construction of the litz wire ensures that the proximity effect is same on each strand at all the points. Thus, the litz wire homogenizes the current density and increases the effective conducting area of the wire, reducing AC losses at high frequency. The other benefits of using litz wire is the lower operating temperatures and reduced weight.

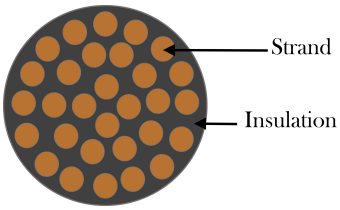

Figure 2.27: Cross-section of a litz wire

The number of strands and the thickness of each strand in a litz wire is determined by the current amplitude and the operating frequency. The AC resistance of a litz wire can be approximately expressed as

$$R = \frac{l}{\sigma \pi r^2}\left[\frac{1}{4} + \frac{r}{2\delta}\right] \tag{2.79}$$

2.6.2 Magnetic wire

The magnetic wire is a solid conductor with very thin insulation coated around the conductor. The magnetic wire is also called as an enameled wire typically used in the construction of transformer windings, motor windings, inductors, and electromagnets. The insulation around the magnetic wire is often made of polymer layers rather than a layer of enamel paint. Figure 2.28 shows a solenoid made of magnetic wire.

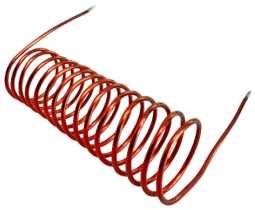

Figure 2.28: Solenoid made of magnetic wire

The thickness of the magnetic wire is calculated based on the current amplitude, frequency and the operating temperature. The magnetic wire provides greater mechanical and thermal strength compared to the litz wire. However, the AC resistance offered by the magnetic wire when operating at high frequency is higher due to skin effect and proximity effect. The extent to which the frequency affects the resistance of the magnetic wire depends on the gauge of the wire. Large gauge wires exhibit more losses than small gauge wire when operating at high frequency. Hence, the magnetic wires can be used for low frequency applications upto 100kHz beyond which the gauge of the wire should be made small according to the operating frequency.

2.6.3 Hallow copper tube

An alternate to the litz wire is the copper hollow tube when operating at high frequency. Although, the litz wire offers less resistance due to skin effect, it is required to reduce the diameter of each strand to operate at much higher frequencies that complicates the packing factor for the litz wire. Also, the strand to strand proximity effect affects the uniformity of current distribution. The hollow conductors have lower skin-effect when compared to other solid conductors with the same cross-sectional area[9]. Figure 2.29 shows an air core solenoid made of copper hollow tube.

Figure 2.29: Solenoid made of hollow copper tube

The other advantages of using a hollow copper tube is easy manufacturing and simplicity in implementing cooling for the coil. If the proximity effect in the hollow conductors are minimised, the hollow tubes can be a good alternative for litz wire in some WPT applications. However, lack of analytical models for the hollow conductors makes it very difficult to analyse the advantages and its limitations.

2.7 Current challenges in wireless power system

The major challenges in the wireless power technology is the efficiency of power transfer, range of power transfer, and alignment between the coils. The efficiency drop in the WPT is due to a number of reasons including distance between the coils, flux leakage, losses in the power converter, and magnetic coupling between the coils and the design form factor of the coils. The form factor is the ratio of the length of the coil to the diameter of the coil and it is one of the parameters that affects the inductance of the coils. However, different coils can have the same form factor. Thus, the combination of different coil geometries can have a coupling factor(k) high enough to transfer power with good efficiency. The wireless power technology is limited by the alignment between the Tx and Rx coils, which can be a major drawback in some applications such as wireless charging of portable electronics where the chances of misalingnment between the coils are more. The following section explains how the misalignment between the coils affect the coupling coefficient and its impact on the power transfer efficiency.

2.7.1 Alignment between transmitter and receiver coils

The inductive wireless power transfer is a technology where the power is transferred by magnetic fields from the Tx coil to the Rx coil through the air gap. The amount of magnetic flux linked between the Tx and Rx coils depends on the magnetic coupling between the coils. The strength of the coupling is defined by the coupling factor or coupling coefficient(k), and is expressed as

$$k = \frac{M}{\sqrt{L_{TX} \times L_{RX}}} \tag{2.80}$$

where L_{TX} and L_{RX} are self-inductances of the transmitter and receiver coil respectively, and M is the mutual inductance induced between the two coils. If current I_1 flowing in a coil produces a magnetic flux ϕ_1, the self-inductance of the coil can be expressed as the ratio of magnetic flux produced to the current in the coil

$$L_1 = \frac{\phi_1}{I_1} \tag{2.81}$$

The mutual inductance with the adjacent coil can be expressed as the magnetic flux generated by coil 1 that passes through the area enclosed by coil 2 divided by the current in coil 1

$$M = L_{21} = \frac{\phi_{21}}{I_1} \tag{2.82}$$

The following are the three types of misalignments that result in poor coupling factor,

- Vertical misalignment
- Lateral misalignment
- Angular misalignment

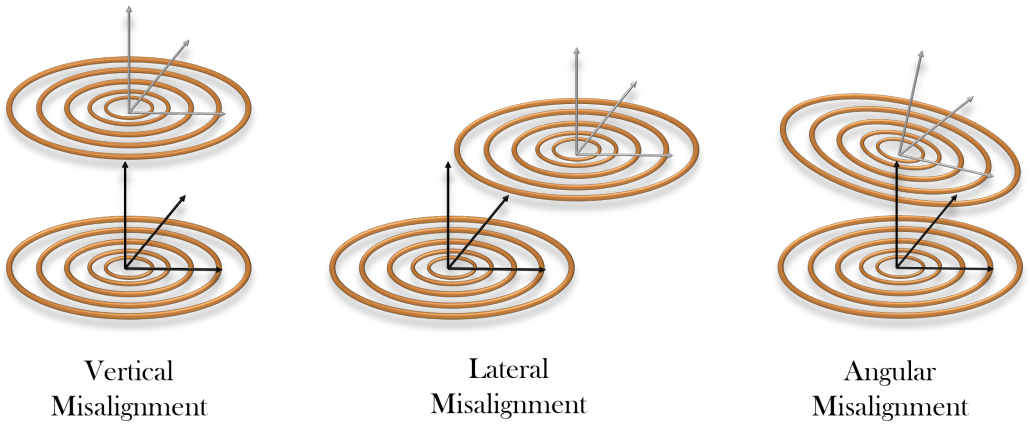

Figure 2.30: Types of misalignment between transmitter and receiver coils

Figure 2.31 shows the Rx coil misaligned with the Tx coil. The Rx coil is laterally misaligned by distance $d = \sqrt{x_1^2 + y_1^2}$. The angles (θ_1, Φ_1) describes the line joining

the centers of the two coils. The receiver coil area vector V_2 is expressed using the angles (θ_0, Φ_0) to describe the angular misalingnment of the receiver coil.

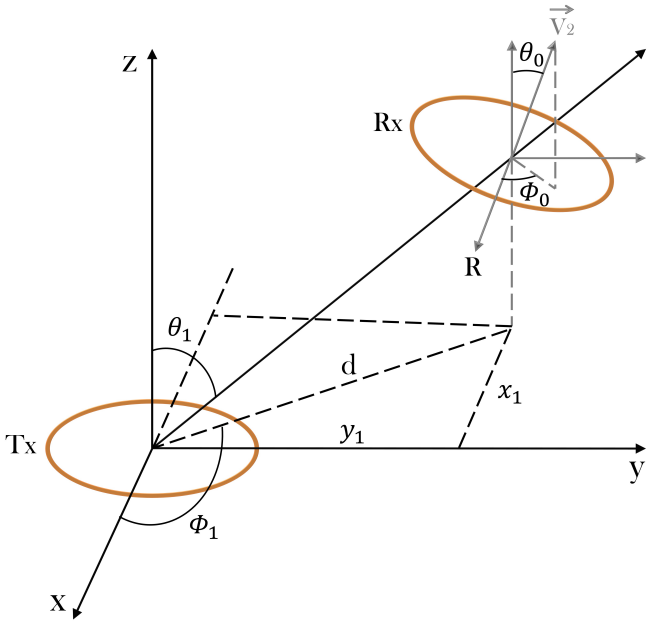

Figure 2.31: Misaligned coils

The general equation for the coupling coefficient between the two coils that are misaligned is calculated using 2.80 and is expressed as[10]

$$k = \left(\frac{\sqrt{r_1 r_2}}{r}\right)^3 \left(\frac{3}{2}\sin\theta_0 \cos\theta_1 \sin\theta_1 \cos\left(\varphi_0 - \phi_1\right) + \cos\left\{\cos^2\theta_1 \frac{\sin^2\theta_1}{2}\right\}\right) \tag{2.83}$$

where r_1 and r_1 are the radius of the Tx and Rx coil respectively, and r can be expressed as

$$r = \sqrt{R^2 + d^2 + r_1^2 - 2d\sqrt{r_1^2 + R^2}\cos\left(90^\circ + \tan^{-1}\left(\frac{r_1}{R}\right)\right)}, r_1 \geq r_2 \tag{2.84}$$

$$r = \sqrt{R^2 + d^2 + r_2^2 - 2d\sqrt{r_2^2 + R^2}\cos\left(90^\circ + \tan^{-1}\left(\frac{r_2}{R}\right)\right)}, r_2 \geq r_1 \tag{2.85}$$

where R is the vertical distance between the centers of the two coils along same axis.

2.7.1.1 Vertical misalignment

The vertical misalignment occurs when the receiver coil is vertically displaced by a distance R in the same plane where the Tx coil is placed as shown in figure 2.32.

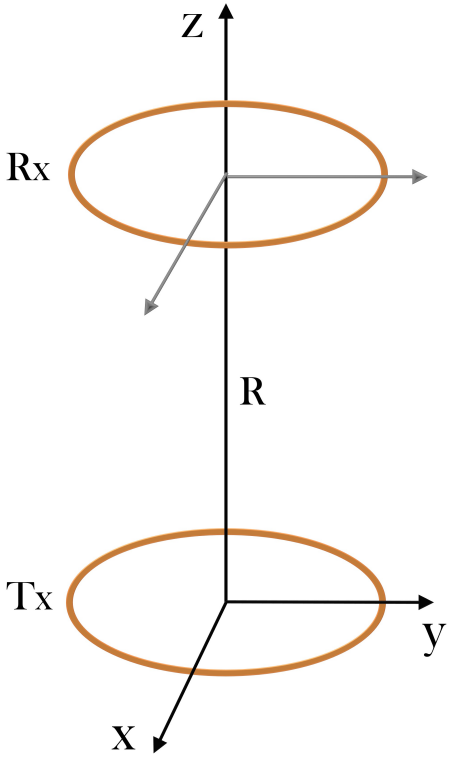

Figure 2.32: Vertical misalignment

In case of vertical misalignment, the variables defined in the general expression for the coupling coefficient becomes $\theta_0 = 0°$,$\theta_1 = 0°$,d=0. Substituting these values in 2.83, we get the expressions for the coupling coefficient under vertical misalignment condition and they are expressed as

$$k = \left(\frac{\sqrt{r_1 r_2}}{\sqrt{R^2 + r_1^2}} \right)^3 , r_1 \geq r_2 \tag{2.86}$$

$$k = \left(\frac{\sqrt{r_1 r_2}}{\sqrt{R^2 + r_2^2}} \right)^3 , r_2 \geq r_1 \tag{2.87}$$

From 2.86 and 2.87, the coupling factor is inversely proportional to the distance between the two coils in the same axis. When the receiver coil is vertically moved away from the transmitter coil, the magnetic field linkage reduces with an increase in distance. At some point, when the receiver coil goes away from the magnetic field range of the transmitter coil, there will be no flux linkage and hence EMF will not be induced in the receiver coil.

2.7.1.2 Lateral misalignment

The lateral misalignment occurs when the receiver coil is laterally displaced with the Tx coil placed in a plane parallel to it as shown in figure 2.33.

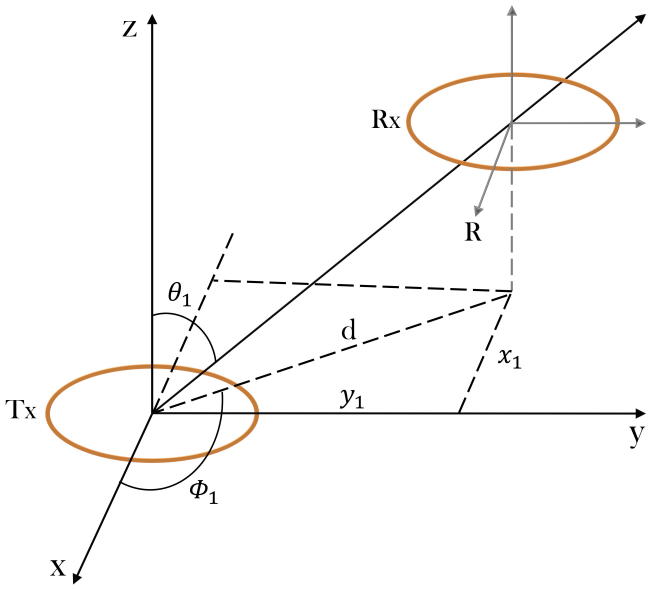

Figure 2.33: Lateral Misalignment

In case of lateral misalignment, $\theta_0 = 0°$ and 2.83 is simplified as

$$k = \left(\frac{\sqrt{r_1 r_2}}{r}\right)^3 \left[\frac{\cos^2\theta_1}{1} - \frac{\sin^2\theta_1}{2}\right] \tag{2.88}$$

2.7.1.3 Angular misalignment

The angular misalignment occurs when the centers of the two coils are on the same axis and the plane of the receiver coil is tilted to form an angle α as shown in figure 2.34.

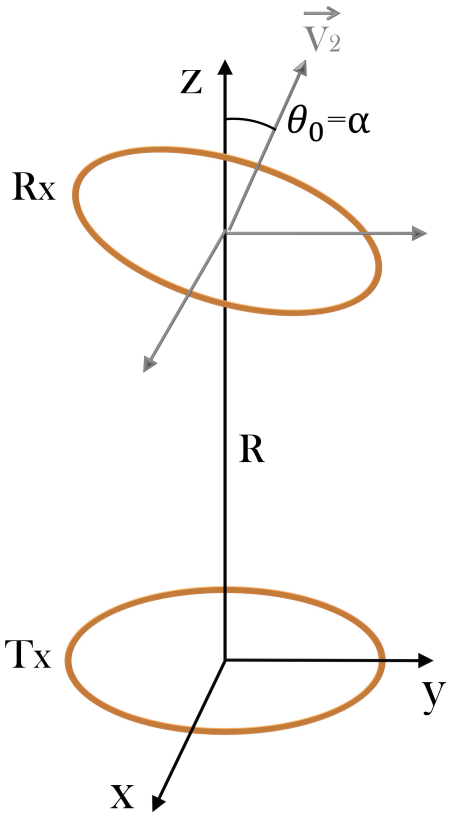

Figure 2.34: Angular misalignment

In case of angular misalignment, the variables defined in the general expression for the coupling coefficient becomes $\theta_0 = \alpha^\circ$,$\theta_1 = 0^\circ$,d=0. Substituting these values in 2.83, we get expression for the coupling coefficient under angular misalignment condition and is expressed as

$$k = \left(\frac{\sqrt{r_1 r_2}}{\sqrt{R^2 + r_1^2}} \right)^3 \cos\alpha, r_1 \geq r_2 \tag{2.89}$$

$$k = \left(\frac{\sqrt{r_1 r_2}}{\sqrt{R^2 + r_2^2}} \right)^3 \cos\alpha, r_2 \geq r_1 \tag{2.90}$$

when $\alpha = 0$, [2.89] and [2.90] reduces to [2.86] and [2.87] respectively. For $\alpha = 90^\circ$, the coupling coefficient becomes zero and hence there will be no power transfer between the two coils.

3

Case Setup

3.1 Investigation of suitable receiver coil geometry

In this section, an investigation of suitable receiver coil geometry is carried out to study the interoperability of different coil geometries, coupling coefficient & the magnetic field distribution. All the coils are tested for aligned & misaligned operation. For the investigation of suitable receiver coil geometry, we have chosen three main commonly used coil geometries which include,

- Concentric coils.
- Solenoid coils.
- Circular coils.

A wireless power system from the Wurth Electronics is used to test the concentric & solenoid coils. We have designed automatically switching transmitter circuits for testing centre-tapped circular coils, as they have three terminals & can't be driven using the WE development kit. Also, the investigation of suitable receiver coil geometry test is conducted by keeping the same transmitter coil to understand the relation between the coupling coefficient & the coil geometry. Table 3.1 shows different transmitter boards & combinations of coils used in the investigation of suitable receiver coil geometry test. The test involves coils with different inductance values, dimensions & coil material as shown in figure 3.1 & figure 3.2. The corresponding coil parameters are shown in table 3.2 & table 3.3.

Table 3.1: Transmitter boards and coil combinations used in the investigation of suitable receiver coil geometry test

Transmitter Board	Transmitter Coil	Receiver Coil
WE development kit	WE concentric coil	Concentric coils
		Solenoid coils
Automatically switching transmitter circuit 1	Circular coil 1	Circular coil 2
Automatically switching transmitter circuit 2	Circular coil 3	Circular coil 4
		Circular coil 5

3.1.1 Measurement of suitable receiver coil geometry

In this thesis, we have conducted measurements & tests on multiple coil geometries with different coil materials. The objective of these measurements is to gain

a comprehensive understanding of the coil geometry & its magnetic properties, as well as to investigate power transfer associated with different coil materials. Among all other coils, we have chosen the WE Tx/Rx coil & solenoid coils to analyze the coupling coefficient. The coil parameters are measured using Agilent's E4980A Precision LCR Meter with a frequency setting of 200KHz which is the closest frequency step available to the operating frequency of 205KHz in the WE development kit. Also, the coils are measured without the resonant capacitors connected.

Even though we have tested several receiver coil geometries, we have chosen custom built solenoid coil to analyze based on the factors affecting the power transfer. The solenoid receiver coil has a similar diameter compared to the WE Tx coil which should result in stronger coupling and the solenoid core reduces the reluctance of the flux path.

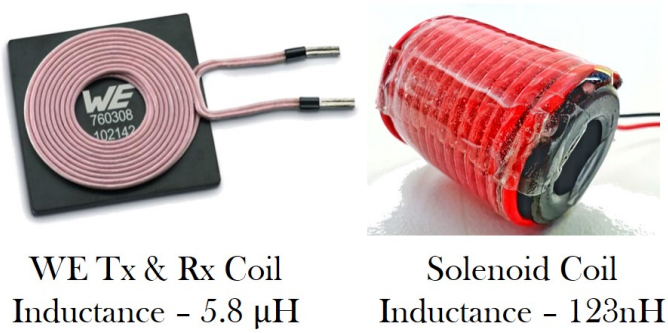

Figure 3.1: Concentric & solenoid coil geometries under test

Table 3.2: Measured coil parameters for concentric and solenoid coils with corresponding resonant capacitors at a resonant frequency of 205KHz

Coil	Inductance	Number of Turns	Q-factor	Resonant Capacitor (μF)
WE Tx/Rx coil	5.8μH	20	13	0.1
Solenoid coil	123nH	13	15	5

The center tapped circular coils investigated are shown in figure 3.2. The measured coil parameters for center tapped circular coils are shown in table 3.3. All the coils are wound using magnetic wire. The coils are mainly varied for the diameter and number of layers/turns. The center tapping and the coil layers are done to boost the magnetic field. Circular coil 1 has the largest diameter of 180mm, to investigate the effect of coil diameter on the range of power transfer. A larger coil diameter helps to accommodate more receiver coils to test point to multi-point power transfer.

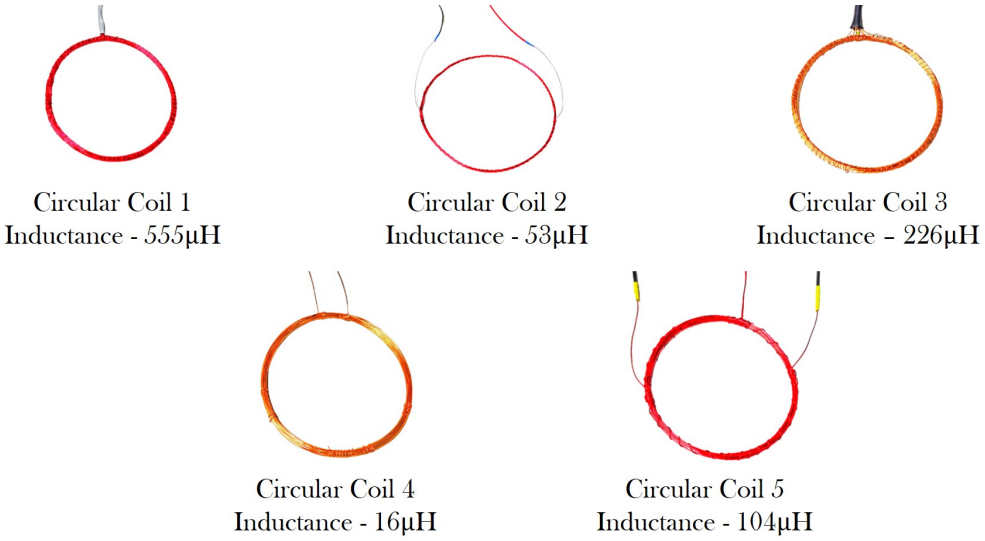

Figure 3.2: Center tapped circular coils under test

Table 3.3: Circular coil parameters and their corresponding resonant capacitors

Coil	Center Tap	Inductance (μH)	Number of Turns	Q-factor	Resonant Capacitor (nF)
Circular Coil 1	Yes	555	120	25	71
Circular Coil 2	No	53	30	32	74
Circular Coil 3	Yes	226	60	225	5
Circular Coil 4	No	16	30	46	80
Circular Coil 5	Yes	103	30	28	12

3.1.2 WE Development kit

In this project, we are using a wireless power transfer system from Wurth Electronics. The power transfer is possible up to 200W when the distance between the coils are less than or equal to 10mm. The wireless power development kit can be used to demonstrate the current wireless power transfer system and that gives an opportunity to develop the system with different concentric & solenoid receiver coils and also has the possibility to vary the resonant frequency accordingly. Table 3.4 shows the key system specification of the WE development kit.

Table 3.4: Key system specification for WE development kit.

Parameters	Specification
Transmitter Input Voltage	24V DC
Receiver Output Voltage	20V DC
Tx & Rx Current	10A
Maximum Transmitted Power	200W
Frequency	205kHz
Load Resistance	6.8Ω | 27Ω | 220Ω
Optimum Coil Distance	10mm

3.1.2.1 Test case

The test set-up for investigation of suitable receiver coil geometry using the Tx and Rx board from the WE development kit is shown in figure 3.3. The test is focused only on studying the magnetic coupling of different concentric and solenoid coils. The test case uses all the components from the WE development kit except the receiver coils and the receiver resonant capacitors, which are changed for different test cases with different coils. A resistive load of 6.8Ω is connected to Rx board. An acrylic sheet of 10mm is used as a spacer between the Tx and Rx coils.

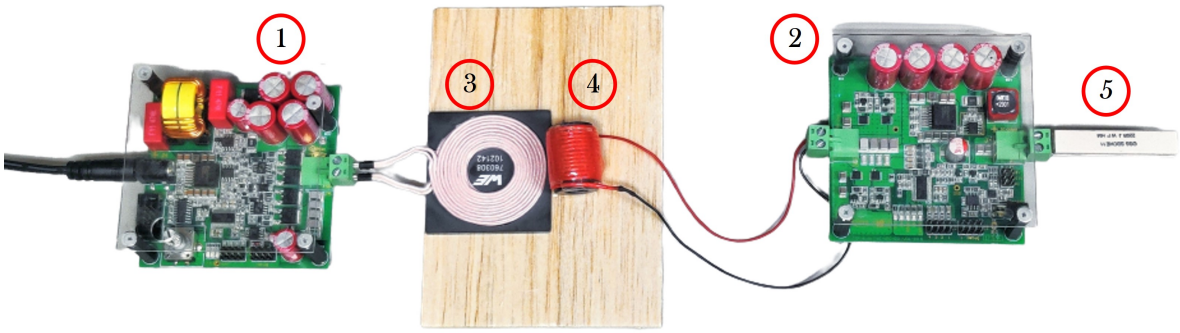

Figure 3.3: Test set up of WE development kit with solenoid Rx coil

1	Transmitter Board
2	Receiver Board
3	Transmitter Coil
4	Receiver Coil
5	Load Resistor

The test case for aligned operation is as follows,

- The Tx and Rx coils are aligned properly with no misalignment.
- The WE development kit is tested for different load conditions with different resistive loads of 6.8Ω, 27Ω and 220Ω.
- For the investigation of a suitable receiver coil geometry test, the voltage and current are measured with a resistive load of 6.8Ω.

- The distance between the Tx and Rx coils is kept constant at 10mm(specified by WE).

The test case for misaligned operation where the receiver coils are misaligned with respect to Tx coil as shown in table 3.5.

Table 3.5: Different misalignment between Tx and Rx coils

Type of Misalignment	Misalignment Value
Vertical	30mm from Tx
Lateral	50% on Tx
Angular	40° angle above Tx

3.1.3 Automatically switching transmitter circuit

A center tapped coil can be used in a wireless power system, as the voltage is injected to the center tapped terminal of the coil, which creates magnetic fields in the 2 sections of the coils and the magnetic fields are in phase with each other which adds to the magnetic field strength. The center tapped coils are built to study the magnetic field strength. Figure 3.4 and figure 3.5 shows the block diagram of the automatically switching transmitter circuit 2 and the receiver respectively.

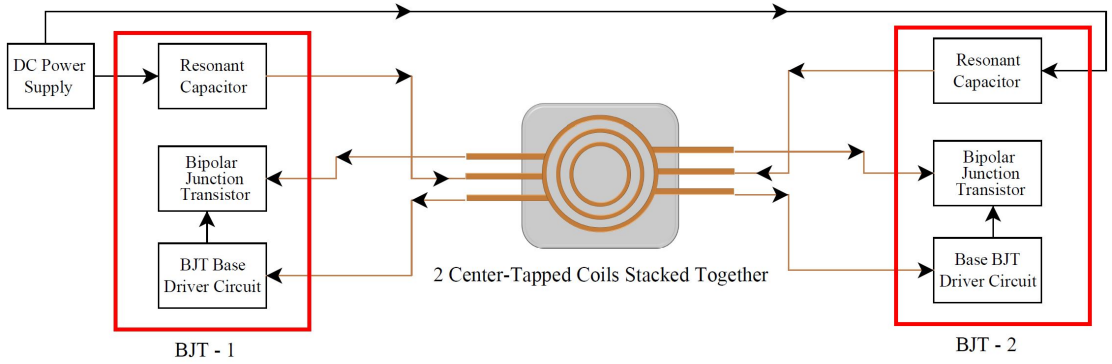

Figure 3.4: Block diagram of automatically switching transmitter circuit 2

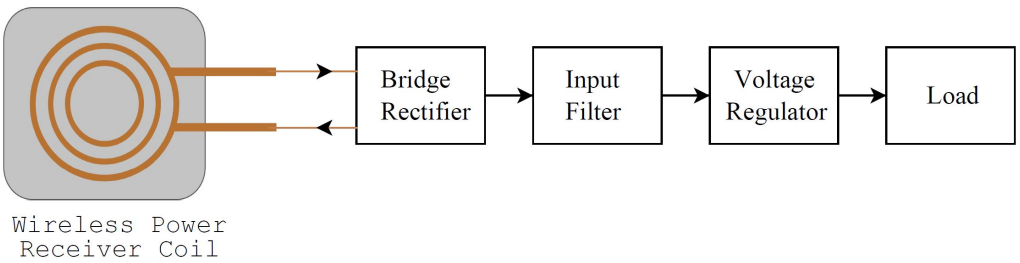

Figure 3.5: Block diagram of a rectifier circuit for wireless power transfer

We have designed 2 automatically switching transmitter circuits, Figure 3.7 shows the schematic diagram of the automatically switching transmitter circuit 1 figure

3.8 shows the schematic diagram of the automatically switching transmitter circuit 2 and figure 3.9 shows the schematic diagram of the receiver. To explain the working of the BJT schematic, a single section of the automatically switching transmitter circuit at different working stages is shown in figure 3.6,

a) A DC power supply is connected to the center tap of the transmitter coil for which a resonant capacitor (C4) is also connected which makes an LC tank. The current flows through both the sections of the coil (L1) and also charges the capacitor (C4).

b) The current flows through the inductor and through the resistor (R2), capacitor (C2) is charged until it reaches a threshold to trigger the BJT.

c) All the capacitors in the circuit gets charged, the energy stored in the capacitors is discharged through the base and a proper base current is supplied to the base of the transistor.

d) The transistor conducts and makes the circuit complete and the Tx coil is fully energized and produces the magnetic field.

The charging and discharging action of the capacitor switches the BJT at a frequency to produce an alternating magnetic field at the coils. Also, the capacitor (C4) and inductor (L1) act as an oscillator that is tuned to a particular resonant frequency. The current flows in the same direction in each coil stacked together to have a strong magnetic field. Figure 3.9 shows the receiver circuit which has a full bridge rectifier that converts AC to DC, then this is fed to a voltage regulator of 5V and 12V and a load is connected to the output of the voltage regulator. It is required to load the receiver all the time as the no load operations may cause higher voltages and break the junctions of the full bridge rectifier and the voltage regulator.

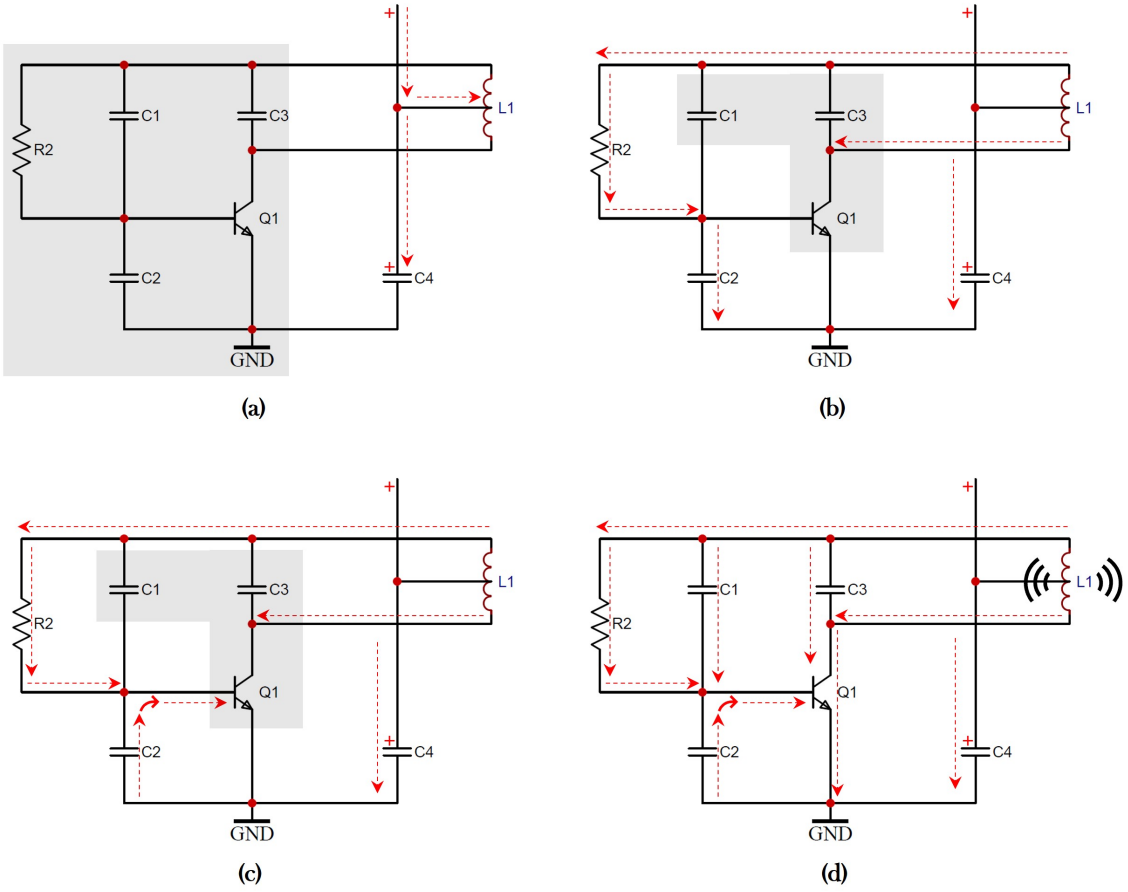

Figure 3.6: Working of a section of the schematic diagram of automatically switching transmitter circuit (figure 3.8)

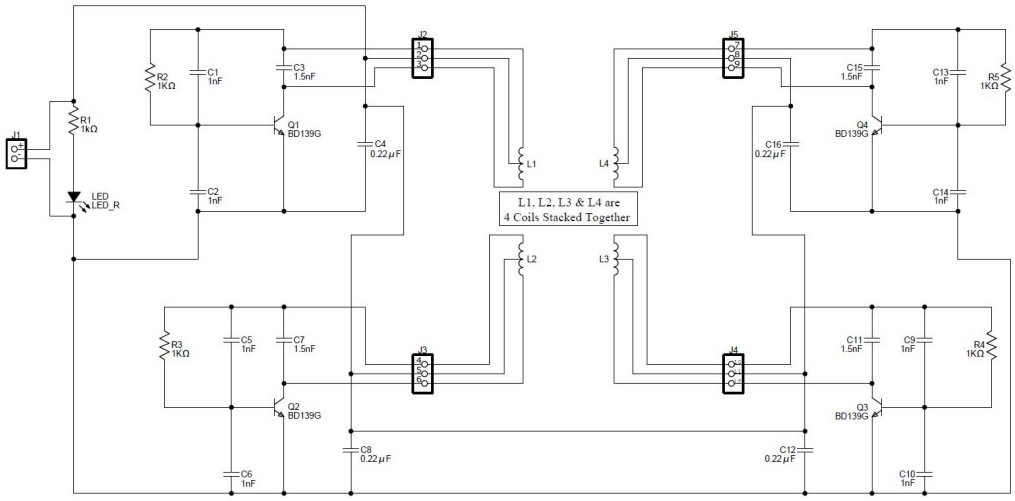

Figure 3.7: Schematic diagram of wireless power transfer for automatically switching transmitter circuit 1

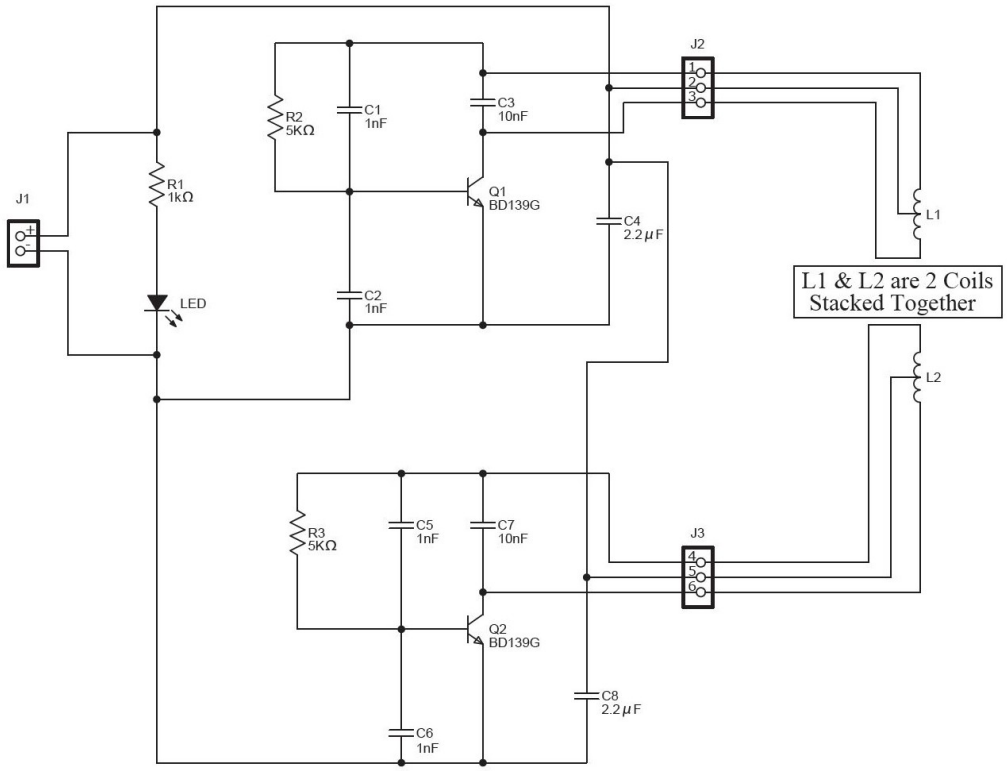

Figure 3.8: Schematic diagram of wireless power transfer for automatically switching transmitter circuit 2

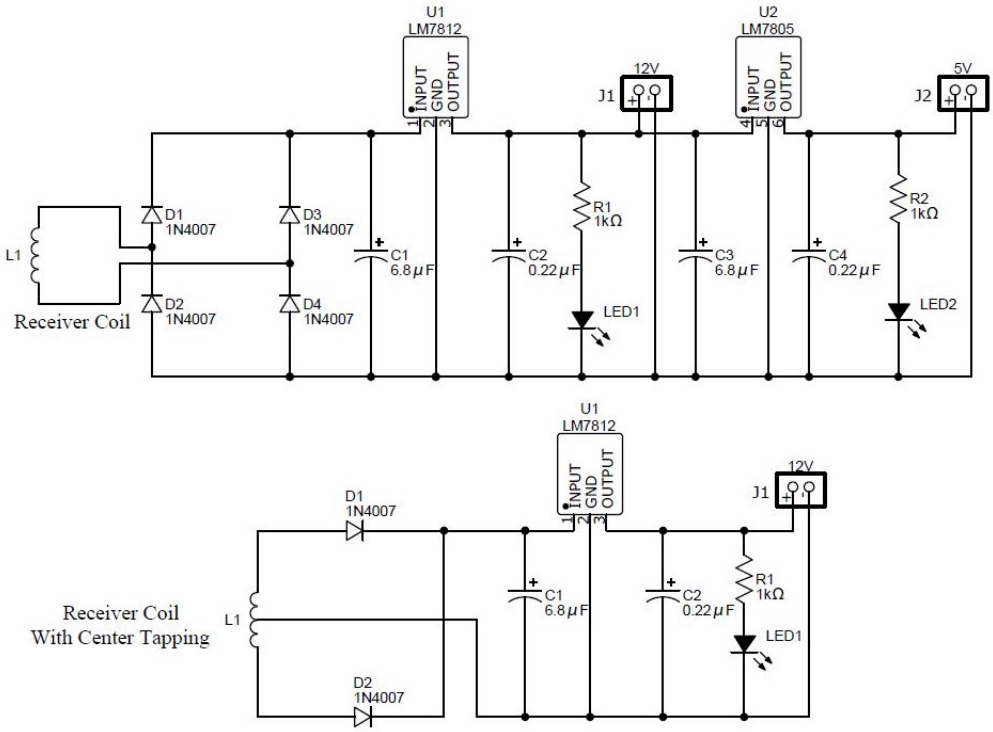

Figure 3.9: Schematic diagram of the receiver rectifier for wireless power transfer

3.1.3.1 Test case

The test case for automatically switching transmitter circuit 1 under aligned operating conditions are as follows,

- The test is carried out with the circular Tx and Rx coils (refer figure 3.10). The positive supply is applied to the center tapping of the Tx coil and the Rx coil is not center tapped.
- The distance between the transmitter coil and the receiver coil is at 50mm and there is no misalignment between the coils.
- The power transmitter board is operating at a switching frequency of 8kHz and supplies 48V to the circular transmitter coil.
- An inductive motor load of 24W is connected to the receiver coil.
- The LC Tank on both the transmitter and receiver board has a parallel resonance.
- The test case for automatically switching transmitter circuit 2 follows the same test case.

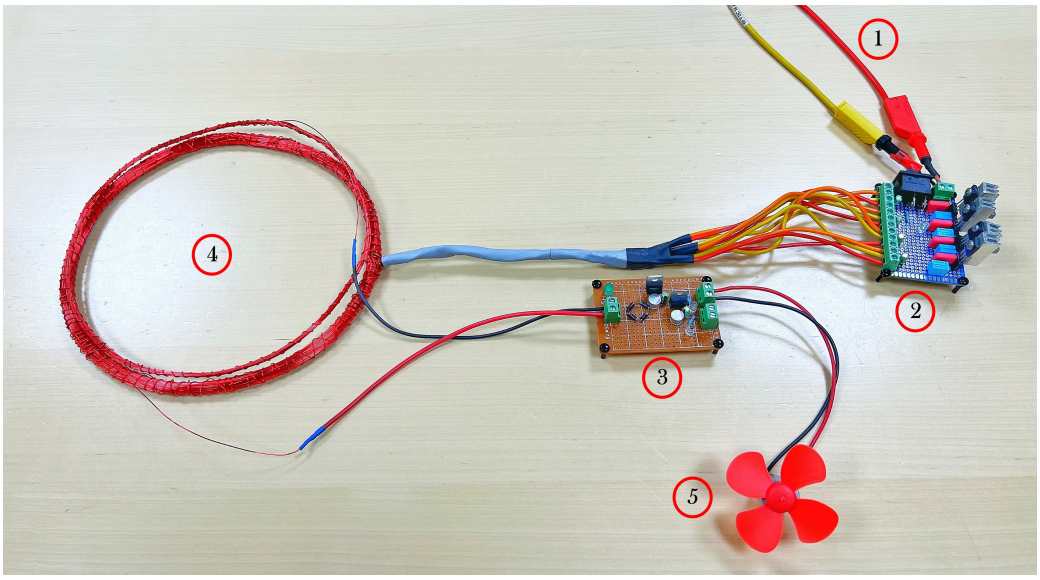

Figure 3.10: Test set-up of 4 parallel center-tapped circular coils

1	Power Supply - 48V DC
2	Transmitter Board
3	Receiver Board
4	Tx and Rx Coils
5	DC Motor

The wireless power system operating under conditions where the circular Tx and Rx coils are tested for the different misalignments. The main objective of this test is to study the induced voltage versus misalignment. The Rx coil of inductance 53μH (circular coil 2) is used to misalign, with the Tx coil. For the

vertical misalignment, the receiver is kept at a 180mm vertical distance from the transmitter, for the lateral misalignment the receiver is 50% (100mm) on the transmitter and for the angular misalignment the receiver is at 40° angle above the transmitter.

3.1.3.2 Point to multi-point power transfer

The main objective of testing the circular coils is to study the point to multipoint power transfer capability of the circular coils with different form factor. The circular coil design has multiple coils which we have used to analyse point to multipoint power transfer. The combination of coils used for this setup are,

- Tx coil - Circular coil 1
- Rx coils - Circular coil 4 & 5

The distance between the transmitter coil and the receiver coil is at 50mm and there is no misalignment between the coils. For driving the centre-tapped Tx circular coil 1, a Tx board with 4 BJTs is used and two 24V DC motors are connected to the Rx circular coil 4 & 5. The LC Tank on both the transmitter and receiver board has a parallel resonance and a corresponding resonant capacitor is used for both the Rx coils.

Table 3.6: Resonant capacitors for circular coils used in point to multi-point power transfer

Coil	Inductance	Resonant Capacitor
Circular Coil 1	555μH	0.7μF
Circular Coil 4	16μH	24μF
Circular Coil 5	1035μH	4μF

3.2 Proposed wireless power system

The main objective of the proposed system is to achieve alignment freedom for the Rx coil in a given space of (15cm x 15cm x 15cm) by generating an electromagnetic field in the space. Additionally, the section aims to investigate suitable coil geometry for Tx. In this section, we utilize different coil geometries on the Tx side and investigate their influence on the magnetic field and coupling. There are two major models in this section where we use concentric coils and series-connected concentric coils as Tx, with a solenoid as Rx for both. From the investigation of different coil geometries for Rx, it is found that the use of a solenoid as Rx has better coupling with the concentric Tx coil under misaligned operation. Hence, concentric coils are connected in series to distribute coil turns into smaller areas to increase coupling with the solenoid Rx coil. The section also presents the half-bridge circuit used to drive the transmitter coils.

3.2.1 Investigation of suitable transmitter coil geometry

This section introduces all the designed coils used in the proposed system and the corresponding coil parameters. There are 2 types of Tx coil geometries investigated namely concentric and series-connected concentric coils. The transmitter and receiver coil geometry combinations are as follows,

- Concentric Tx coil - Concentric Rx coil.
- 2 Series connected concentric Tx coil - Solenoid Rx coil.
- 8 Series connected concentric Tx coil - Solenoid Rx coil.

The coil parameters are measured using Agilent's E4980A Precision LCR Meter with a frequency setting of 800KHz & 1MHz based on the operating frequency of half-bridge transmitter circuit used to drive the coils. Also, the coils are measured without the resonant capacitors connected. Figure 3.11 and table 3.7 show the concentric coils and their parameters respectively. Concentric coil 1 is used as Tx, and concentric coil 2 & 3 are used as Rx. concentric coil 1 & 2 have equal diameters, while concentric coil 3 is smaller in diameter compared to the other two coils.

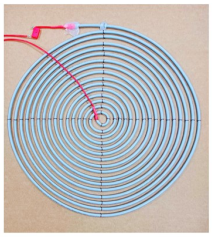

Concentric Coil 1
Inductance - 32µH

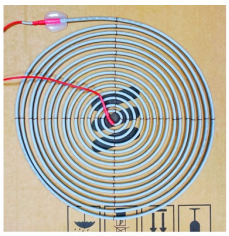

Concentric Coil 2
Inductance - 28µH

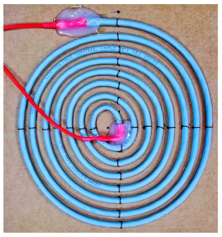

Concentric Coil 3
Inductance – 60nH

Figure 3.11: Custom-built concentric coils wound using cable magnetic wire

Table 3.7: Concentric coil parameters and their corresponding resonant capacitors at a resonant frequency of 800KHz

Coil	Inductance	No. of Turns	DC Resistance	Inductive Reactance	Q Factor	Resonant Capacitor
Concentric Coil 1	32.29μH	15	1.08Ω	161.73Ω	145.75	1.60nF
Concentric Coil 2	27.95μH	15	0.78Ω	140.53Ω	178.56	1.41nF
Concentric Coil 3	59.25nH	7	0.37Ω	25.96Ω	105.35	872.48nF

Figure 3.12 and table 3.10 show the series-connected concentric Tx and solenoid Rx coils and their respective parameters. The dimensions of the series-connected coils and solenoid coils are shown in tables 3.8 and 3.9, respectively. 2 series-connected coils are used to generate a horizontal magnetic field and investigate the possibility of increasing coupling with the solenoid Rx coil. This system is then expanded to 8 series-connected coils on the Tx side to form a space with dimensions of (15 cm x 15 cm x 15 cm). The electromagnetic field generated by the 8 series-connected coils is picked up by the solenoid Rx coil to power a DC lamp load.

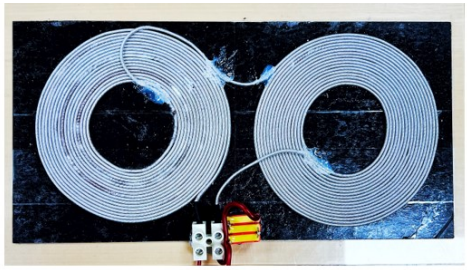

2 Series-Connected Coil
Inductance - 82µH

Solenoid Coil 1
Inductance - 37µH

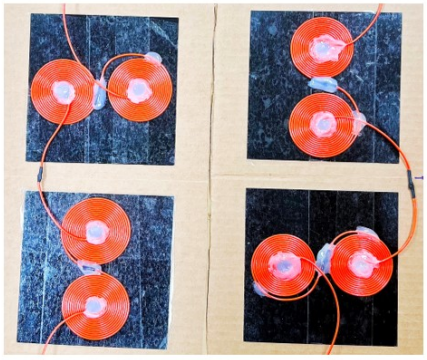

8 Series-Connected Coil
Inductance - 72µH

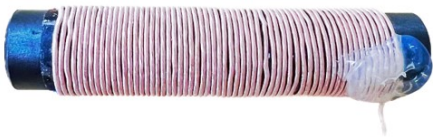

Solenoid Coil 2
Inductance - 160µH

Figure 3.12: Series connected concentric Tx and solenoid Rx coils used in proposed system

Table 3.8: Series connected concentric coil dimensions

Coil	Coil Thickness	Coil Inner Diameter	Coil Outer Diamter	Shielding Thickness
2 Series Connected Coil	1.5mm	45.20mm	105mm	1mm
8 Series Connected Coil	1.5mm	10mm	49.5mm	1mm

Table 3.9: Dimensions of solenoid Rx coils used in proposed system

Coil	Coil Thickness	Coil Inner Diameter	Coil Outer Diameter	Coil Hieght
Solenoid Coil 1	1.5mm	5mm	11.5mm	20mm
Solenoid Coil 2	1.5mm	5.45mm	7.8mm	40mm

Table 3.10: Series connected concentric and solenoid coil parameters and their corresponding resonant capacitors at a resonant frequency of 1MHz

Coil	Inductance	Number of Turns	DC Resistance	Inductive Reactance	Q Factor	Resonant Capacitor
2 Series-connected	81.65μH	46	1.30Ω	0.40Ω	8.32	0.63nF
8 Series-connected	71.90μH	112	0.25Ω	451.75Ω	166.74	0.35nF
Solenoid Coil 1	37.25μH	26	2.33Ω	233.52Ω	101.49	0.68nF
Solenoid Coil 2	160μH	70	0.021Ω	998.12Ω	37.15	0.15nF

3.2.2 800kHz Half bridge converter

The main objective of testing different coils using half-bridge circuit is to increase the operating frequency and voltage of the transmitter circuit. The half-bridge circuit helps in increasing the range and can operate at higher power levels. Going higher in frequency can help to study the effect of frequency on the range, misalignment and power transfer. Figure 3.13 shows the block diagram of the proposed high frequency half bridge Tx circuit and Rx circuit.

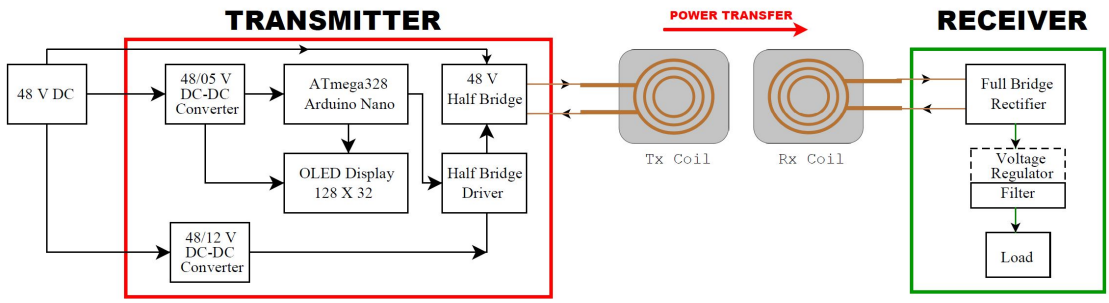

Figure 3.13: Block diagram of proposed 800KHz half bridge transmitter circuit & receiver circuit

Table 3.11 shows the key specification of the proposed half bridge circuit. Table 3.12 and table 3.13 shows the list of components required to build the proposed transmitter and receiver board respectively.

Table 3.11: Key system specification of 800kHz half bridge circuit

Parameters	Specification
Input Voltage	48V DC
Maximum Current	10A
Rectifier Input Voltage	48V AC
Frequency	800kHz
Maximum Power	480W
Coil Distance	10cm

Table 3.12: Components required to build proposed 800kHz half bridge circuit

Sl No	Component	Value
01	Resistors	1kΩ & 1.2kΩ
02	Potentiometer	50kΩ & 1MΩ
03	Inductors	20μH & 100μH
04	Capacitors	100μF, 1000μF, 2200μF & 100nF
05	LED	3mm
06	Zener Diode	1N5822 & MUR460
07	MOSFET	IRF540N
08	MOSFET Driver	IR2184PBF
09	12V Voltage Regulator	LM2576HVT
10	5V Ericsson Flex Converter	PKU4717YA
11	μ Controller	ATmega328 Arduino Nano
12	Display	OLED Display

Table 3.13: Components required to build receiver rectifier circuit

Sl No	Component	Value
01	Diode	ERC84009
02	Inductor	20μH
03	Capacitor	100μF
04	Resistor	1kΩ
05	LED	3mm

Figure 3.15 and 3.16 shows the schematic diagram of the high frequency half bridge Tx and Rx circuits respectively. For explaining the working of the half bridge circuit, 2 MOSFETs with the transmitter tuned inductor and the capacitor section is shown in the figure 3.14,

a) DC power supply of 48V is connected to the drain of the MOSFET(Q1). When the PWM is applied to the gate of the MOSFET(Q1) and MOSFET(Q2)

is off. The current flows through the MOSFET(Q1) and charges the LC tank CTx and LTx.

b) When the MOSFET(Q1) is off the PWM is applied to the MOSFET(Q2). The energy stored in the CTx and LTx is discharged as the MOSFET(Q2) is closed and completes the circuit.

The charging and discharging action of the LC tank creates an alternating magnetic field. This magnetic field is alternating at high frequency according to the frequency set by the PWM. Figure 3.15 has the power circuit and the half bridge circuit. The 48V DC is converted to 5V DC with Ericsson flex converter (series DC-DC converter) to supply the micro-controller and the OLED display. The 48V is converted to 12V DC with a high voltage version of linear voltage regulator - LM2576HVT. The arduino nano is programmed to generate 800kHz at the digital pin D9 where a smoothing resistor R5 is connected. The IC IR2184PBF takes the high frequency PWM from the arduino and then drives the MOSFETs Q1 and Q2. The Tx coil and a resonant capacitor is connected to the drive point to the ground in the circuit where the high frequency at 48V is generated.

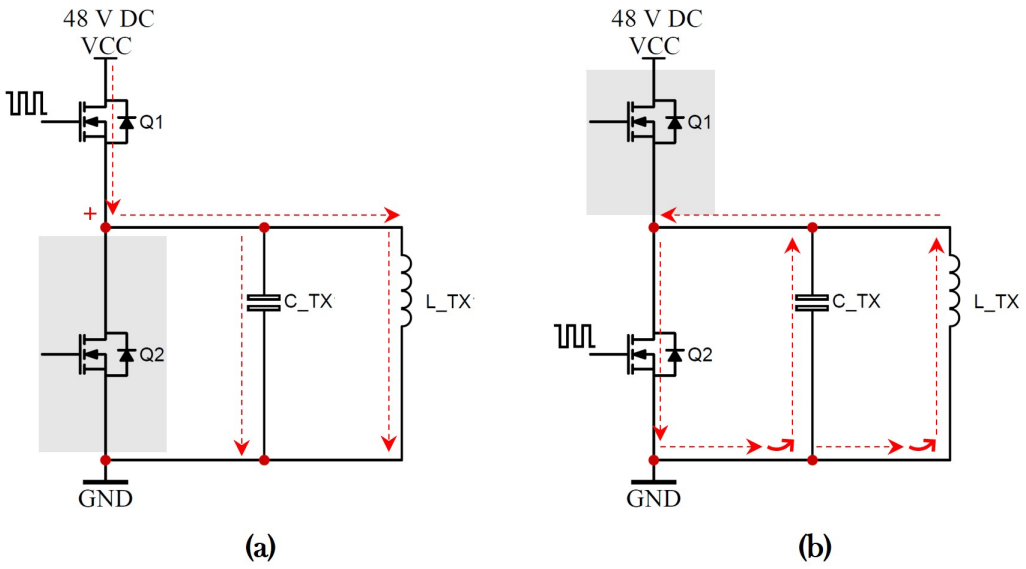

Figure 3.14: Working of proposed half bridge transmitter circuit

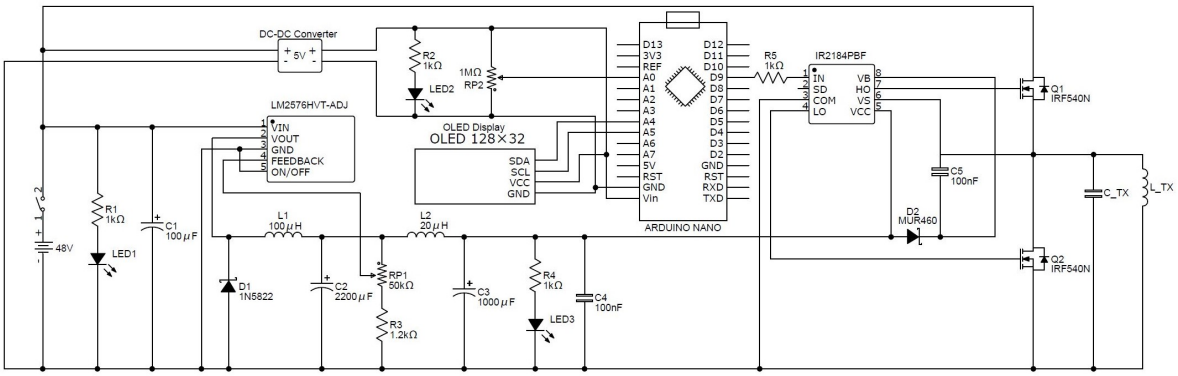

Figure 3.15: Schematic diagram of proposed 800kHz half bridge transmitter circuit

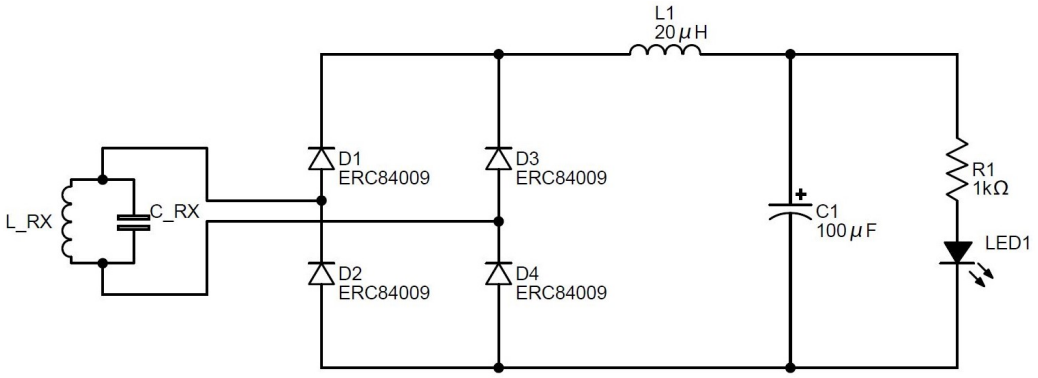

Figure 3.16: Schematic diagram of the receiver rectifier circuit

3.2.2.1 Concentric coils

The concentric coil combination is intended to investigate the possibility of increasing the range and power transfer by increasing the coil diameter. Figure 3.17 shows the test setup of concentric coils 1 & 2 using 800kHz half-bridge converter.

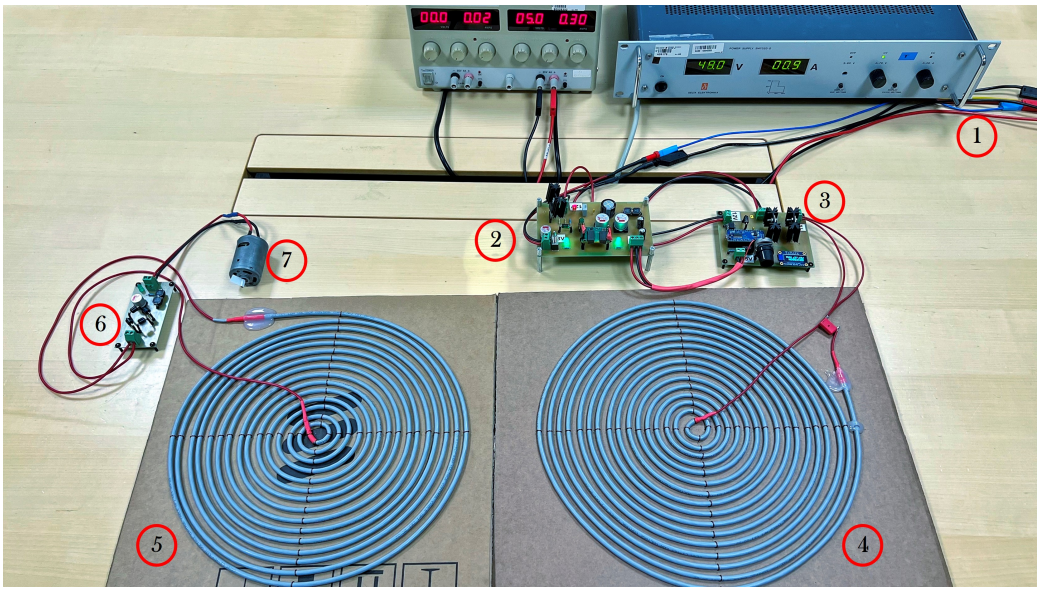

Figure 3.17: Test set-up of concentric coil 1 as Tx & concentric coil 2 as Rx using 800kHz half-bridge converter

1	Power Supply - 48V DC
2	Power Board
3	Transmitter Board
4	Tx Coil
5	Rx Coil
6	Receiver Board
7	DC Motor

The test case for the concentric coils under aligned operating conditions are as follows,

- The distance between the concentric Tx coil 1 and concentric Rx coil 2 is at 17.5cm and there is no misalignment between the coils.
- After testing the concentric Rx coils 2 & 3 under normal operation for the induced voltage, the best coil is selected for misalignment and in this case concentric coil 2 is misaligned.
- The power transmitter board is operating at a switching frequency of 800kHz and supplies 48V to the concentric transmitter coil.
- A 50W motor is connected to the receiver coil as load.
- The changing coils on the Tx and Rx boards change the resonant frequency of the LC Tank and hence a suitable tuned capacitor is used for each coil to maintain the system resonant frequency at 800KHz.
- The LC Tank on both the transmitter and receiver board has a parallel resonance.

The test case for the concentric coils under misaligned operating conditions has a value for the vertical misalignment, the receiver is kept at a 180mm vertical distance from the transmitter, for the lateral misalignment the receiver is 50% (100mm) on the transmitter and for the angular misalignment the receiver is at 40° angle above the transmitter. The voltage and current plots of the Tx and Rx coils are measured at the input terminal of the receiver board.

3.2.2.2 2 Series-connected concentric coils

Figure 3.18 shows the test set-up of 2 series-connected concentric Tx coil & solenoid Rx coil 1 using 800kHz half-bridge converter. The test case for the 2 series connected concentric coils under aligned operating conditions are as follows,

- The test is carried out with 2 series-connected concentric coil as Tx coil and solenoid coil 1 as Rx coil.
- The distance between 2 series-connected concentric Tx coil and solenoid Rx coil 1 is at 30mm and there is no misalignment between the coils.
- The power transmitter board is operating at a switching frequency of 800kHz and supplies 48V to the concentric transmitter coil.
- A DC load of 10W is connected to the receiver coil.
- The LC Tank on both the transmitter and receiver board has a parallel resonance.

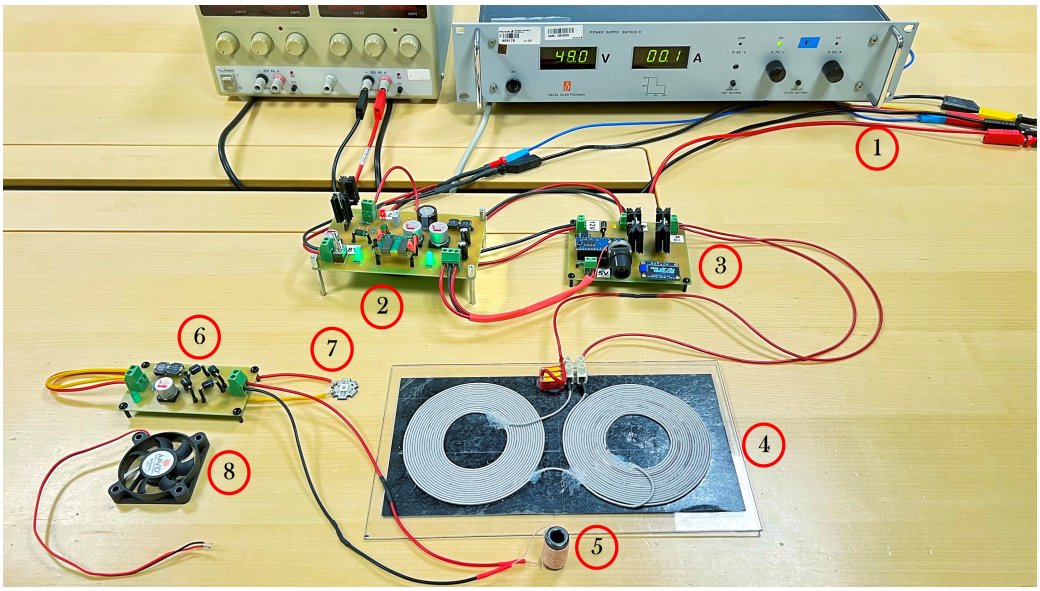

Figure 3.18: Test set-up of 2 series-connected concentric Tx coil & solenoid coil 1 as Rx using 800kHz half-bridge converter

1	Power Supply - 48V DC
2	Power Board
3	Transmitter Board
4	Tx Coil
5	Rx Coil
6	Receiver Board
7	LED
8	DC Motor

The test case for 2 series-connected concentric coils under misaligned operating conditions has a value for the horizontal and vertical rotation 180° at a distance of 30mm. The voltage and current plots of the Tx and Rx coils are measured at the input terminal of the receiver board.

3.2.3 1MHz half-bridge converter

Infineon half-bridge converter board is used to drive 8 series-connected concentric transmitter coil to demonstrate the equal distribution of magnetic field in a given space of (15cm X 15cm X 15cm). The Infineon converter is a GaN based half-bridge circuit with dedicated gate driver ICs and isolated power supplies for the gate drivers. The board consists of a half-bridge of GaN power transistors, GaN gate driver ICs, power supply for gate drivers, and input logic to adjust the deadtime. The converter can be configured to operate in either buck or boost mode by connecting an external inductor. The half-bridge converter board is shown in figure 3.19. The specifications of the Infineon half-bridge converter board is shown in table 3.15.

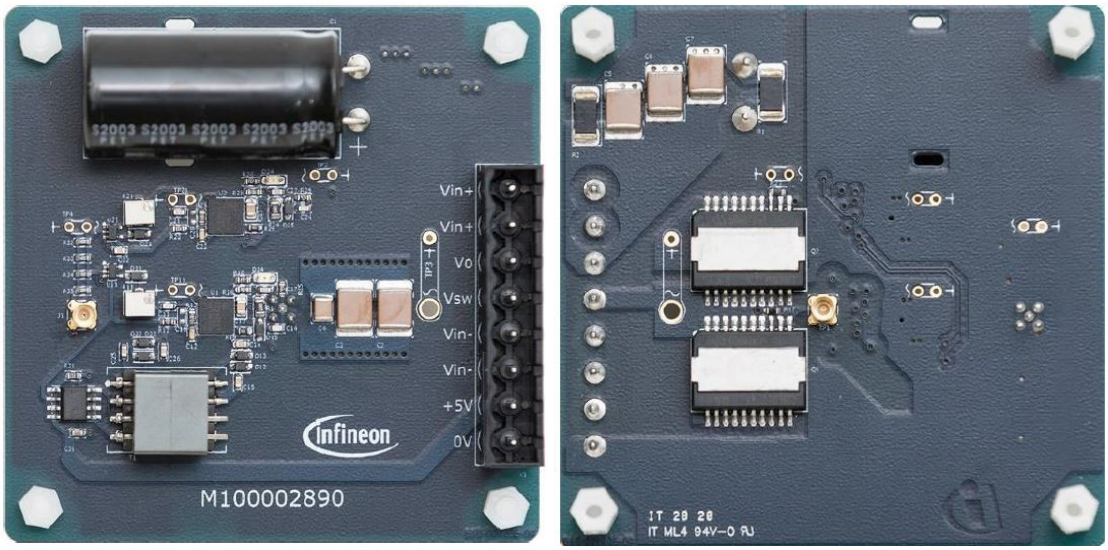

Figure 3.19: Front & back view of Infineon's GaN based half-bridge converter

The block diagram of half-bridge converter board setup is shown in figure 3.20. Table 3.14 has the list of equipment required for series connected coils using Infineon's GaN based half-bridge converter test setup. The transmitter block has 48V DC line power supply for the half bridge and 5V DC is supplied as the board power which supplies control and logic circuits. In the board power supply of 5V, the current is limited to 250mA as the high current flow may destroy the control and logic ICs. The parameters in the signal generator are set according to the table 3.16 and then connected to the board by a 50Ω MMCX coaxial connector. The circuit connection and the terminals in the Infineon's GaN based half-bridge converter is as shown in the figure 3.20. The Tx coil is connected to the V_o and V_{sw} of the Infineon's GaN based half-bridge converter which refers to the inverted double-pulse test from the data sheet (Infineon datasheet). The receiver coil is a solenoid and is directly connected to an LED to demonstrate the concept of the equal distribution of electromagnetic field in a space. Table 3.15 lists the specifications for GaN based half-bridge converter.

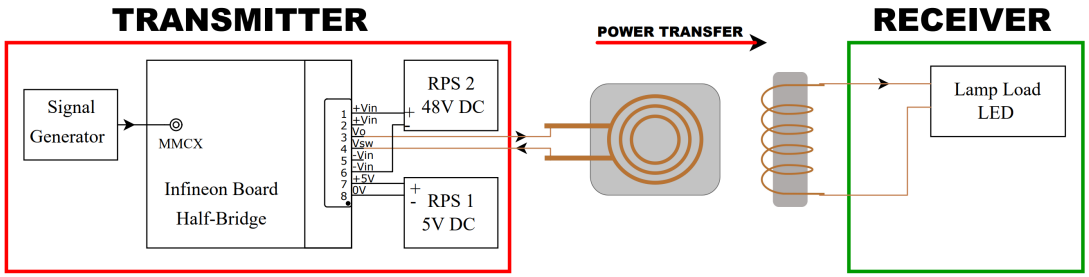

Figure 3.20: Block diagram of proposed wireless power system with 8 series connected concentric transmitter coil

Table 3.14: Equipment required for series connected coils using Infineon's GaN based half-bridge converter test setup

Equipment Required	Specification
Signal Generator	2MHz
Coaxial Connector	50Ω MMCX
DC Power Supply	5V, 48V
Infineon's Half Bridge	GaN based

Table 3.15: Specifications for GaN based half-bridge converter obtained from Infineon datasheet

Parameters	Specifications
Board Input Voltage	5V
Board Input Current	50 - 250mA
PWM Input Level	5V
Half-bridge Input Voltage	0 - 450V
Half-bridge Maximum Current	35A
Operating Frequency	≤ 3 MHz
Deadtime Adjustment Range	0 - 180ns

Table 3.16: List of parameters for signal generator in the case setup of series connected concentric Tx and solenoid Rx

Parameters	Value
Frequency	1MHz
Amplitude	3 Vpp
Offset	1.6 V
Phase	0°
Duty Cycle	50%

The half-bridge converter is configured to be operated in buck topology to drive 8 series connected concentric transmitter coil as shown in figure 3.21 and the procedure to set-up the board is listed below,

- A DC power supply unit is used to provide 5V input voltage and 100mA current as power supply to the circuit. This provides power supply to the board including the gate driver circuits.
- The PWM input signal is provided by a signal generator. The board has a dedicated connection J1 that is terminated by 50Ω MMCX coaxial connector for PWM input that can be connected using a BNC male to MMCX plug cable. A square wave signal of 3V at a frequency of 1MHz is supplied from the signal generator.

- Bus voltage supply up to 450V DC with sufficient current to supply the power needed for the load can be connected between V_{in+} and V_{in-} in pluggable terminal block X1. In this case, the bus voltage is set to 48V with maximum current of 10A to supply the series connected transmitter coils.

- The load in our case is the series connected coils which is connected between the V_{SW} and V_o in terminal block X1. This connection enables the circuit to operate in buck mode.

- In buck mode, the voltage applied to the coil will be proportional to the input voltage times the PWM duty-cycle.

- All the input and output connections to the board are made to the pluggable terminal block X1 except the connection for PWM signal that is made using a coaxial cable.

- The deadtime circuit is used to ensure that the high side and the low side GaN transistors are never turned on simultaneously. In this case, the deadtime is kept at default setting of 100ns.

3.2.3.1 8 Series-connected concentric coils

The Infineon's half-bridge converter board is used to drive the 8 series-connected transmitter coil. In this test case, as the Tx and Rx coils have different coil geometries, the misalignment is done by rotating the Rx solenoid coil 180° vertically and horizontally in the given space of (15cm X 15cm X 15cm). Figure 3.21 shows the test set-up of 8 series-connected concentric Tx coil & solenoid Rx coil 2 using Infenion's converter.

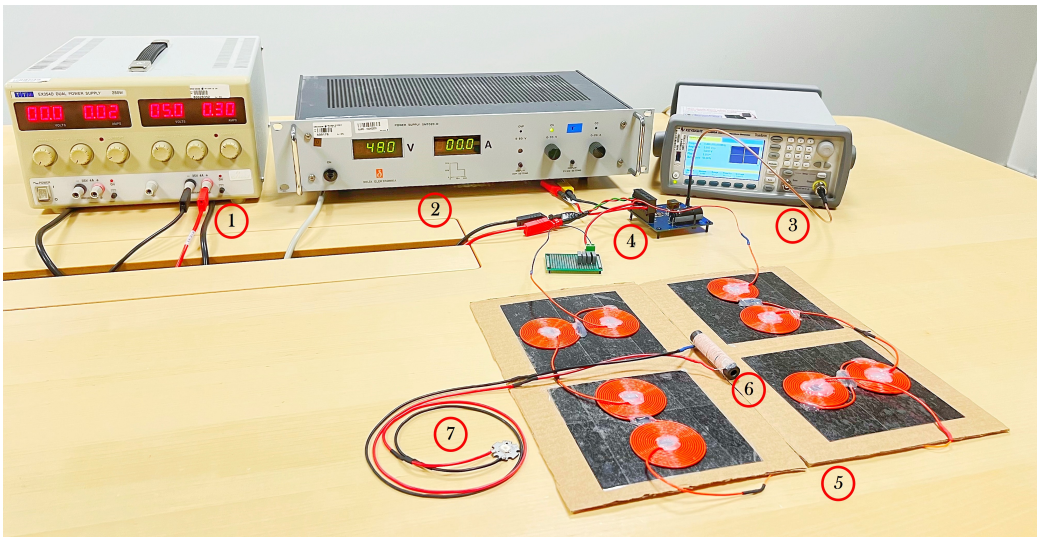

Figure 3.21: Test set-up of 8 series-connected concentric coil as Tx & solenoid coil 2 as Rx using Infenion's converter

1	Auxiliary Supply - 5V DC
2	Power Supply - 48V DC
3	Signal Generator
4	Transmitter Board
5	Tx Coil
6	Rx Coil
7	LED Load

The test case for 8 series-connected concentric Tx coils and solenoid Rx coil 2 under aligned operating conditions are as follows,

- The distance between the Tx coil and Rx coil is at 15cm.
- The Rx coil is tested for both vertical and horizontal rotation in a test space of (15cm X 15cm X 15cm).
- The power transmitter board is operating at a switching frequency of 1MHz and supplies 48V to the series connected concentric Tx coil.
- A load of 10W is connected to the receiver coil.
- The LC Tank on both the transmitter and receiver board has a parallel resonance.

4

Simulation Setup

In this project, we utilize the finite element method(FEM) software known as Ansys Maxwell to model a range of wireless power transfer setups. The aim is to conduct a comprehensive FEM analysis, which serves two main purposes; validating experimental measurements and investigating the influence of coil parameters and coil geometry on the coupling factor (k) and magnetic field distribution.

The models are verified against the analytical calculations and experimental measurements. The FEM models are designed to calculate the inductance and resistance of coils, coupling factor between Tx and Rx coils, determine the magnetic field density produced by the coils, and evaluate the induced voltage in the Rx coil during wireless power transfer operations. The solution types 'Electrostatic' and 'Magnetostatic' were used to analyse the 3D models in FEM software.

All the wireless power transfer set-ups modelled in the Ansys Maxwell consists of two coils, a transmitter coil and a receiver coil. Multiple models of different coil geometries are simulated in Ansys Maxwell, however only the set-ups that are used to evaluate the experimental measurements and analytical calculations are presented in this chapter.

4.1 Modelling of different coil geometries in Ansys

The concentric and solenoid receiver coil geometries used with concentric transmitter coil is modelled in Ansys as shown in figure 4.1 and figure 4.2 respectively. To emulate the WE concentric coil as shown in figure 3.1, a single turn 3D cylinder is used with stranded terminals to replicate turns on the concentric coil. The coil and shielding dimensions are set according to the measured dimensions. Similarly, the solenoid Rx coil with hollow core as shown in figure 3.1 is emulated using 3D cylinder that is extruded vertically to form a solenoid structure. The number of turns on the solenoid is set using stranded terminals.

Ansys maxwell uses FEM to solve Maxwell's equations and in order to solve these equations, the 3D geometry of the model needs to discretized in to smaller blocks. The classic mesh set-up is used for both the models as the transmitter in both the models is thin and flat which generates coarse mesh at the beginning and refines the mesh at the edges. To further refine the mesh on coils and ferrite shielding

or core, skin depth based mesh operation is utilized that allows to calculate skin depth based on the operating frequency of 205kHz.

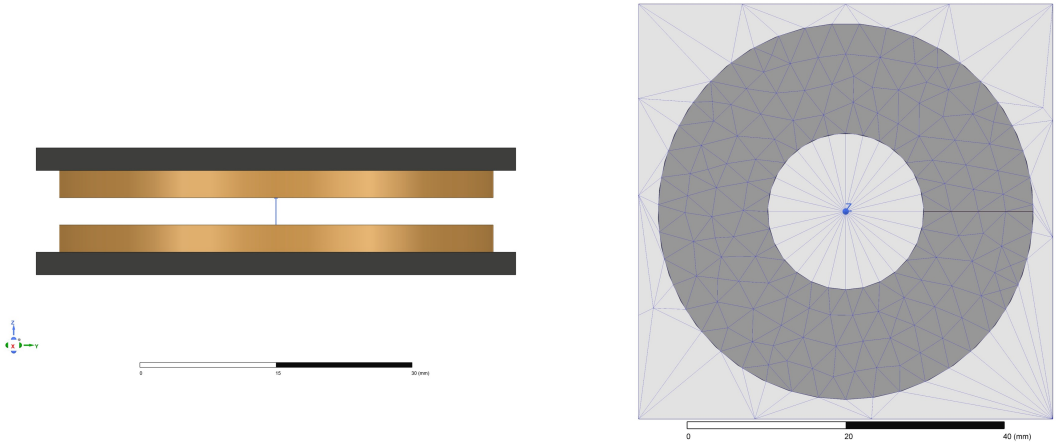

Figure 4.1: The 3D model and mesh plot of the WE concentric Tx & Rx coils with ferrite shielding

Table 4.1: Mesh statistics for WE concentric coils with ferrite shielding

Mesh Statistics	Coils	Shielding	Boundary
Mesh Type	Classic		
Refinement	Skin Depth	Skin Depth	Length Based
Skin Depth	0.093mm	0.093mm	NA
Layers	2	2	NA
Total Number of Elements	173284		

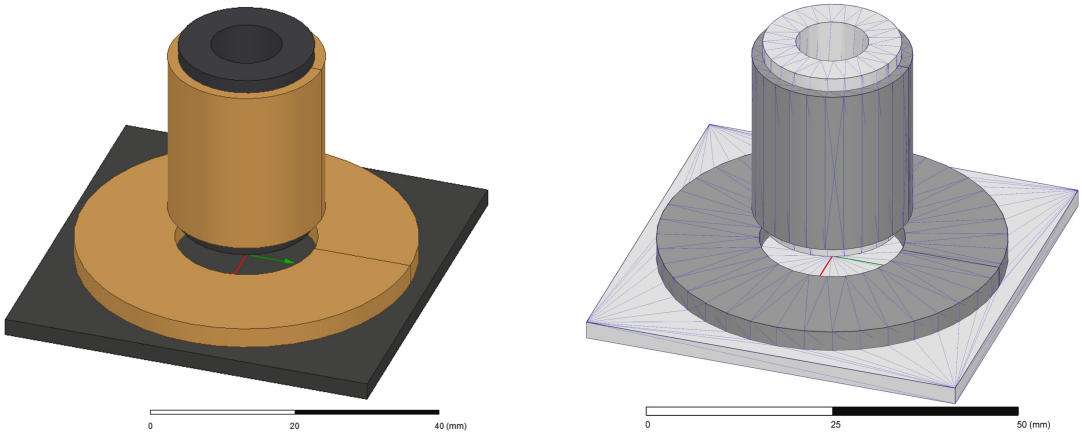

Figure 4.2: The 3D model and mesh plot of the WE concentric Tx coil with ferrite shielding and solenoid Rx coil with hollow core

Table 4.2: Mesh statistics for WE concentric coil with ferrite shielding and solenoid coil with hollow core

Mesh Statistics	Coils	Core	Boundary
Mesh Type	Classic		
Refinement	Skin Depth	Skin Depth	Length Based
Skin Depth	0.145mm	351.51mm	NA
Layers	2	2	NA
Total Number of Elements	38217		

After designing the models in Ansys Maxwell 3D, the lumped models are simulated using magneto static and electrostatic solver. The coils are excited using DC current and hence the magneto static solver helps to solve static magnetic fields and to determine magnetic field distribution. While electrostatic solver is used to determine the induced voltage is receiver coil.

The excitation current is applied to the coils by splitting the geometry into two and assigning current to one face of the coil in magneto static solver to determine self-inductance, mutual inductance, and coupling coefficient between the transmitter and receiver coil. The analysis set-up is used to assign number of passes which is set to 20 with a percentage error of 10%. The operating frequency of 205kHz is also set in the analysis set-up. The simulation results for misaligned operation is obtained using optimetrics set-up where linear sweep for change in distance between the transmitter and the receiver is set to measure the values at various steps.

4.2 Modelling of point to multi-point power transfer using circular coils in Ansys

The different circular coils used in the point to multi-point power transfer is modelled in Ansys as shown in figure 4.3. The simulation set-up consists of one transmitter and two receiver coils to demonstrate point to multi-point power transfer capability of circular coils. To emulate the circular coils as shown in figure 3.2, a torus geometry is utilized to model the circular coils in Ansys. The number of turns in the coils is set using the stranded coil option in the excitation field. It is to be noted here that there is no center tapping on the coils in the simulation set-up as it will make the model complex and assigning current excitation becomes difficult.

The Tau mesh set-up is used to descretize the circular coil model. The Tau mesh option is a strict mesher suitable for curved surfaces and generates mesh more accurately. To further refine the mesh on the circular coils, skin depth based mash operation is utilized to calculate skin depth based on the operating frequency of 8kHz.

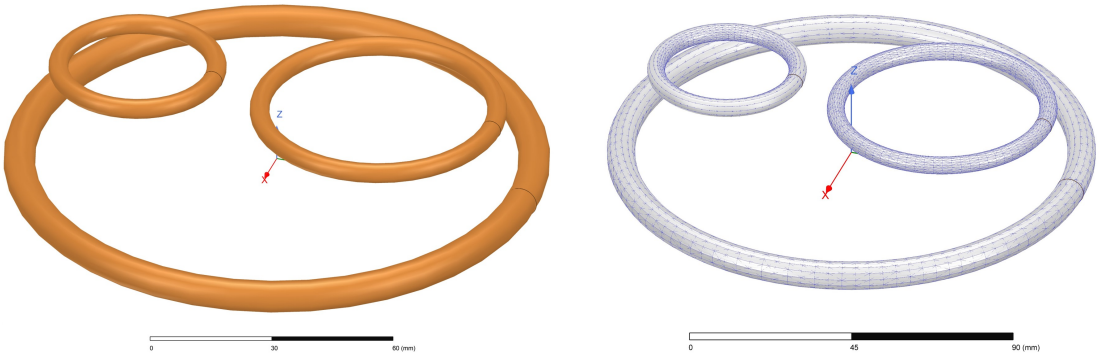

Figure 4.3: The 3D model and mesh plot of the custom built circular coils

Table 4.3: Mesh statistics for custom built circular coils

Mesh Statistics	Coils	Boundary
Mesh Type	Tau	
Refinement	Skin Depth	Length Based
Skin Depth	0.176mm	NA
Layers	2	NA
Total Number of Elements	250835	

After designing the model in Ansys Maxwell 3D, the lumped model is simulated in both magneto static and electrostatic solver to determine magnetic field distribution and induced voltage respectively. The operating frequency is set to 8kHz and the number of passes is set to 20 with a percentage error of 10% in the analysis set-up.

4.3 Modelling of proposed wireless power system in Ansys

The proposed wireless power systems namely consists of the custom built concentric coils and series connected concentric coils as shown in figure 3.11 and figure 3.12 respectively are modelled in Ansys Maxwell. All the models in this section are simulated using magneto static and electrostatic solvers. The self-inductance, mutual inductance,coupling coefficient between the transmitter and the receiver, and magnetic field distribution is calculated using the magneto static solver. The induced voltage in the receiver coil is calculated using the electrostatic solver. For all the three models, the analysis set-up is set with 20 number of passes with a percentage error of 10%. The operating frequency is set to 800kHz for custom built concentric coils and 2 series connected concentric coil. While the operating frequency for 8 series connected concentric coil is set to 1MHz.

4.3.1 Custom built concentric coils

The custom built concentric coil are modelled in Ansys as shown in figure 4.4 using cylindrical geometry and the number of turns on the coil are represented using stranded conductors. The dimensions of the model are set according to the measured dimensions of coils.

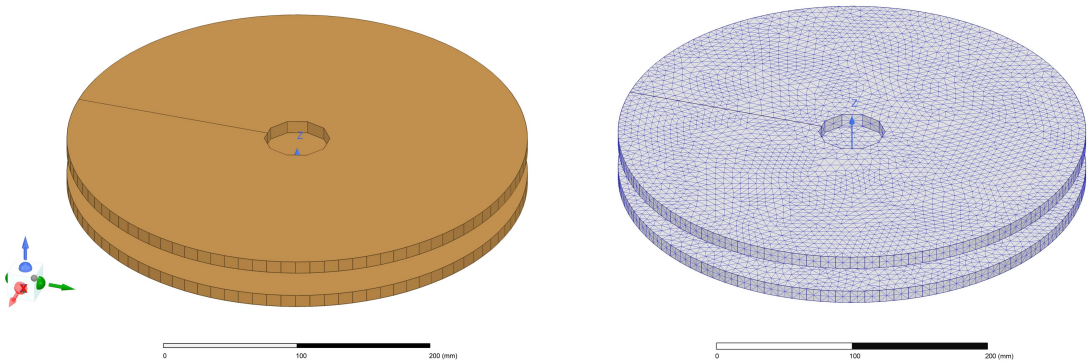

Figure 4.4: The 3D model and mesh plot of the custom built concentric coils

Table 4.4: Mesh statistics for custom built concentric coils

Mesh Statistics	Coils	Boundary
Mesh Type	Auto	
Refinement	Skin Depth	Length Based
Skin Depth	0.073mm	NA
Layers	2	NA
Total Number of Elements	896526	

In this model the mesh settings is set to auto as the coil geometry is thin and flat. It is important to generate a good mesh for problems with a high frequency where the skin effect in the conductor is to be modelled. Hence, the auto mesh type discretizes the model accurately to solve the Maxwell's equations. The mesh is refined using skin depth meshing for the operating frequency of 800kHz.

4.3.2 Series connected concentric coils

The series connected concentric coils with solenoid coil as shown in figure 3.12 is emulated using spiral geometry for series connected concentric coils and cylindrical geometry for solenoid coil. The dimensions of the transmitter and receiver coil are set according to the measured dimensions. The 3D models and mesh plots are shown in figure 4.5 and 4.6. Both the models are simulated using Tau mesh to generate meshing on the curved surfaces more accurately. Further the mesh is refined using skin depth refinement set to 800kHz for 2 series connected model and 1MHz for 8 series connected model. The excitation current to the series connected concentric coils is applied by adding winding to the coil and then assigning terminals to each winding.

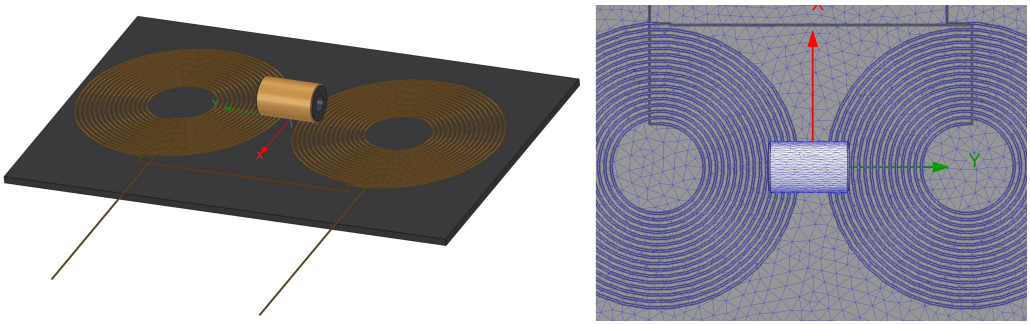

Figure 4.5: The 3D model and mesh plot of the 2 series connected concentric coil with ferrite shielding and solenoid coil with hollow core

Table 4.5: Mesh statistics for 2 series connected concentric coil and solenoid coil

Mesh Statistics	Coils	Core	Shielding	Boundary
Mesh Type	Tau			
Refinement	Skin Depth	Skin Depth	Skin Depth	Length Based
Skin Depth	0.073mm	0.135	151.21mm	NA
Layers	2	2	2	NA
Total Number of Elements	1711391			

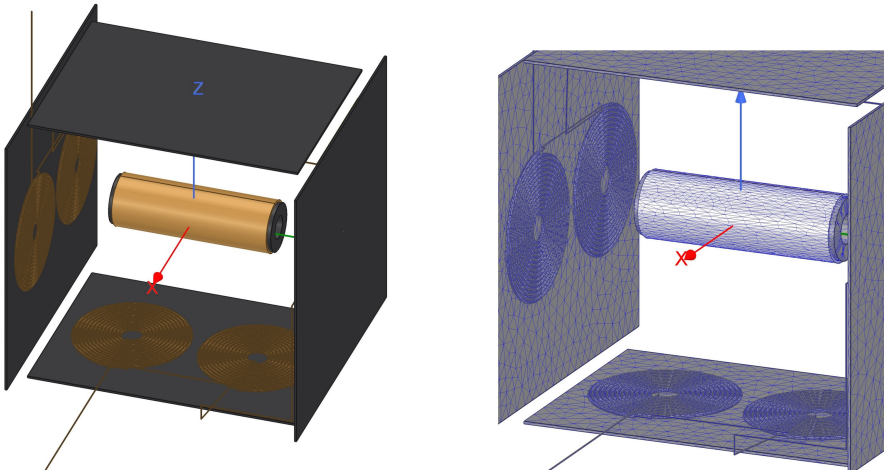

Figure 4.6: The 3D model and mesh plot of the 2 series connected concentric coil with ferrite shielding and solenoid coil with hollow core

Table 4.6: Mesh statistics for 8 series connected concentric coil and solenoid coil

Mesh Statistics	Coils	Core	Shielding	Boundary
Mesh Type	Tau			
Refinement	Skin Depth	Skin Depth	Skin Depth	Length Based
Skin Depth	0.073mm	159.15mm	0.073mm	NA
Layers	2	2	2	NA
Total Number of Elements	2033755			

5
Analysis

5.1 Investigation of suitable receiver coil geometry

In this section different Rx coil geometries are analysed to utilize most suitable Rx coil geometry for the proposed wireless power system. The plots in figure 5.1 & 5.2 show the voltage & current waveforms across the WE Tx & Rx coils respectively. The initial spike in the Tx coil is due to the charging & discharging of voltage across the LC tank. The reduction of amplitude in the Rx coil is due to leakage flux & the loose coupling. The Rx plot is distorted because of a mismatch in LC tank tuning which induces a harmonic in the circuit.

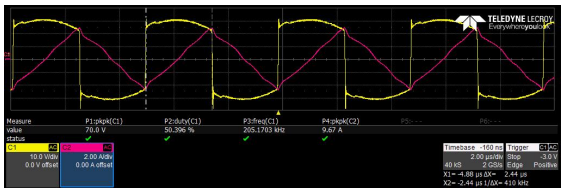

Figure 5.1: Voltage and current plot across the Tx coil under aligned operation for WE development kit

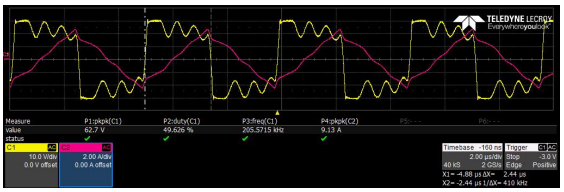

Figure 5.2: Voltage and current plot across the Rx coil under aligned operation for WE development kit

Table 5.1 shows the measurement data for different load conditions under aligned operation which helps in the performance evaluation for the different load impedance characteristics of the WE development kit. It can be seen that the efficiency reduces with an increase in load resistor value this is because it effectively presents a larger impedance to the receiver coil. According to the voltage division rule, a larger portion of the transmitted voltage drops across the load resistance, leading to a reduced voltage across the receiver coil and less power being transferred to the load.

Table 5.1: Measurement data for different load conditions under aligned operations for WE development kit

Load Resistor	Supply Voltage (V_S)	Supply Current (I_S)	Supply Power (P_S)	Load Voltage (V_L)	Load Current (I_L)	Load Power (P_L)	Efficiency
6.8Ω	24V	3.41A	81.84W	22.16V	3.22A	71.35W	87.18%
27Ω	24V	0.91A	21.84W	22.56V	0.83A	18.72W	85.73%
220Ω	24V	0.2A	4.8W	22V	0.1A	2.2W	45.83%

Table 5.2 shows the measurement data for the WE development kit under misaligned operation. When there is a misalignment between the coils the power transfer reduces drastically as the resonant peak shifts either to the inductive or capacitive side. Among the three misalignments, the angular misalignment presents the least power transfer followed by the lateral & vertical misalignments. At some point in the range, during VMA, if the Rx coil goes out of the transmitter boundary the Tx & Rx will be disconnected and there will be no power transfer.

Table 5.2: Measurement data for WE development kit under misaligned operation

Type of Misalignment	Misalignment Value	Voltage (V_{rms})	Current (I_{rms})	Power (P_L)	Efficiency
Aligned	10mm from Tx	22.16	3.22	71.35W	87.18%
Vertical	30mm from Tx	6.78	0.73	4.94W	6.04%
Lateral	50%(26.75mm) on Tx	6.29	0.60	3.77W	4.61%
Angular	40° angle above Tx	4.52	0.35	1.58W	1.93%

The concentric Tx & Rx coils used in the WE development kit are simulated using FEM & the plot for magnetic field density is shown in figure 5.3. The Tx & Rx coils are excited with measured rated current of $I_{Tx} = 3.41A$ and $I_{Rx} = 3.22A$ respectively. The maximum Mag_B is found to be 1.57mT at the center of the two coils. The Mag_B gradually reduces towards the outer edge of the coils. The shielding blocks the flux above & below, helps in confining the magnetic flux between the coils, prevents the flux from escaping outside & helps in reducing the reluctance of the magnetic path.

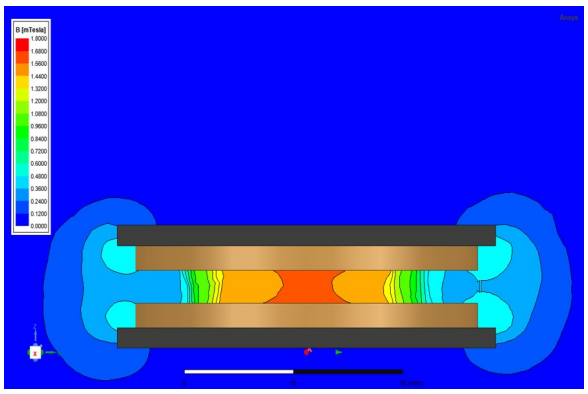

Figure 5.3: *B*-field distribution of WE development kit

5.1.1 Solenoid Rx coil

The distortions in the waveforms start as soon as there is a misalignment between the coils, affecting the magnetic coupling and leading to less efficient power transfer. The distortion tries to stabilize when the power transfer reaches a new equilibrium state corresponding to the new alignment. However, this new equilibrium state is less efficient than the original state when the coils were perfectly

aligned. The voltage & current plots follow the same trend as WE development kit coils. However, the power transfer for misalignment values is much better in solenoid coil as shown in table 5.3. As solenoid coil has a core and is wound using litz wire has a better power transfer and efficiency compared to other coils.

Table 5.3: Measurement data for WE development kit with solenoid coil as Rx under misaligned operation

Type of Misalignment	Misalignment Value	Voltage V (V_{rms})	Current A (I_{rms})	Power W (P_L)	Efficiency (%)
Aligned	10mm from Tx	17.78	1.21	21.51	26.28
Vertical	30mm from Tx	6.11	0.41	2.50	3.06
Lateral	50%(26.75mm) on Tx	5.30	0.44	2.33	2.84
Angular	40° angle above Tx	3.86	0.54	2.08	2.54

The plot for magnetic field density of WE concentric Tx and solenoid Rx coil is shown in figure 5.4. The Tx and Rx coils are excited with measured rated current of $I_{Tx} = 3.41A$ and $I_{Rx} = 1.21A$ respectively. The maximum simulated magnetic field density is found to be 1.23mT at the centre of the two coils as the magnetic flux is concentrated inside the solenoid Rx with a hollow core. The magnetic field density gradually reduces towards the outer edge of the two coils and reduces drastically below the Tx shielding.

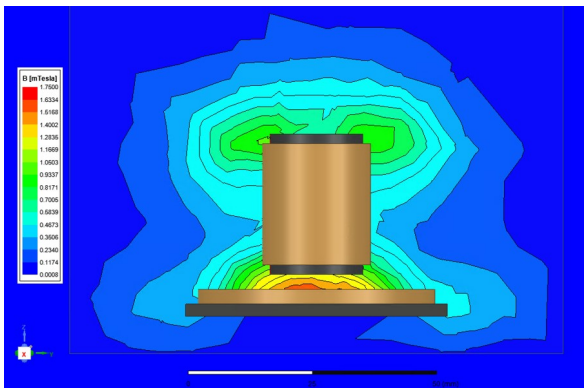

Figure 5.4: *B*-field distribution of WE development kit with solenoid coil as Rx

Table 5.4 shows the comparison of measured, analytical & simulated parameters for coil. The higher values of self-inductance & coil resistance in the measured & analytical columns indicate that there are some parasitic effects in the actual system that are not accounted for in the simulation model. These effects are due to the coil geometry, the wire material, the air gap & the surrounding environment. The lower values of mutual inductance & coupling coefficient in the analytical column suggest that the calculations assume ideal magnetic coupling between the coils, uniform flux distribution, & negligible leakage flux.

Table 5.4: Comparison of measured and simulated parameters for WE development kit with solenoid coil as Rx

Parameters	Measured	Analytical	Simulation
Self-Inductance Tx	5.8μH	4.88μH	5.42μH
Self-Inductance Rx	123.25nH	118.21nH	126.23nH
Coil Resistance	115.15mΩ	110.20mΩ	105.89mΩ
Mutual Inductance (M)	NA	0.34μH	0.38μH
Coupling Coefficient (k)	NA	0.44	0.45
Magnetic Field Density (B)	NA	1.16mT	1.23mT

5.1.2 Circular Rx coil

In this section, we have used center-tapped circular coils to analyze the power transfer, range & coupling of circular coils and to investigate if center-tapped circular coil can be used as Tx and Rx in wireless power systems. The circular coil is driven using the BJT circuit, which generates a duty cycle of around 90% at 8kHz as shown in figure 5.5. The initial spike in the voltage is due to the charging of the base capacitor connected across the center-tapping of the circular coil. A high-duty cycle indicates that the coils are active for most of the time, potentially leading to more efficient power transfer under aligned & misaligned operation as shown in the table 5.5 & the efficiency is shown in the table 5.6.

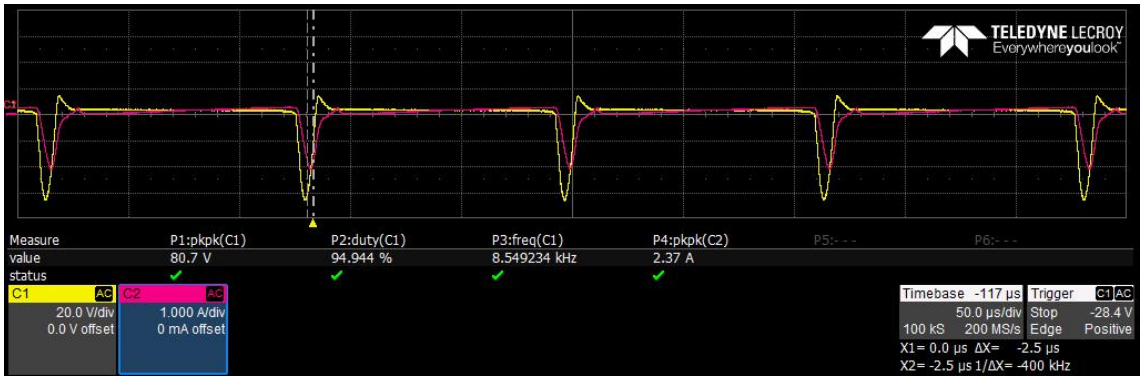

Figure 5.5: Voltage & current plot across the circular receiver coil 2 under normal operation between the Tx & Rx coils

Circular coil 2 is used to misalign, the power transfer & efficiency are better compared to other coils. This is because of the larger diameter of the coil which gives better coupling & range for circular coils as it has more uniform magnetic field distribution compared to other coil shapes, which helps in efficient magnetic coupling. Circular coil 2 has more turns compared to circular coil 4 & 5 which enables more power transfer & strong coupling. Due to the power losses in coils at high frequencies, the magnetic wire wound circular coils are not recommended for wireless power transfer.

Table 5.5: Voltage & current measurements for different center-tapped circular coils under aligned and misaligned operation

Coil	Type of Misalignment	Misalignment Value	Voltage V (V_{rms})	Current A (I_{rms})	Frequency (kHz)
4 Parallel Center-tapped Circular Coil					
Circular Coil 2	Aligned	50mm from Tx	28.53	0.83	8.54
	Vertical	180mm from Tx	26.16	0.58	8.49
	Lateral	50%(100mm) on Tx	24.74	0.50	9.02
	Angular	40° angle above Tx	23.58	0.39	8.38
2 Parallel Center-tapped Circular Coil					
Circular Coil 4	Aligned	20mm from Tx	19.44	1.07	136.01
Circular Coil 5	Aligned	20mm from Tx	20.50	0.96	133.12

Table 5.6: Power transfer & efficiency for different center-tapped circular coils

Coil	Type of Misalignment	Power W (P_L)	Efficiency (%)
4 Parallel Center-tapped Circular Coil			
Circular Coil 2	Aligned	26.67	31.01
	Vertical	15.17	19.88
	Lateral	12.37	16.20
	Angular	9.19	12.04
2 Parallel Center-tapped Circular Coil			
Circular Coil 4	Aligned	28.80	58.33
Circular Coil 5	Aligned	19.68	55.20

The FEM model and plot for magnetic field density of circular Tx(Circular Coil 1) and Rx(Circular Coil 2) is shown in figure 5.6. The Tx and Rx coils are excited with measured rated current of $I_{Tx} = 1.69A$ and $I_{Rx} = 0.96A$ respectively. The maximum simulated magnetic field density is found to be 1.35mT between the coil turns of Tx and Rx as the magnetic flux is concentrated around the coil turns in the circular coils unlike concentric coils where the magnetic field is distributed. The magnetic field density is considerably lower at the center and gradually reduces towards the outer edge of the two coils.

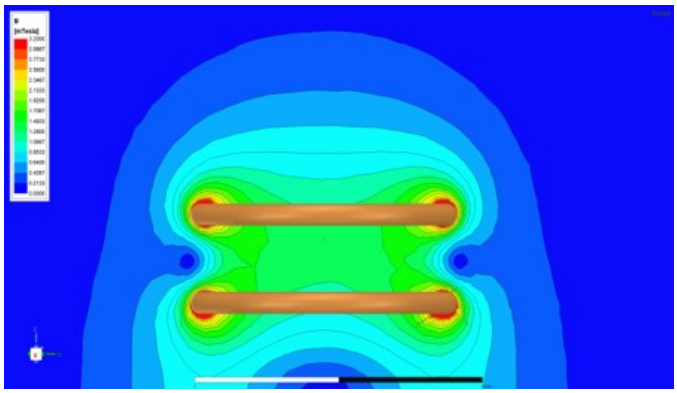

Figure 5.6: *B*-field distribution of between center tapper circular coils

5.1.3 Comparison of Rx coil geometries

This section compares and analyzes various coil geometries for investigating suitable Rx coil for the proposed wireless power system in terms of coupling coefficient and magnetic field density under different misaligned conditions. Plots illustrate how the coupling factor and *B*-field density change with misalignment for different Rx coil geometries. Three scenarios, vertical, lateral, and angular misalignments, are considered, with misalignment values presented as percentages for clarity.

The coupling factor variation under three misaligned conditions is simulated for concentric, solenoid, and circular coils in the investigation of a suitable Rx coil. Figure 5.7 illustrates the simulation plot for changes in k across different Rx coil geometries under misaligned conditions. It is observed that the k value for concentric and circular coils remains stable during vertical misalignment until a certain point, after which it decreases linearly with increasing misalignment, aligning with expectations. This occurs because the Rx coil moves away from the region with a stronger magnetic field in the vertical direction, leading to a reduction in coupled flux. However, the k value for the solenoid coil in vertical misalignment remains relatively constant throughout the entire misalignment. This stability is attributed to the high permeability core in the solenoid, providing a lower reluctance path that prevents a significant reduction in magnetic flux linkage between the Tx and Rx coils.

Similarly, the k value for concentric and circular coils decreases linearly with lateral and angular misalignment, as they move away from the Tx coil. This reduction results from fewer turns on the Rx coil linking with the Tx coil's magnetic flux. In contrast, the k value for the solenoid under lateral and angular misalignment remains more stable compared to concentric and circular coils.

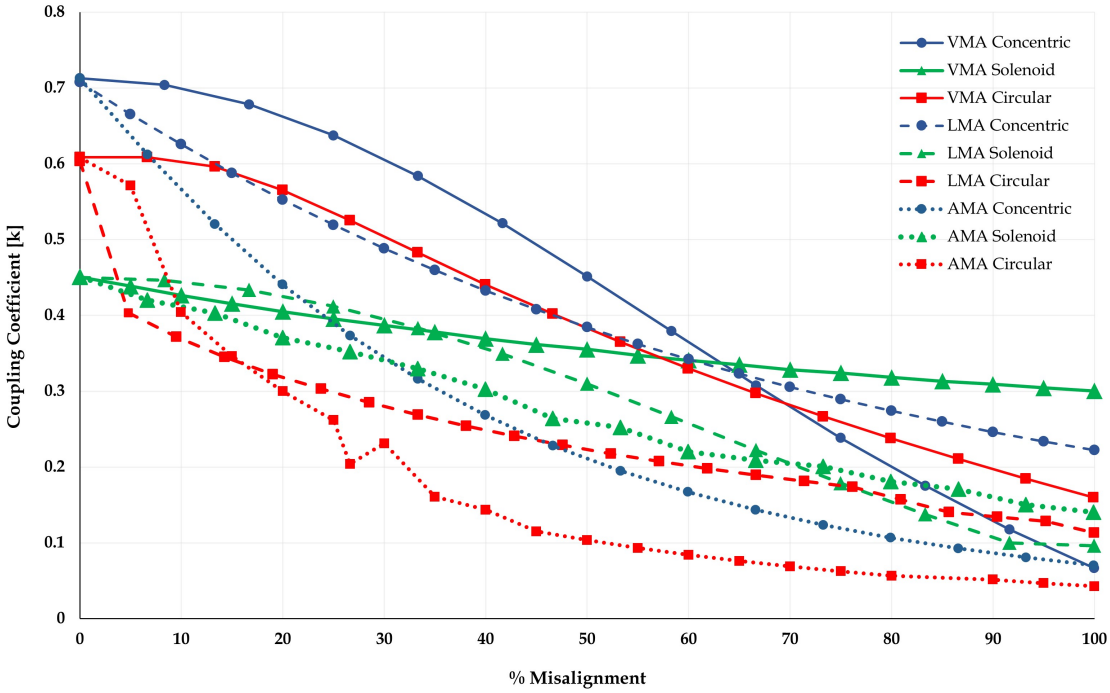

Figure 5.7: Coupling coefficient vs vertical, lateral, & angular misalignment for different Rx coil geometries

Figure 5.8 illustrates the magnetic field density change with misalignment for different Rx coil geometries. The plot reveals that the magnetic field density for concentric coils decreases linearly during lateral and angular misalignment, whereas for vertical misalignment, it consistently remains higher. In the case of vertical misalignment, the magnetic field density remains consistent until the Rx coil surpasses 45% misalignment, decreasing linearly beyond 50%. This is because all turns on the Rx coil stay linked to the magnetic field generated by the Tx coil until 50% misalignment, with the Rx coil staying in the vicinity of a strong magnetic field throughout the misalignment.

Similarly, the solenoid plot for vertical misalignment exhibits the trend seen in the plot for the change in k with vertical misalignment. For lateral misalignment, the magnetic field density stays consistent until 50% misalignment, decreasing significantly thereafter. The plot for angular misalignment decreases linearly, coinciding with the centers of the two coils with a low reluctance path. However, the circular coil plots deviate from the k change plot trend due to the strong magnetic field between the two circular coils, where numerous turns are stacked together.

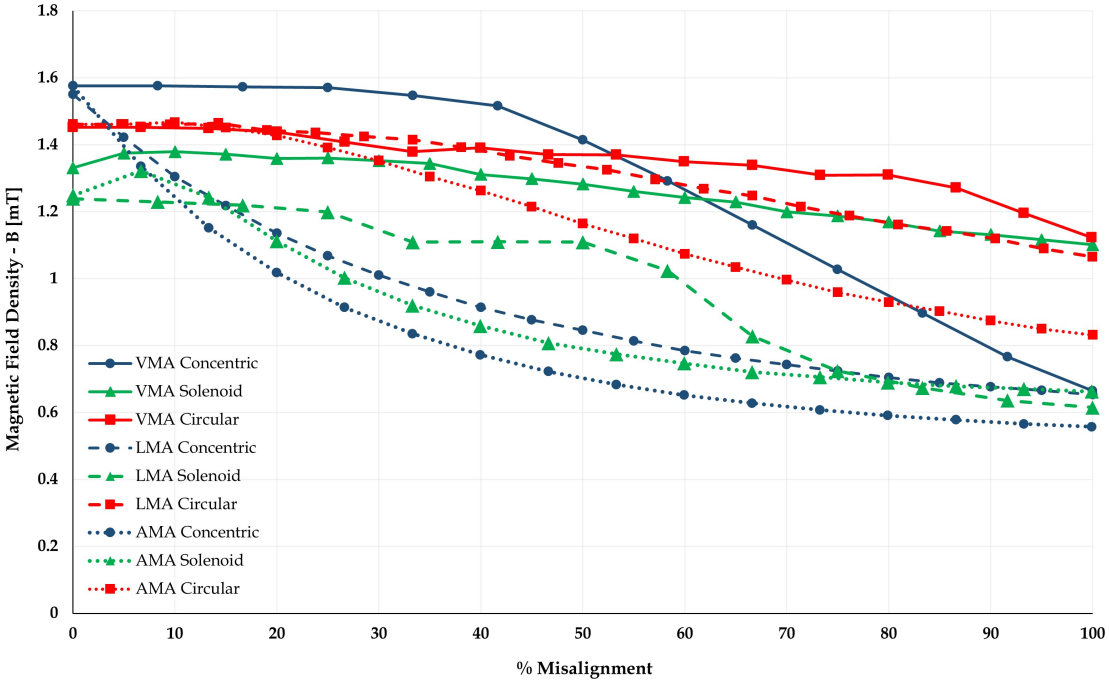

Figure 5.8: Magnetic field density vs vertical, lateral, & angular misalignment for different Rx coil geometries

It can be concluded from the plots that the solenoid coil geometry proves advantageous as a suitable Rx coil due to its stable k value under various misalignment conditions. The presence of a high permeability core in the solenoid maintains a consistent magnetic flux linkage between the Tx and Rx coils, preventing a significant reduction even under misalignment. This stability is particularly notable in all three misalignment conditions making the solenoid coil a robust choice for maintaining a stable coupling coefficient.

5.2 Proposed wireless power system

In this section, we will analyze the wireless power systems that we have designed, focusing on everything from coils to Tx and Rx boards. It's important to note that, we have used an Infineon converter (evaluation board) with 8-series connected concentric Tx coil, all other coils and circuits were designed by us. The objective of this section is to address the concerns of misalignment by using different coil geometries. The concentric coils with larger diameters are built to analyse the range & power transfer. The concentric coils are then connected in series on the Tx side & solenoid is used as Rx to provide alignment freedom to the Rx.

5.2.1 Concentric coils

In this setup, we can see that all the three misalignments have better power transfer efficiency compared to any other system used before as we have a better capacity to drive the coils in the transmitter board and the transmitter and the receiver have more coil area which creates better coupling between the coils. Also with higher frequency, we are able to achieve more range and a better power transfer during VMA. Concentric coils have an even distribution of magnetic field compared to other coil shapes, which helps in efficient magnetic coupling between the transmitter and receiver coils.

The pk-pk voltage measured at concentric Tx coil 1 is 70V ($24V_{rms}$) and the current is 7.50A ($2.65A_{rms}$) at a frequency of 800kHz. The misalignment has a significantly lower amplitude compared to the aligned case, indicating a less efficient power transfer. However, the optimization in the coil geometries, use of cable litz wire & better tuning on both the transmitter and the receiver have significantly reduced the distortion in the signals. The concentric Rx coil 2 is used to misalign as the coil has better power transfer due to a similar coil diameter to the Tx coil as shown in table 5.7. Also, compared to all other coils concentric Tx coil 1 and concentric Rx coil 2 have a bigger diameter of 30cm which gives a stronger coupling and better power transfer during misalignment and hence has a better efficiency.

Table 5.7: Measured values for concentric coil 2 as Rx under different misaligned operation

Type of Misalignment	Misalignment Value	Voltage (V_{rms})	Current (I_{rms})	Power (P_L)	Efficiency
Aligned	175mm from Tx	21.21	2.49	52.81W	83.03%
Vertical	1000mm from Tx	19.09	2.46	46.96W	78.83%
Lateral	50%(175mm) on Tx	17.67	2.48	43.82W	68.90%
Angular	40° angle above Tx	16.61	2.42	40.19W	63.20%

The FEM model and plot for magnetic field density of custom built concentric Tx and Rx is shown in figure 5.9. The Tx and Rx coils are excited with measured rated current of $I_{Tx} = 2.65A$ and $I_{Rx} = 2.49A$ respectively. The maximum simulated

magnetic field density is found to be 0.95mT at the center of the two coils as the magnetic flux is concentrated at the center of the concentric coils. The magnetic field density gradually reduces towards the outer edge of the two coils.

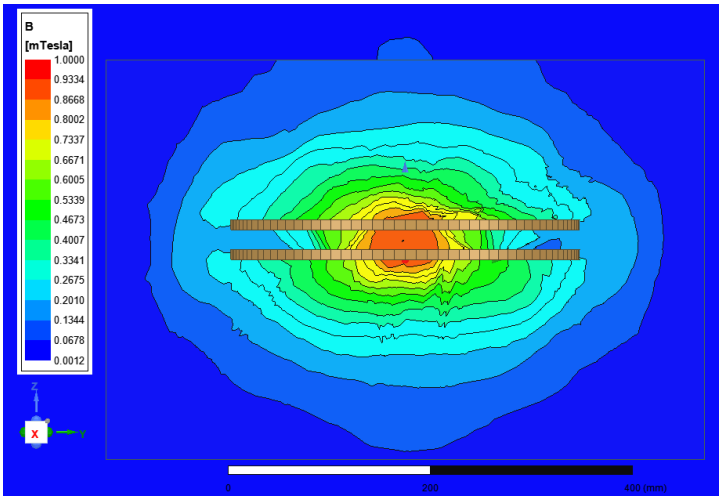

Figure 5.9: *B* field distribution between concentric coil 1 & concentric coil 2 under aligned condition

Figure 5.10 shows the plot for change in *k* with misalignment for concentric coil 1 & 2. It is observed from the plot that the value of *k* for vertical misalignment reduces slowly up to a certain misalignment and then reduces linearly as the percentage of misalignment increases which is as expected. This is because the Rx coil moves away from the region where the magnetic field is stronger in vertical direction, and hence the coupled flux between the coils reduces. It can also be observed that the coupling between the coils is better at maximum misalignment for lateral displacement than vertical displacement. This could be due to in lateral misalignment, a number of coil turns of Rx coil remain in the vicinity of the strong magnetic field.

The change in *k* with angular misalignment shows greater decline in *k* with misalignment which is lower than the plot for vertical and lateral misalignment. In angular misalignment, one part of the Rx coil remains in the vicinity of strong magnetic field while the other end slowly moves away from the magnetic field. Hence, not enough magnetic field lines generated by Tx coil cut the Rx coil. Also, the air gap between the two coils increases the reluctance of the magnetic circuit leading to lower coupling.

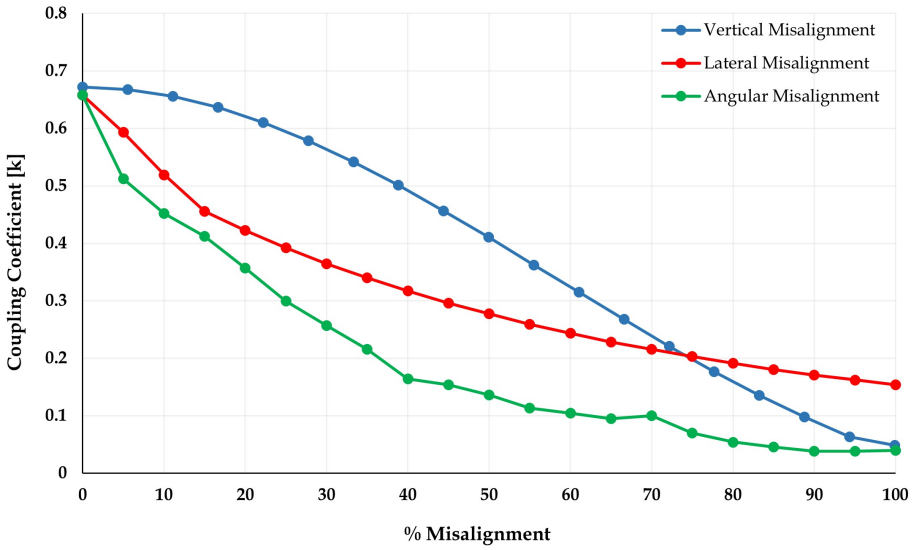

Figure 5.10: Coupling coefficient vs vertical, lateral, and angular misalignment between concentric coil 1 & 2

Figure 5.11 shows change in magnetic field density with misalignment. The plot follows same trend as seen in figure 5.10 where at maximum misalignment between coils, the magnetic field density at lateral and angular displacement is much higher compared to vertical displacement.

Figure 5.12 shows change in induced voltage with misalignment. Similar to the plot for k and B, the trend follows here. However, it can be seen that the induced voltage drops suddenly at around 15% of angular misalignment. This could be due to magnetic flux not cutting the Rx coil turns as the Rx coil moves in angular direction.

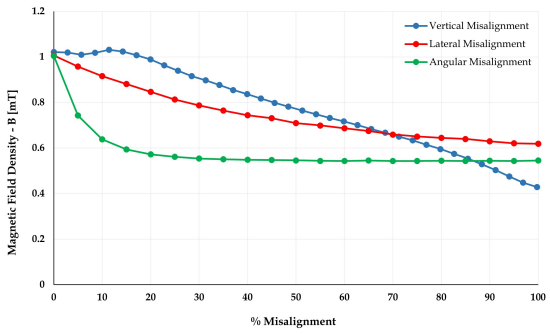

Figure 5.11: Magnetic field density vs misalignment between concentric coil 1 & 2

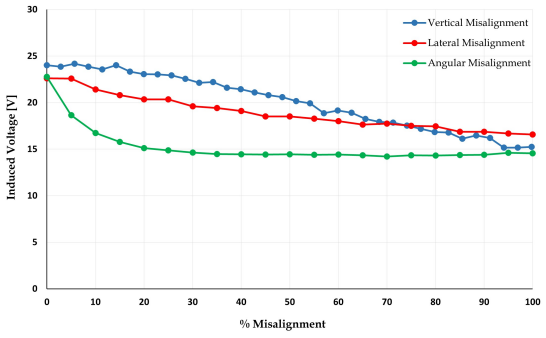

Figure 5.12: Induced voltage vs misalignment between concentric coil 1 & 2

5.2.2 Series connected coils

In this section, we will analyse 2-series connected & 8-series connected Tx coils with the solenoid Rx coils. The transmitter magnetic field is distributed to generate

horizontal field lines & hence the receiver is misaligned by rotating it horizontally & vertically. Figure 5.13 shows the voltage & current plot from Rx under aligned operation. Horizontal rotation(HR) reduces the magnetic coupling which leads to a decrease in the efficiency of power transfer. Vertical rotation(VR) can lead to a more drastic reduction in magnetic coupling compared to horizontal rotation. In extreme cases, if the receiver is rotated 90 degrees, the coupling can be almost completely lost.

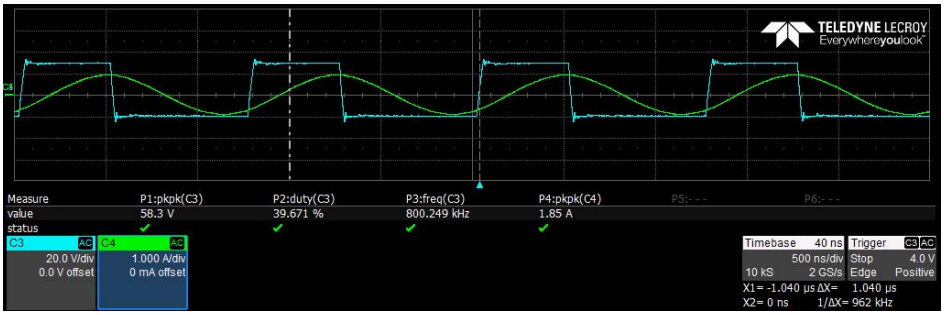

Figure 5.13: Voltage and current plot across hollow core solenoid Rx coil under aligned operation

In order to achieve the best coupling, the transmitter is connected in series such that 2 coils are placed on each side together forming 8 series connected coils. Even though the coils distribute the magnetic field there are some voids in the 3D space due to the cross-magnetizing effect. The plots of Tx and Rx coils are shown in figure 5.14 & figure 5.15 respectively which has an initial spike due to the interaction of magnetic fields & charging of LC tank. Figure 5.16 shows the plot for the Void at 40° angle which has reduced amplitude due to poor coupling and the waveforms look distorted due to misalignment. The efficiency & the power transfer are listed in the table 5.8. The increase in efficiency for 8-series connected Tx coil with solenoid Rx under misaligned condition is due to the distributed Tx coil turns in smaller areas which enables better distribution of magnetic field and consequently improves the coupling with the Rx coil.

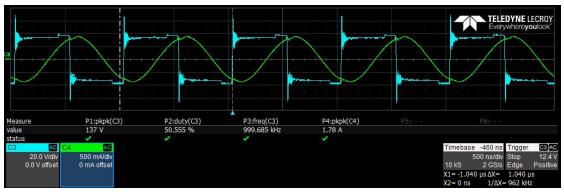

Figure 5.14: Voltage and current plot across 8 series connected concentric Tx

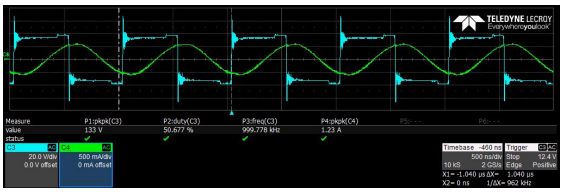

Figure 5.15: Voltage and current plot across hollow core solenoid Rx coil

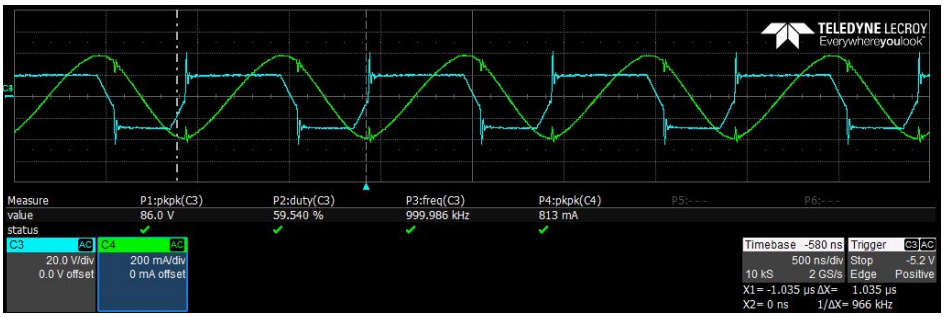

Figure 5.16: Voltage and current plot across solenoid Rx coil when it is placed in the magnetic field voids

Table 5.8: Measurement values for 2 series & 8 series connected coils with solenoid Rx coil 1 & 2 respectively

Coil	Type of Misalignment	Voltage V (V_{rms})	Current A (I_{rms})	Frequency (kHz)	Power W (P_L)	Efficiency (%)
2 Series Connected Coil(Tx)	Aligned	21.21	0.65	800.24	13.78	NA
Solenoid Coil 1(Rx)	Aligned	20.61	0.50	800.07	10.30	74.78
	Horizontal Rotation	20.61	0.32	800.07	6.59	47.82
	Vertical Rotation	19.44	0.31	800.17	6.02	43.68
8 Series Connected Coil(Tx)	Aligned	24.04	0.62	998.68	14.90	NA
Solenoid Coil 2(Rx)	Aligned	23.68	0.49	999.77	11.60	77.87
	Misaligned	23.33	0.41	999.98	9.56	64.16

The FEM model and plot for magnetic field density of custom built 2-series connected concentric Tx and solenoid Rx is shown in figure 5.17. The Tx and Rx coils are excited with measured rated current of I_{Tx}=0.65A and I_{Rx}=0.5A respectively. The maximum simulated magnetic field density is found to be 1.13mT between two coils. The magnetic field density gradually reduces towards the outer edge of the two coils and drastically reduces below the shielding. It can be observed from the figure that the B field generated by the Tx coil travels from one concentric coil to another concentric coil connected in series completing a loop. These magnetic field lines link with the solenoid coil placed parallel to the magnetic field lines generated by series connected concentric coils. The two scenarios are included namely horizontal rotation and vertical rotation. Horizontal rotation is when the Rx coil is placed perpendicular to the magnetic field lines generated by the Tx coil and it is rotated through 180° in the horizontal direction. While vertical rotation is when the Rx coil is rotated through 180° in the vertical direction.

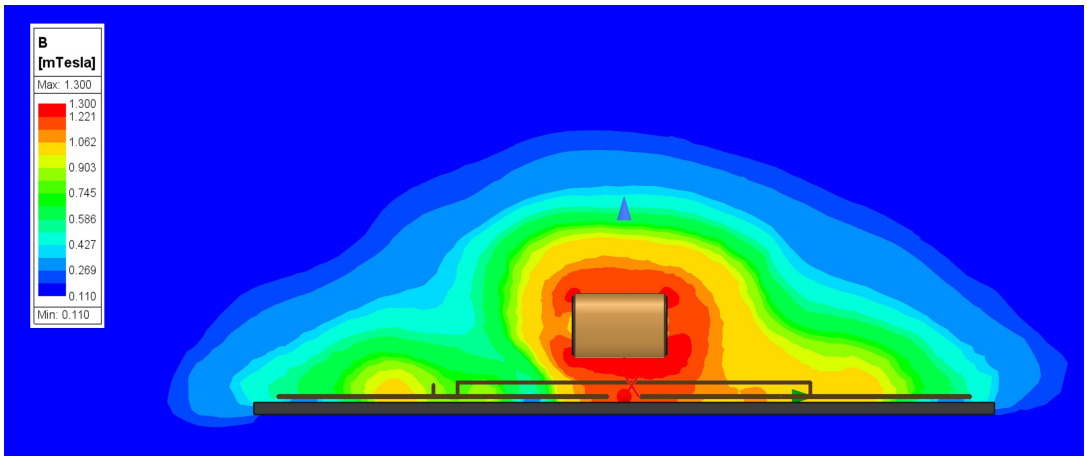

Figure 5.17: *B* field distribution between 2 series connected concentric Tx coil and solenoid Rx coil

The FEM model and plot for magnetic field density of custom built 8-series connected concentric Tx and solenoid Rx is shown in figure 5.18. The Tx and Rx coils are excited with measured rated current of $I_{Tx} = 0.62A$ and $I_{Rx} = 0.49A$ respectively. The maximum simulated magnetic field density is found to be 1.5mT between two coils. All the 8 series connected concentric coils are supported by shielding forming a closed space in which a solenoid coil with hollow core is placed. It can be observed that there are areas in the closed space where the magnetic field density is lower as the magnetic linkage between two consecutive series connected concentric coils is not strong enough.

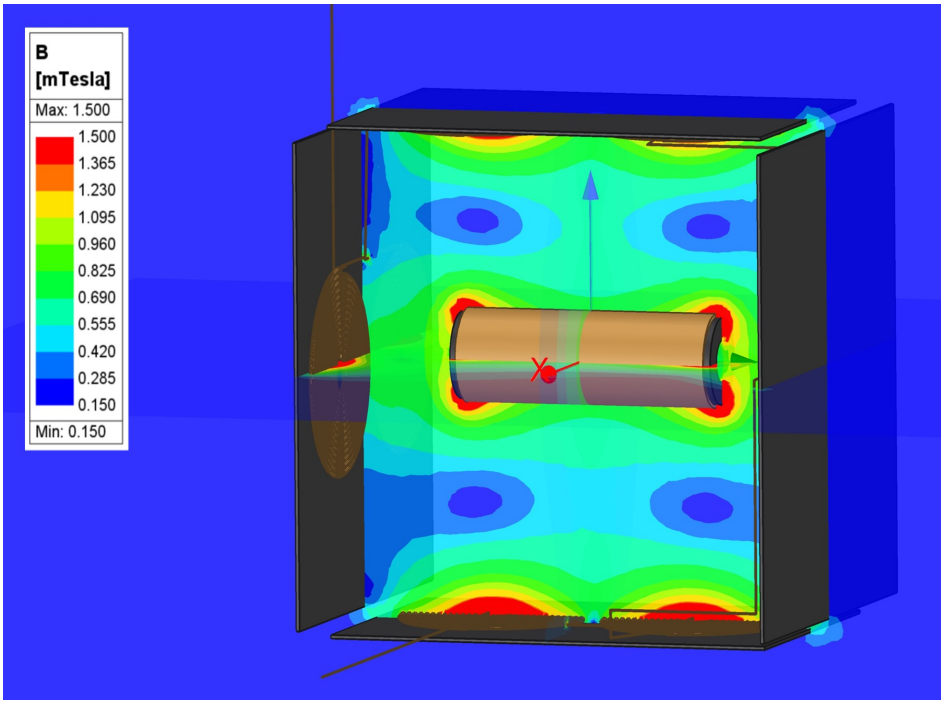

Figure 5.18: *B* field distribution between 8 series connected concentric Tx coil and solenoid Rx coil

Table 5.9 shows the comparison of measured, analytical & simulated parameters for 8-series connected Tx coil and solenoid Rx coil.

Table 5.9: Comparison of measured and simulated parameters for 8-series connected concentric Tx & Solenoid Rx coil in normal operation

Parameters	Measured	Analytical	Simulation
Self-Inductance Tx	71.90μH	74.46μH	72.30μH
Self-Inductance Rx	160μH	167.33μH	162.51μH
Coil Resistance Tx	0.25Ω	0.3Ω	0.53Ω
Coil Resistance Rx	0.021Ω	0.02Ω	0.041Ω
Mutual Inductance (M)	NA	85.94μH	85.63μH
Coupling Coefficient (k)	NA	0.77	0.79
Magnetic Field Density (B)	NA	1.47mT	1.5mT

The change in coupling coefficient with horizontal rotation and vertical rotation of solenoid Rx in combination with 2 series connected and 8 series connected Tx coil is shown in figure 5.19. It can be seen that the coupling coefficient for solenoid Rx with 8 series connected concentric coil remains stable when rotated both in horizontal and vertical direction. This is due to the magnetic field generated by the 8 series connected concentric Tx coil which is equally distributed in the given space except the corners where the coupling is lowest as shown in the plots.

However, it can be observed that the coupling coefficient for solenoid Rx with 2 series connected concentric coil has the maximum value at 90° and lowest value at 0° and 180°. This is because at 90°, the solenoid Rx is parallel to the magnetic field lines generated by the series connected concentric Tx coil. And at 0° and 180°, the solenoid Rx coil is perpendicular to the magnetic field lines.

It can also be interpreted as the 2 series connected concentric Tx coil generates 2-dimensional magnetic field while the 8 series connected concentric Tx coil generates 3-dimensional magnetic field.

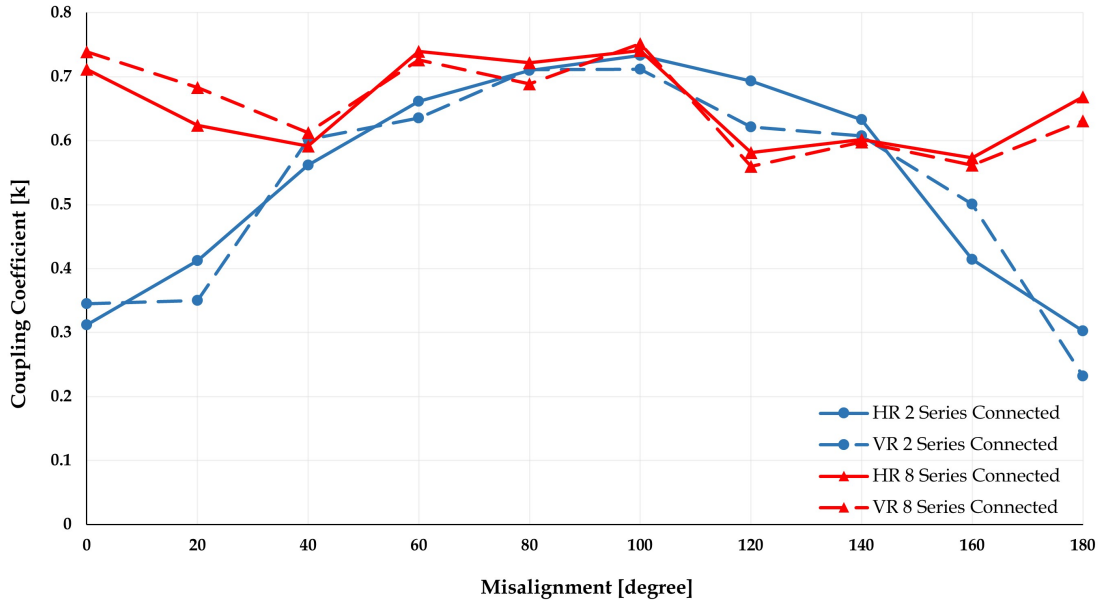

Figure 5.19: Coupling coefficient vs misalignment for solenoid Rx coil with 2 and 8 series connected concentric Tx coil

Figure 5.20 show the change in magnetic field density with misalignment. The magnetic field density is lowest at the corners of the closed space. Similar to the plot for change in k with misalignment, the same trend follows here. However, the plot for change in magnetic field density with vertical misalignment for solenoid Rx with 2 series connected coil do not follow the same trend. This could be due to computational error in the parametric sweep operation.

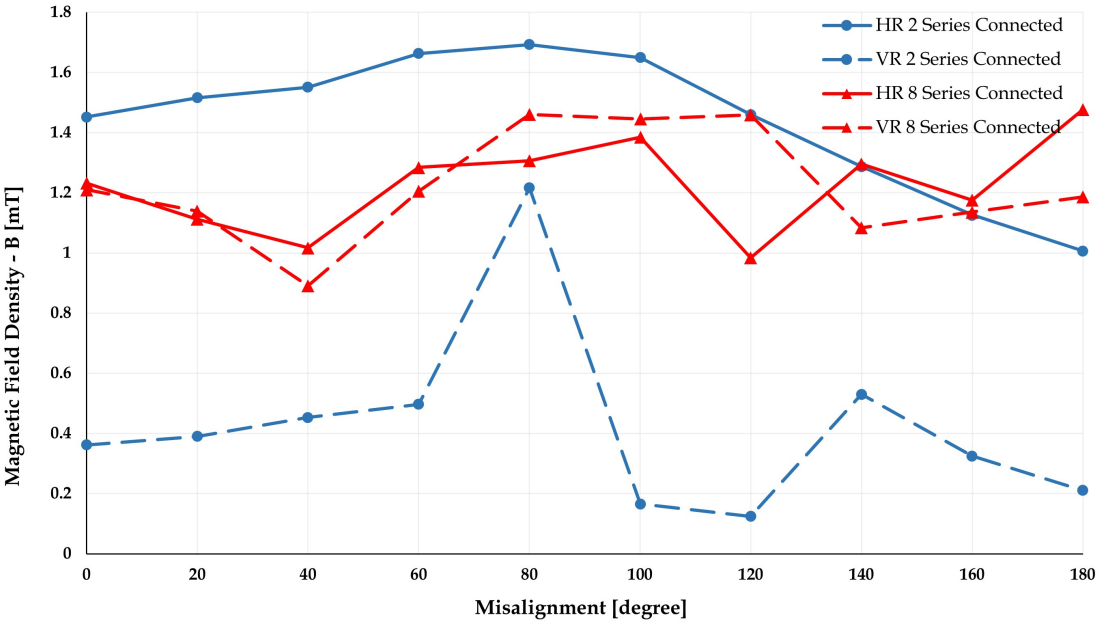

Figure 5.20: Magnetic field density vs misalignment for solenoid Rx coil with 2 and 8 series connected concentric Tx coil

Figure 5.21 show the change in induced voltage with misalignment. The magnetic field density is lowest at the corners of the closed space. However, the magnetic linkage of Rx coil with one set of concentric coil is strong enough to induce voltage in all directions.

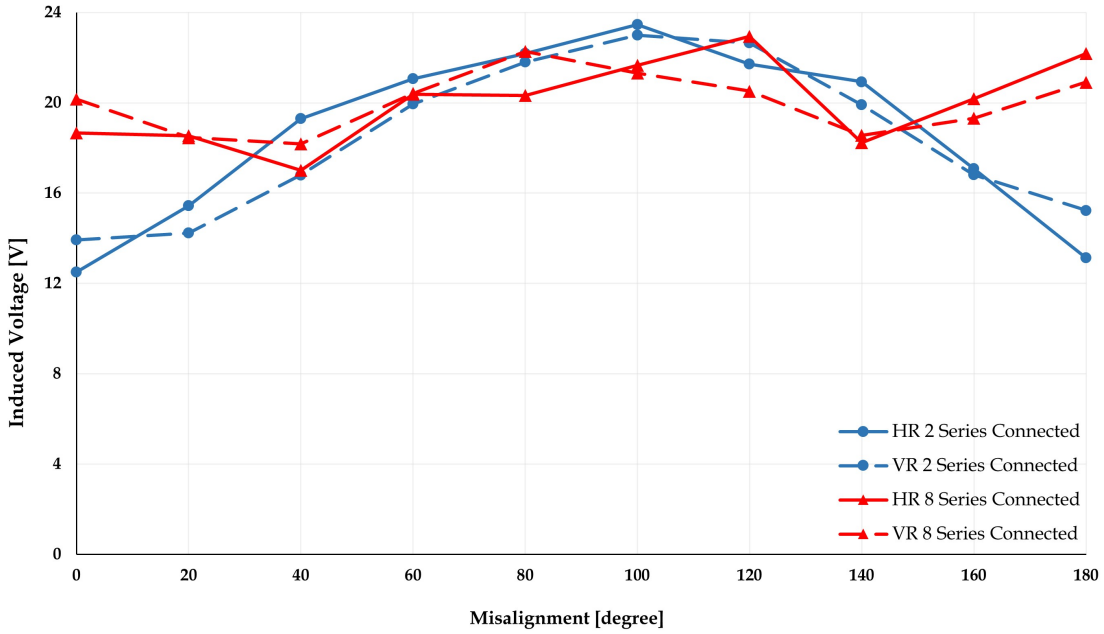

Figure 5.21: Induced voltage vs misalignment for solenoid Rx coil with 2 and 8 series connected concentric Tx coil

5.3 Comparison & results

5.3.1 Power transfer

The alignment between the Tx and Rx has a significant impact on efficiency. This is primarily due to a greater reduction in the coupling coefficient between the coils with a small misalignment between the Tx and Rx. Figure 5.22 shows the transferred power and efficiency of each wireless power model under aligned and misaligned conditions. The efficiency of each model under aligned operation is significantly higher compared to the efficiency under misaligned conditions. This is because, during aligned operation, the Tx and Rx are perfectly aligned, enabling the maximum possible coupling between the coils. Additionally, the Tx and Rx coils resonate at the same frequency under aligned conditions, resulting in maximum efficiency. In contrast, efficiency reduces drastically under misaligned operation.

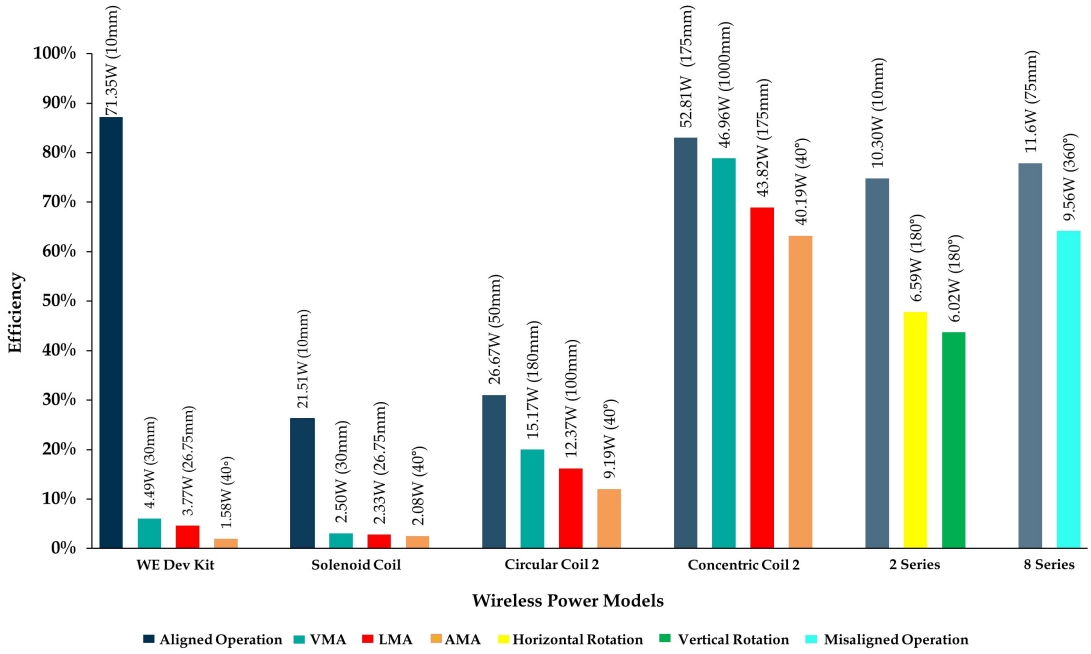

Figure 5.22: Comparison of power transfer efficiency

It can be observed that under aligned operation, the WE development kit has an efficiency of 87%, which is higher compared to the efficiency of the solenoid Rx coil, where the efficiency drops by more than 60% under aligned operation. This is due to the different coil geometry used as Rx with the concentric Tx coil, as changes in coil type, number of turns, self-inductance, and core type reduce the coupling between the concentric Tx and Rx coil. However, it can be observed that the solenoid Rx coil provides better efficiency under angular misalignment compared to the WE development kit. This is mainly due to the strong magnetic field at the center of the solenoid Rx with a hollow core, offering a lower reluctance path when displaced in an angular direction compared to the concentric Rx coil.

The power transfer efficiency for the center-tapped circular coil is higher under misaligned conditions when compared to the WE development kit and solenoid Rx coil. However, the power transfer efficiency under aligned operation is lower since the coil turns are stacked together in the circular coil, resulting in a less distributed B-field due to the higher reluctance offered by the air gap. But under misaligned operation, the B-field and induced voltage do not reduce and remain stable until the maximum misalignment is reached, as explained in section 5.1.3. Hence, there is a relatively higher efficiency under misaligned operation.

Similarly, the power transfer efficiency for concentric coil 2 is much higher in both aligned and misaligned conditions compared to other models. This is due to the same coil geometry on Tx and Rx having similar coil parameters, a larger radius of coils, and a higher number of turns on both Tx and Rx. The change in k, B, and induced voltage with misalignment for concentric coil 2 is explained in section 5.2.1.

The 2-series connected and 8-series connected concentric coils with solenoid Rx offer good power transfer efficiency in both aligned and misaligned operations. The distributed magnetic field created by the series-connected concentric coils enables better coupling with the solenoid Rx in all directions. The 2-series connected concentric coil has an efficiency of 75% when the solenoid Rx is parallel to the magnetic field lines generated by the series-connected Tx. However, this efficiency drops to 45% when the solenoid is placed perpendicular to the magnetic fields generated by the series-connected Tx.

The 8-series connected concentric coil creates a distributed and uniform magnetic field in the given space. Hence, power can be transferred efficiently in the provided space with the solenoid Rx in all directions, achieving an efficiency of 78%. However, there is a void between the consecutive 2-series connected coils, and when the solenoid Rx is facing towards the void where the magnetic field is lowest, the efficiency drops to 64%.

In comparison, the proposed 8-series connected concentric Tx coil with a solenoid Rx coil outperforms the conventional wireless power system from WE. The efficiency is improved by more than 60% under misaligned operation and offers similar efficiency and performance under aligned operation.

5.3.2 Point to multi-point power transfer

The circular coil geometry is also used to study the point to multipoint power transfer capability of the circular coils with different form factor. The circular coil design has multiple coils which we have used to analyse point to multipoint power transfer. The combination of coils used for this setup are,

- Tx coil - Circular coil 1
- Rx coils - Circular coil 4 & 5

The distance between the transmitter coil and the receiver coil is at 50mm and there is no misalignment between the coils. For driving the centre tapped Tx circular coil 1, a Tx board with 4 BJTs is used and two 24V DC motors are connected to the Rx circular coil 4 & 5. The LC Tank on both the transmitter and receiver board has a parallel resonance and a corresponding resonant capacitor is used for both the Rx coils.

Table 5.10: Measurement data from the test setup for point to multi-point power transfer

Coil	**Inductance (μH)**	**Voltage(V)**		**Current(A)**		**Frequency (kHz)**
		pk-pk	rms	pk-pk	rms	
Circular Coil 1	555.35	132	46.66	4.50	1.59	8.79
Circular Coil 4	16.11	76.05	26.89	5.03	1.77	8.68
Circular Coil 5	103.55	72.03	25.47	2.60	0.92	8.71

The efficiency in the circular coil 4 is better compared to circular coil 5, as the diameter of the circular coil 4 is bigger than the diameter of the circular coil 5. In spite of the presence of the center tapping in the circular coil 5, we can see lower efficiency as the coil dimensions should also align with the Tx coil. The overall efficiency of the system will not be affected if we have multiple Rx coils with the loads within the range of the system. The power transfer efficiency for different receiver coils used in point to multi-point power transfer are presented in 5.11. The magnetic field distribution in point to multi-point is shown in figure 5.23.

Table 5.11: Power transfer efficiency

Coil	Power (P_L)	Efficiency
Circular Coil 4	47.59W	64.15%
Circular Coil 5	23.43W	31.58%

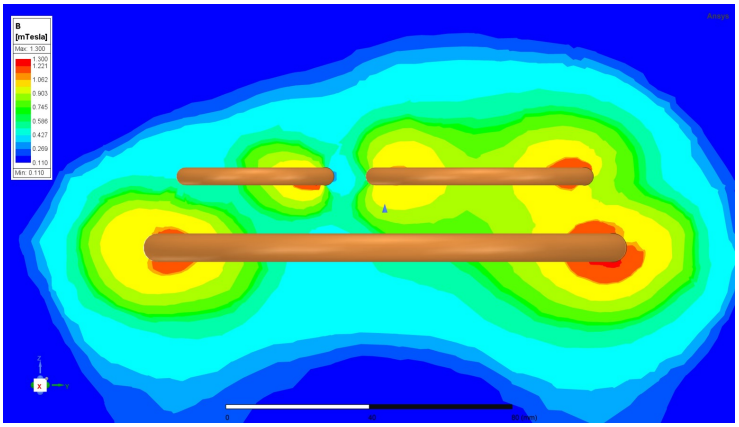

Figure 5.23: *B* field distribution in point to multi-point power transfer

6
Conclusion

In this thesis, we have designed concentric coils that are connected in series to create a distributed magnetic field, which acts as a Tx along with a solenoid Rx coil, it improves the alignment and the power transfer efficiency compared to conventional wireless power system. Thus, the high-frequency resonant inductive coupling method proved to be highly effective, especially when combined with the optimized coil geometry. We have analyzed different coil geometries to investigate suitable Tx and Rx coil for the proposed wireless power system.

6.1 Investigation of suitable Tx and Rx coil

The conventional wireless power system from WE employs identical concentric coil geometry for the Tx and Rx. The test results show that the maximum range of power transfer in the vertical direction, until the receiver coil stays coupled, is 30mm, beyond which the coils will disconnect. The efficiency drops by about 80% when the Rx coil is moved 30mm away from the Tx coil in the vertical direction, and the power transfer further reduces in LMA and AMA. The decline in efficiency is attributed to a significant reduction in the coupling coefficient with misalignment. The simulation results obtained from the FEM model designed in Ansys Maxwell also indicate that the coupling between the coils reduces by 80% with increasing misalignment. We were able to validate the misalignment results and the coupling factor from the hardware model and simulation model through analytical calculations with around a 1.5% error.

A result found was that for better efficiency with concentric coils, it is optimum to have an identical Rx geometry. However, when a solenoid is used as Rx, there is an efficiency improvement of 1% during misalignment. The solenoid coil has a core, and the coil is wound using litz wire, enabling better efficiency for both aligned and misaligned operation. These results are validated using simulation and analytical calculations. Also, the simulation results shows that the solenoid Rx coil provides stable coupling coefficient under different misalignment conditions as shown in figure 5.7. The investigation of center-tapped circular coil shows that a maximum range upto 180mm between Tx and Rx can be achieved, which is around a 15% increase in range compared to the conventional system. The increase in range is attributed to a greater number of coil turns stacked together in the circular coils, leading to better mutual coupling. The circular Rx coil is connected to a 24W DC motor, and there is an increase in efficiency of 10% during

both aligned and misaligned operation. The center-tapped circular coils are also utilized to test point-to-multi-point power transfer. It is found from the test results that multiple circular Rx coils can be used in combination with a single circular Tx coil with better efficiency compared to the WE development kit. Although center-tapped circular coils help in improving range and efficiency, the higher number of coil turns and a unique BJT based automatically switching transmitter circuit to drive the center-tapped circular coils make it a non-viable solution.

6.2 Proposed wireless power system

The measurement and simulation results from the WE development kit show that, as expected, it is required to perfectly align the Tx and Rx coils to achieve maximum power transfer efficiency. Hence, the conventional system does not provide geometric and alignment freedom to the receiver. In the proposed wireless power system, it is possible to generate a distributed magnetic field, which enables better range, and efficiency, and provides geometric and alignment freedom to the receiver.

To achieve a distributed magnetic field and higher power transfer efficiency, a high-frequency half-bridge transmitter board is designed to reduce losses in the power electronics. Concentric coils with relatively large diameters are used as both Tx and Rx coils, with the half-bridge transmitter board operating at 800 kHz. The maximum power transfer is found to be 52.8W up to a range of 175mm with an efficiency of 83%. In contrast, the WE development kit has a maximum range of 30mm. Hence, more coil turns and a larger coil diameter help in improving the range.

The half-bridge Tx board is also utilized to drive a custom-built 2-series connected concentric Tx coil. The 2-series connected concentric Tx coil generates a magnetic field that travels from one concentric coil to another concentric coil connected in series, forming a horizontal loop of magnetic field lines. These horizontal field lines contribute to better coupling with the solenoid Rx coil. It was possible to transfer 10.3W of power at an efficiency of 75%. With the 2-series connected concentric coil and the solenoid as Rx, power transfer was achieved at an approximate efficiency of 48%, and 44% when the Rx was rotated in the horizontal and vertical directions, respectively. The measurement and simulation results reveal limitations in this coil geometry setup, as the coupling between the 2-series connected concentric coil and the solenoid Rx coil significantly reduces when the solenoid Rx is at an angle where the magnetic field lines generated by the Tx coil are perpendicular to the Rx coil, leading to a reduction in efficiency.

The limitations of the 2-series connected concentric coil are overcome by developing an 8-series connected concentric Tx coil, where 4 pairs of 2-series connected concentric coils are connected in series to form a closed space of dimensions (15cm x 15cm x 15cm). Similar to the 2-series connected concentric coils, which generate a loop of magnetic field lines traveling from one coil to the other, placing 4

pairs of 2-series connected coils to form an enclosed area results in a space with an equally distributed magnetic field. When a solenoid Rx coil is placed in this enclosed space, as shown in Figure 3.21, we achieve a power transfer of 11.6W at 78% efficiency. In this setup, we are also able to transfer approximately 10W at 64% efficiency when the solenoid Rx coil is rotated in a direction relative to the Tx coil where the magnetic field density is lowest. Thus distributing coil turns into smaller areas help in better distribution of magnetic field and improves the coupling between the Tx and Rx. The simulation results for the 8-series connected coil model also show stable coupling between the series-connected concentric Tx coil and solenoid Rx when Rx is rotated, justifying the outcomes of the test results.

In comparison, the proposed wireless power system exhibits approximately the same efficiency of 80% under aligned operation and an increased efficiency by more than 60% under misaligned operation compared to the WE development kit. Additionally, the proposed wireless power system offers alignment freedom to the Rx coil, allowing it to be rotated in any direction and still be coupled with the Tx coil. In contrast, in the WE development kit, a significant drop in efficiency is observed with even small misalignment.

7

Future Scope

Wireless Power Transfer (WPT) has emerged as a promising technology, offering convenience and efficiency in charging devices without the need for physical connectors. While our thesis project has made significant strides in WPT, there are several areas for enhancement and optimization.

- BJTs are used in the transmitter board for driving circular coils, which has resulted in heating issues. Transitioning to MOSFETs or IGBTs could mitigate this problem due to their superior efficiency and heat dissipation. Additionally, designing the receiver board with Schottky diodes, voltage regulators, and filters can stabilize the power output to loads, ensuring consistent and reliable power transfer.
- Moving from a half-bridge circuit to a full-bridge circuit for driving series-connected coils holds the potential to boost efficiency. The utilization of a full bridge circuit enables better control and management of power flow, potentially reducing losses and optimizing the power transfer.
- The 8 series connected coils are designed for a smaller area of $260cm^2$ and this can be scaled to a larger area to supply power to multiple loads.
- Certain applications, such as charging laptops, demand higher power. To address this, exploring coils with reduced losses becomes crucial. Hollow copper tubes offer promising characteristics, such as minimal resistance and mitigated skin effects at high frequencies, making them a potential solution for high-power transfer. Additionally, PCB-etched coil is tested in coil compatibility which opens doors for diverse applications in various power transfer scenarios.
- The absence of accounting for losses in both power electronics and coils during system modelling presents an opportunity for improvement. Incorporating these losses into the calculations will lead to more precise estimations of power transfer efficiency, allowing for better optimization and real-world performance predictions.

8

Environmental & Ethical Aspects

Wireless power transfer has emerged as a promising technology, revolutionizing how we charge portable electronics and power IoT devices. Its potential to enhance convenience and flexibility comes hand in hand with its environmental and ethical implications. One of the key advantages of wireless power transfer lies in its potential to reduce carbon dioxide emissions. By eliminating the need for multiple wired chargers and adapters, it curtails the production of these accessories, consequently lessening the environmental footprint associated with their manufacturing and disposal. However, a potential environmental concern arises from the increased usage of copper in winding coils, essential components in wireless power transfer systems. Mining and processing copper can be environmentally taxing due to habitat disruption, water usage, and emissions. Yet, the benefits of wireless charging in reducing overall energy consumption often outweigh the initial environmental costs of increased copper usage.

From an ethical standpoint, the adoption of wireless power transfer raises questions about access and equity. While this technology offers convenience, it might exacerbate the digital divide. Affordability and accessibility of wireless charging technology could potentially create disparities, leaving certain demographics or regions behind if they cannot afford or access these advancements. Additionally, there are ethical implications regarding the disposal of obsolete wired chargers and devices as the transition to wireless power transfer accelerates.

To address the environmental impact of increased copper usage, research and development efforts should focus on enhancing the efficiency of wireless power transfer systems, thereby reducing the amount of copper required in coils. Additionally, emphasizing the use of recycled copper and promoting responsible mining practices can help mitigate the environmental consequences of copper extraction. Ethically, efforts must be made to ensure equitable access to wireless charging technology, potentially through subsidies, incentives, or community programs.

In conclusion, while wireless power transfer presents remarkable advantages in reducing CO2 emissions and enhancing convenience, it necessitates a comprehensive approach to address its environmental impact and ethical considerations. Strategic technological advancements, responsible material sourcing, and equitable accessibility are pivotal in harnessing the full potential of wireless power transfer while minimizing its drawbacks.

Bibliography

[1] Cem Som and Dr. Michael A. de Rooij. *Trilogy of Wireless Power Transfer*, 1st edition. Germany: Wurth Elektronik eiSos GmbH & Co. KG, 2019.

[2] Dr. Thomas Brander, Alexander Gerfer, Bernhard Rall and Heinz Zenkner. *Trilogy of Magnetics*, 5th edition. Germany: Wurth Elektronik eiSos GmbH & Co. KG, 2018.

[3] Wenxing Zhong, Dehong Xu and Ron Shu Yuen Hui. Wireless Power Transfer Between Distance and Efficiency, *CPSS Power Electronics Series*, China, 2020, Springer.

[4] Shah, M. H., Abosaq, N. H. Wireless power transfer via inductive coupling. 3C Tecnología. Glosas de innovación aplicadas a la pyme. Edición Especial, April 2020, 107-117.

[5] V. Shevchenko, O. Husev, R. Strzelecki, B. Pakhaliuk, N. Poliakov and N. Strzelecka, "Compensation Topologies in IPT Systems: Standards, Requirements, Classification, Analysis, Comparison and Application," in IEEE Access, vol. 7, pp. 120559-120580, 2019, doi: 10.1109/ACCESS.2019.2937891.

[6] P. Nalinnopphakhun, W. Onreabroy and A. Kaewpradap, "Parameter Effects on Induction Coil Transmitter of Wireless Charging System for Small Electric Motorcycle," 2018 IEEE International WIE Conference on Electrical and Computer Engineering (WIECON-ECE), 2018, pp. 145-148, doi: 10.1109/WIECON-ECE.2018.8783005.

[7] J. D. Jackson. Classical Electrodynamics. Wiley, New York, 3rd. edition, 1999.

[8] Hussain, I.; Woo, D.-K.Inductance Calculation of Single- Layer Planar Spiral Coil. Electronics 2022, 11, 750. https://doi.org/10.3390/electronics11050750

[9] Z. Pantic and S. Lukic, "Computationally-Efficient, Generalized Expressions for the Proximity-Effect in Multi-Layer, Multi-Turn Tubular Coils for Wireless Power Transfer Systems," in IEEE Transactions on Magnetics, vol. 49, no. 11, pp. 5404-5416, Nov. 2013, doi: 10.1109/TMAG.2013.2264486.

[10] U. Azad and Y. E. Wang, "Impact of receiver coil misalignment on near-field communication system performance," Proceedings of the 2012 IEEE International Symposium on Antennas and Propagation, 2012, pp. 1-2, doi: 10.1109/APS.2012.6347948.

[11] ELEKTRISOLA Dr. Gerd Schildbach GmbH Co KG, "Litz wire", https://www.elektrisola.com/en/Litz-Wire/Info (accessed 20 Sept. 2022)

[12] Eric Persson, Yalcin Haksoz, "CoolGaN™ 600 V half-bridge evaluation platform featuring GaN EiceDRIVER™," Infineon Technologies AG, 2020.

A

Appendix 1

A.1 Conventional Wireless Power System

Figure A.1 shows the transmitter and the receiver board which has LEDs for error indication, warns of a faulty condition, power transfer conditions, and data communication. Figure A.2 shows the block diagram of the 200W WPT development kit. Table A.1 show the description of the junction blocks of 200W WPT development kit. Figure A.3 and table A.2 shows the details of the mains adapter and it's specifications. Figure A.3 also shows 3 different mains adapter plugs. The development kit has three major blocks namely,

1. Power Transmitter
2. Power Receiver
3. Tx and Rx Coils

The transmitter block has to be supplied with a voltage of 24V DC, for this a mains adapter/switch-mode power supply of input voltage 100V-240V AC, 50/60Hz frequency and a maximum current of 2.5A is used. The 24V DC output from the switch-mode power supply is then fed to the transmitter block which contains an EMI filter to suppress electromagnetic noise and extract and bypass any unwanted current from the wires and cables, allowing only desirable current to flow through the circuit. Then the power flows through the reverse polarity protection block and then to the full-bridge inverter. The full-bridge inverter block contains four MOSFETs. The high frequency input to the gates of the MOSFETs allow them to switch at high frequency and the controller turns on only two MOSFETs at different limbs of the H-bridge at a time to avoid a short circuit current flow. The power transfer is fully digitally controlled by the XMC1302 series microcontroller. The high frequency generation, the dead time and the control signals for the full-bridge is generated by the MCU which can be controlled in automatic mode or manual mode. The manual mode features the change in frequency with an encoder, this can be used to change the output voltage or for optimising the efficiency. The *MagI*^{3}*C* power module supplies a controlled power to the full-bridge inverter. The MCU block has a feedback from the data receiver communication block and over-voltage protection block. The power from the full-bridge inverter is then fed to a LC-resonant tank which will be pre-tuned for the frequency generated at the full-bridge inverter.

The receiver coil is connected with a tuned capacitor which forms a RLC-resonant tank similar to the transmitter block. The power received from the receiver coil is fed to the full-bridge synchronous rectifier. The full-bridge synchronous rectifier consists of four MOSFETs controlled by a full-bridge MOSFET driver where the power is converted from high frequency AC to a DC voltage which is then fed to the load. The controlled voltage for driving the MOSFETs, the $MagI^3C$ power module is used which gets a controlled signal generated by the MCU. The microcontroller unit gets feedback from data transmitter communication block and IoT I2C block where all the sensor outputs are connected.

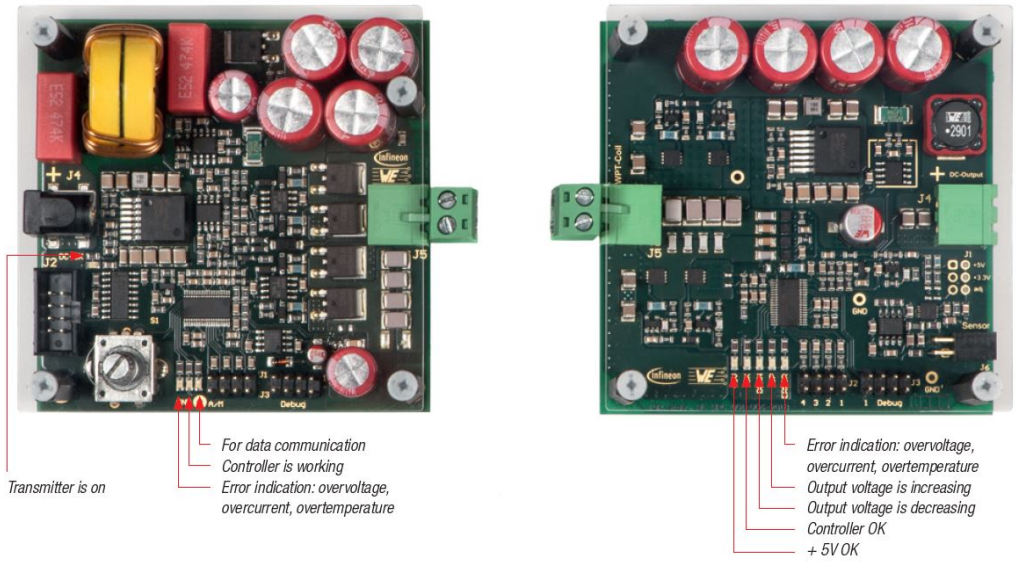

Figure A.1: WPT transmitter and reciecer board with status indicating LEDs

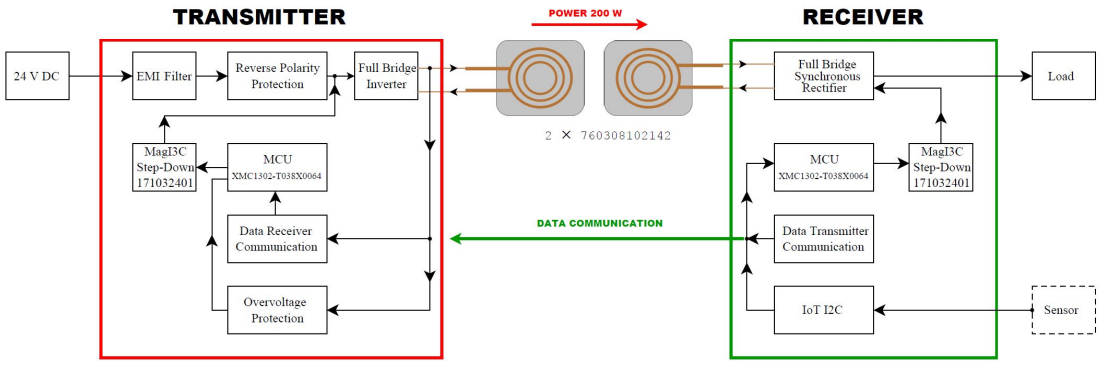

Figure A.2: Block Diagram of 200W WPT Development Kit From Wurth Electronics

Table A.1: Junction Blocks of 200W WPT Development Kit

Junctions	Description
J1	Automatic / Manual Opration Modes
J2	RS232 Interface
J3	Debug / Program
J4	DC input to the Tx board and The load point on the Rx board
J5	Tx/Rx Coil Connectors
J6	Sensor Output Connector

The overall system operates at a voltage level of 24V DC which is obtained from the switch-mode power supply. The switch-mode power supply converts the mains AC voltage to a desired voltage of 24V DC which can be connected to a DC plug at junction J4 of the transmitter board. The voltage level from the input of the transmitter board to the output of the receiver board is maintained at 24V DC with a maximum current of 10A and the circuit is operating at a frequency of 205KHz. Figure A.3 show the image of the mains adapter with 3 different mains adapter plugs and table A.2 shows the details of the mains adapter and it's specifications.

Table A.2: Mains Adapter Specifications

Parameters	Specifications
Input Voltage	100 - 240V AC, 50/60Hz
Output Voltage	24V DC
Output Current Rating	6.25A

Figure A.3: Mains adapter with 3 different mains adapter plugs

Electric Power Engineering
Chalmers University of Technology
Gothenburg, Sweden
www.chalmers.com/en/